A NONLINEAR COMPUTER FOR THE SOLUTION OF SERVOMECHANISM PROBLEMS

Thesis by

Clement Joseph Savant Jr.

In Partial Fulfillment of the Requirements

for the Degree of

Doctor of Philosophy

California Institute of Technology

Pasadena, California

1953

Preface

The author's interest was first aroused in the subject of nonlinear mechanics while taking the graduate course entitled Engineering Mathematical Physics (EE 226) at the California Institute of Technology. Subsequent courses (AM 257, AM 150, and AM 200) intensified this interest in the nonlinear field. During these courses, the available material was studied (Cf. Refs. 1, 2, and 3) and the various methods of solution (analytical, topological, and computer) were investigated.

At the same time, the author was also engaged in the direction of the servomechanism laboratory, where numerous nonlinear systems were encountered. The existence of nonlinear feedback control systems and the difficulty of their solution led the author to the conclusion that an improved analog computing method should be found so that the nonlinearities, dodged by most engineers, could be handled. It was further reasoned that if a control system had an unavoidable forward-loop nonlinearity, then an appropriate nonlinear feedback system might produce a better response than linear feedback.

A study of current arbitrary function generators was discouraging because of the inflexibility of these devices when operating as an arbitrary function of a dependent variable.

About this time, the author found that two other graduate students, R.C. Howard and R.S. Neiswander, had similar interests in nonlinear problems. Together the three men

conceived of a new arbitrary function generator which used the logarithm function as its principle. The basic unit, the log-taking element, was developed by the three. Being convinced that the computer was feasible, R.C. Howard and the author of this thesis went on and developed the greater part of the computer: inverse-log-taking element, input polarity inverter, output polarity inverter, linear and exponential sweep generators, power supplies, etc.

Because of the magnitude of the project the efforts of the three men were necessarily pooled in the development of the log-taking element. This work is summarized in a joint article pending publication in the magazine Electronics. The remaining portion of the work was performed cooperatively by R.C. Howard and C.J. Savant. However, since the work was divided, these two men wrote their theses separately, each placing emphasis on the particular projects upon which he did most of the work. For sake of completeness, however, the entire computer is described in both theses.

The author wishes to express his appreciation to Dr. W.H. Pickering, who was his research adviser. Appreciation is also expressed to the members of the analysis laboratory for their technical assistance and to Dr. G. Housner and Dr. D. Hudson for their interest in the project.

Abstract

This thesis describes the details of an electronic computer capable of generating arbitrary functions of one or more dependent variables. The design of the essential equipment is discussed, and operating instructions as well as complete circuit diagrams are included for easy reference of future researchers.

The computer is used to generate arbitrary functions of an independent variable, and a wide range of functions is shown. Various classical nonlinear problems including Duffing's equation and Van der Pol's equation are solved on the computer and compared with known theory. A discussion, augmented by oscillograms, is presented on nonlinear damping. The computer then is used to improve the response of two feedback control systems. Both systems, which were taken from actual devices met in practice, have inherent nonlinearities. With the aid of the electronic computer the response of these systems is improved. In the solution of the servo system, an interesting nonlinear phenomenon was discovered which is discussed in detail.

Table of Contents

I. INTRODUCTION

The engineer need not look far in his work to find a nonlinear problem. The mechanical engineer knows that springs and dashpots are linear in only small regions near the origin. Familar stress-strain diagrams, gas-expansion laws, and even the simple pendulum cannot be described in all regions by linear equations. The electrical engineer is familiar with the saturation of iron-core inductors and electrical machinery using iron magnetic circuits. Nonlinear vacuum tube characteristics and curved torque-speed curves of servo motors are further examples. These are just a few of the common relationships which engineers linearize in order to obtain a simple solution, i.e., based on classical linear theory. Practically all of the problems in nature are nonlinear, and the linearizations commonly practiced are only approximations. Notice that such linearizations are most valuable and quite sufficient for many purposes. There are, however, cases in which the linear treatment is inadequate. This statement is especially true in nonlinear systems where essentially new phenomena occur which cannot in principle exist in linear systems. In nonlinear vibrations the occurrence of subharmonic forced oscillations is an example of one strictly nonlinear phenomenon. Self-excited stable oscillations and jump phenomena of nonlinear resonance are further examples.

Mathematicians have attacked the second-order nonlinear differential equation with iteration and perturbation techniques. Although some results have been obtained (Cf.

Ref. 2), the problem soon becomes unwieldy even for small nonlinearities, and hence these methods are not satisfactory for engineers. Since the convergence of these methods often depends upon the nonlinearity's being small, the methods are not even applicable when the nonlinearity is large. Topological methods (Cf. Ref. 1) have aided in the solution of second-order systems, but little has been done with higher-order equations by graphical techniques.

One might ask why the solution of nonlinear differential equations of second degree or greater requires such special care. Basically the answer is, of course, that the principle of superposition is invalid. Hence if y_1 is a solution to the homogeneous differential equation and y_2 is a solution to the steady-state equation, then $y_1 + y_2$ is a solution only if the equation is linear. The division of the solution into steady-state and transient parts for classical solution, the operational method of solution, Fourier series or integral, and the method of Duhamel's integral are all invalid because these methods require summation or integration, operations which cannot be performed unless the principle of superposition holds.

In the study of feedback control systems, much of the equipment exhibits inherent nonlinear operation except for small regions near the null. Great strides have been made recently in improving accuracy and speed of response of servomechanisms. Such improvement has resulted from the development of highly refined techniques of linear analysis.

It is becoming more difficult to make further improvement in the transient performance of control systems designed upon the basis of linear analysis without (1) reducing the time delays or energy storages of the system or (2) improving the acceleration characteristics of existing servo motors. Significant improvements in controllers and servo motors are now being made less frequently and with less ease than in the past.

If nonlinear elements are used in servomechanisms, system performance can sometimes be improved without increased improvements in the characteristics of existing controllers and servo motors. Unfortunately the use of nonlinear elements in a closed-loop system has been avoided because of the extreme difficulty encountered in handling and solving the nonlinear differential equations.

Both analog and digital computers have been employed in the solution of nonlinear equations. In many of these solutions, considerable time is expended in setting the nonlinearity into the computer. For example, in digital equipment a change of the form of the nonlinearity would involve considerable labor since elaborate programming is required for each problem. The multiple linear segment type of function generator, often used in analog equipment, requires careful setting of a number of potentiometers to change the nonlinear function. Also with the photoformer a new card must be cut for each new function; hence analog function generators are often not versatile enough. Although

the accuracy of the solution is fairly high, especially with the digital machine, existing techniques do not lend themselves to easy change of the nonlinear function.

The need for a versatile arbitrary function generator of a dependent variable is strongly felt in feedback control system design. For example, consider a control system, the response of which requires improvement. It may be possible to better the performance if appropriate nonlinear functions be added, either in the forward loop or in the feedback path. In determining the nature of this nonlinear function, one is not so concerned with a high degree of accuracy as in the case of modifying one function into another in an attempt to discover an optimum. The nature of the design problem then demands a highly versatile computer with only a reasonable accuracy (perhaps 5%) required.

The arbitrary function generator discussed in this thesis satisfies the needs of the designer in that the form of the nonlinearity can be changed by the setting of two knobs.

The present generator boasts another advantage. In many problems it may be necessary to generate products of arbitrary functions of two or more variables. The computer described in this thesis permits products of the general form

$$[f(x)]^{\alpha}\ [g(y)]^{\beta}\ [h(z)]^{\gamma}$$

where f(x), g(y), and h(z) may be the dependent variables of

a given problem or may be any independent variables. The exponents α, β, and γ may be either positive or negative.

The principle of operation of the multiplier is based on the logarithmic function, which has the following property:

$$\alpha \log_a f(x) + \beta \log_a g(y) + \gamma \log_a h(z) = \log_a \left\{ [f(x)]^{\alpha} [g(y)]^{\beta} [h(z)]^{\gamma} \right\} \quad (1)$$

where "a" is any number greater than unity.

Since summation is an easy operation with electronic circuits, the logarithms of three voltages can be added simply, and the inverse logarithm of the sum results in the product. Hence the difficult operation of analog multiplication (or division) is performed easily by adding voltages. Thus the first and most important work centered about the development of two electronic circuits which have the required logarithmic and inverse logarithmic characteristics. This development resulted in two basic units: the log-taking element (LTE) the output of which is the negative logarithm of the input voltage, and the inverse-log-taking element (ILTE) the output voltage of which is the inverse logarithm of the input. These two units plus necessary polarity inverting equipment comprise the arbitrary function generator of a dependent variable (subsequently called AFDEV). Besides the basic computer equipment, a number of auxiliary pieces such as power supplies, dc amplifiers, linear sweep generator, exponential generator, voltage test units, tube aging rack,

and oscilloscope calibrator were developed.

Section II of the thesis gives a description of the four basic computer parts: the LTE, the ILTE, the input polarity inverter, and the output polarity inverter. The remaining equipment is discussed in the Appendices. Section III describes the use of the computer as an arbitrary function generator of an independent variable. Section IV gives the solution to various classical nonlinear differential equations. Section V discusses several forms of nonlinear damping. Section VI presents a nonlinear pneumatic servomechanism in which the response has been improved. Section VII describes a closed-loop position servomechanism which is improved with the aid of nonlinear rate feedback. Section VIII presents the conclusions of this work.

II. COMPUTER COMPONENTS

The first part of this section describes the development of the log-taking element (LTE) in a joint paper* pending publication in the magazine Electronics. The article is included here approximately in the form which was submitted for publication. As mentioned in the introduction, all components except the four basic elements are discussed in the Appendices. The fundamental elements are described in this section.

A Practical Linear-to-Logarithm Converter

In almost every electronic field, the need occasionally arises for linear-to-logarithmic conversion of data. Probably the most popular use has been in one-dimensional instrument displays and recorders, in which, for advantageous scale compression, linear inputs are converted to logarithmic values (such as decibels). This use can be extended to two-dimensional, semi- and log-log oscilloscope presentations. In electric-analog computing, the logarithmic converter in conjunction with an antilogarithmic converter conveniently performs multiplication and division by addition and subtraction of voltages and as readily produces integer and noninteger exponent functions. This last application, analog computing, initiated a recent investigation of linear-to-logarithmic converters.

At first, a survey of proposed converters, fortified by laboratory tests, was made, and the triode circuit was

*Prepared by R.C. Howard, C.J. Savant Jr., and R.S. Weiswander.

selected as having the greatest promise. In the process of optimizing this circuit, a new logarithmic conversion region of tube operation was found which had unusually high gain and good stability. Further modifications were made to provide reproducibility of converter characteristics. After the resultant converters were set to a predetermined standard, they were entirely interchangeable.

Evaluation Criteria

A linear-to-logarithmic converter is defined herein as an electronic device which, when presented with an input x (x is some number scaled into dc voltage), produces an output $y = \log_a x$ (y is also a number scaled into voltage, and a is the base of the logarithm). Over 20 years ago a vacuum-tube triode circuit* was developed which would accomplish this purpose (Cf. Ref. 4). Since then many converters have appeared: devices employing germanium diodes, selenium rectifiers, exponential time decays, vacuum-tube diodes, triodes, tetrodes, and pentodes (Cf., for example, Refs. 5 through 9). Analog-computer, arbitrary-function generators, such as photoelectric cathode-ray-tube devices, can also be used as logarithmic converters.

To evaluate this diverse group, some means of comparison had to be established; here the selected criteria were the requirements dictated directly by the application of the converter:

1. High-level, moderate-range, voltage input.

---

*In actuality, the tube was a UX-222 tetrode, triode-connected.

An input range of 1 volt minimum and 300 volts maximum was chosen, keeping the level as high as practicable in order to minimize effects of drift and noise.

2. High conversion gain.

Changes in input should produce changes as large as possible in the logarithmic output. This high gain means that a low logarithm base is desired. Note that as the base a approaches unity, the conversion gain approaches infinity. With low gain, very small changes in output become important, greatly increasing the difficulty of design with regard to drift and noise.

3. Stable and accurate conversion.

The stability and accuracy of conversion should be such that the total error (referred to the input) anywhere in the operating region is of the order of or less than the minimum input.

4. Reproducible characteristics.

In all applications, the characteristics such as logarithm base and offset voltage must be known. In many applications including the present analog computer, it is necessary to adjust all converters to duplicate some predetermined set of characteristics.

5. Practicable design.

The converter should be simple and should have both

input and output work to ground. Desirably, the input impedance should be high, and the output impedance low. The converter should operate over a frequency range of 0 to 1000 cyc/sec.

Evaluation of Logarithmic Converters

After the basis for comparison had been established, several types of logarithmic converters known to the writers were considered. The simplest types, devices using nonlinear passive elements, were investigated first.

1. Selenium rectifiers and germanium diodes.

The voltage across a selenium rectifier is the logarithm of the current for a very wide range of "pass" currents. For voltage-to-voltage conversion, a large series resistance is added, and the circuit becomes that of Figure 1. The response of a typical six-plate rectifier is shown in Figure 2.

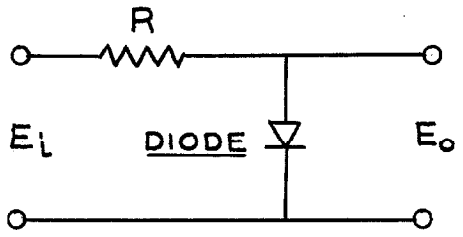

Figure 1. Selenium Rectifier Circuit

Despite the appeal of simplicity and excellent range of logarithmic characteristics, the rectifier was found to have relatively low gain and large drift. Defining

output volts as output number, i.e., 1:1 scaling, the logarithm base for a six-plate, 75-ma rectifier was about 10, and for a one-plate, 75-ma rectifier, about 10^8. Thus, for example, in the case of the one-plate rectifier, a change of 100:1 input produced only $\log_{10^8}(100) = 1/4$ volt in the output. In all rectifiers tested, large output drifts occurred which were functions not only of temperature but also of aging and undetermined factors.

The germanium diodes, when used in the circuit of Figure 1, exhibited characteristics similar to those of the selenium rectifiers but with a more limited range and better stability.

2. Vacuum-tube diodes.

   Vacuum-tube diodes also demonstrated logarithmic conversion in their very low current regions when tested as nonlinear elements in the circuit of Figure 1. Conversion yielded unusually low output voltage levels and logarithm bases comparable to those of the passive elements.

3. Vacuum-tube triodes.

   The most common triode circuit utilizes the fact that a logarithmic relation exists between grid current and plate current in some triodes operating at low plate voltages (Cf. Refs. 4, 5, and 9). Again if a large grid resistor is added for voltage-to-voltage conversion, the basic circuit becomes

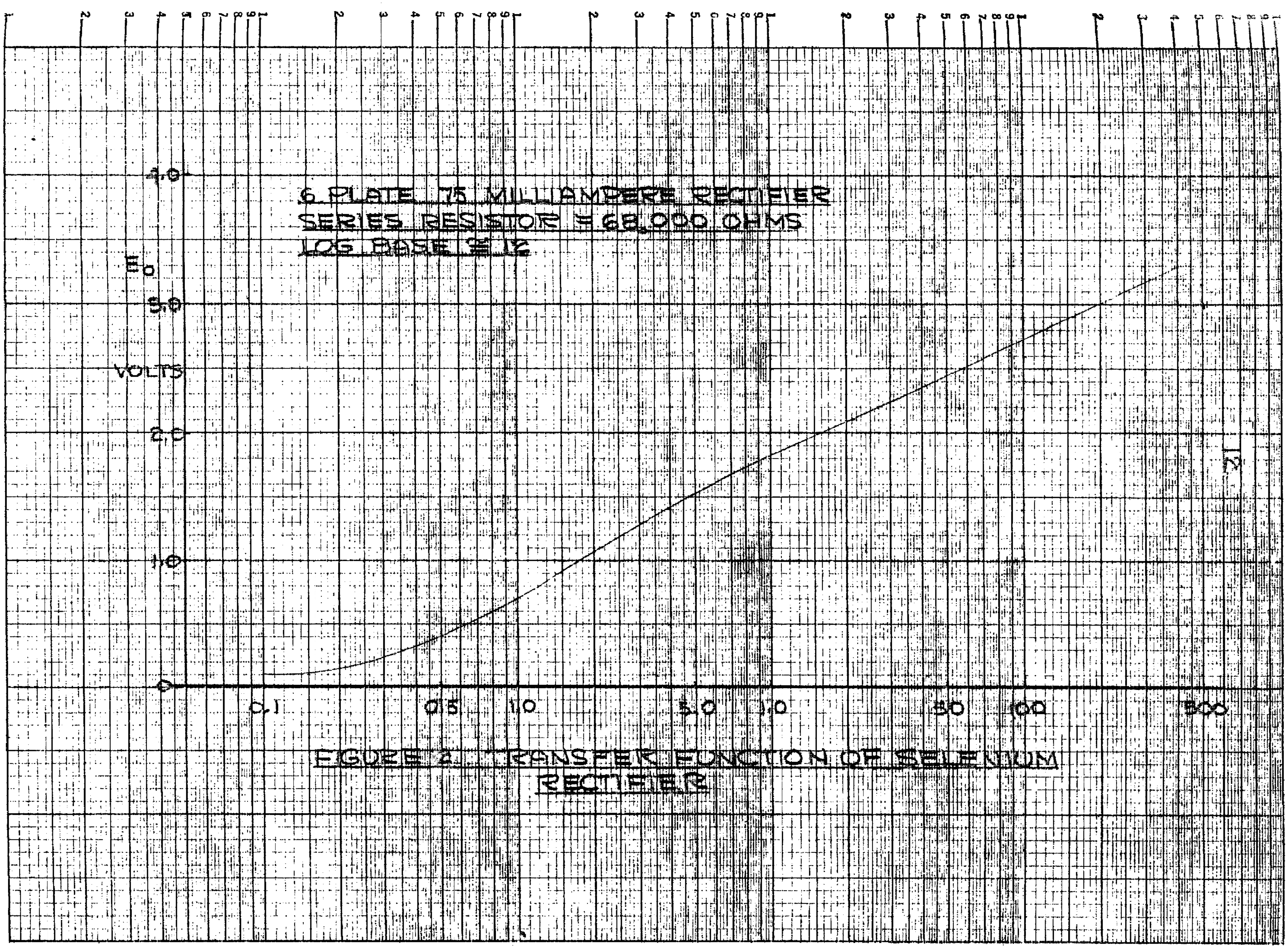

FIGURE 2. TRANSFER FUNCTION OF SELENIUM RECTIFIER

that of Figure 3.

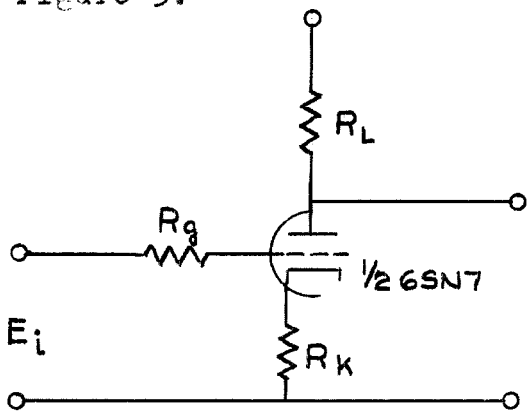

Figure 3. Basic LTE Circuit

Resistors R_L and R_K and the plate voltage are adjusted to produce an output $E_o = - \log_a(E_i) + E_{offset}$. With this basic circuit, Albert N. Nadel* succeeded in obtaining a remarkably accurate conversion with a logarithm base of about 3 over a range of 1 to 300 volts.

4. Vacuum-tube tetrodes and pentodes.

In general, converters using tetrodes and pentodes rely upon a variable mu to produce plate currents as logarithms of grid voltages. The range of a single-tube circuit is small, and the base of the logarithm is several times higher than that of the triodes just discussed.

Modified Triode Converter

Since triode converters appeared most promising on all counts, it was concluded that development work on this item should be furthered. First, an attempt was made to determine

*Tests at North American Aerophysics Laboratory, 1950.

the optimum performance of the basic triode circuit; second, modifications were made which would provide for reproducibility.

In the optimization process, an exceedingly high-gain conversion characteristic was discovered in the high-plate-voltage region of a few triodes. The response curve is presented in Figure 4. The input-to-cathode resistor was added to improve the low-input-voltage response; the resistor does not affect higher-level conversion. Tubes do not have to be preselected to maintain reasonably similar characteristics, and good stability (75 mv/hr) was attained by 500-hour tube aging.

The output of the converter is of the form $E_o = - \log_a E_i + E_{offset}$. Both E_{offset}, which arises from the large-positive-plate voltage, and the logarithm base, a, vary for different tubes. For reproducibility, E_{offset} can be canceled in each converter, and the logarithm base, a, can be made to coincide with some standard. The removal of E_{offset} was directly accomplished by adding a cathode follower to the triode and subtracting out E_{offset} at the follower's grid. This addition introduced the further advantage of isolating the triode converter from the actual output. Adjustment of the logarithm base requires a simple adjustment of gain after the logarithmic conversion; and this restricted-range gain control is inserted at the cathode follower's output. The final circuit for linear-to-logarithmic conversion is shown in Figure 5, and several plug-in, interchangeable converters are pictured

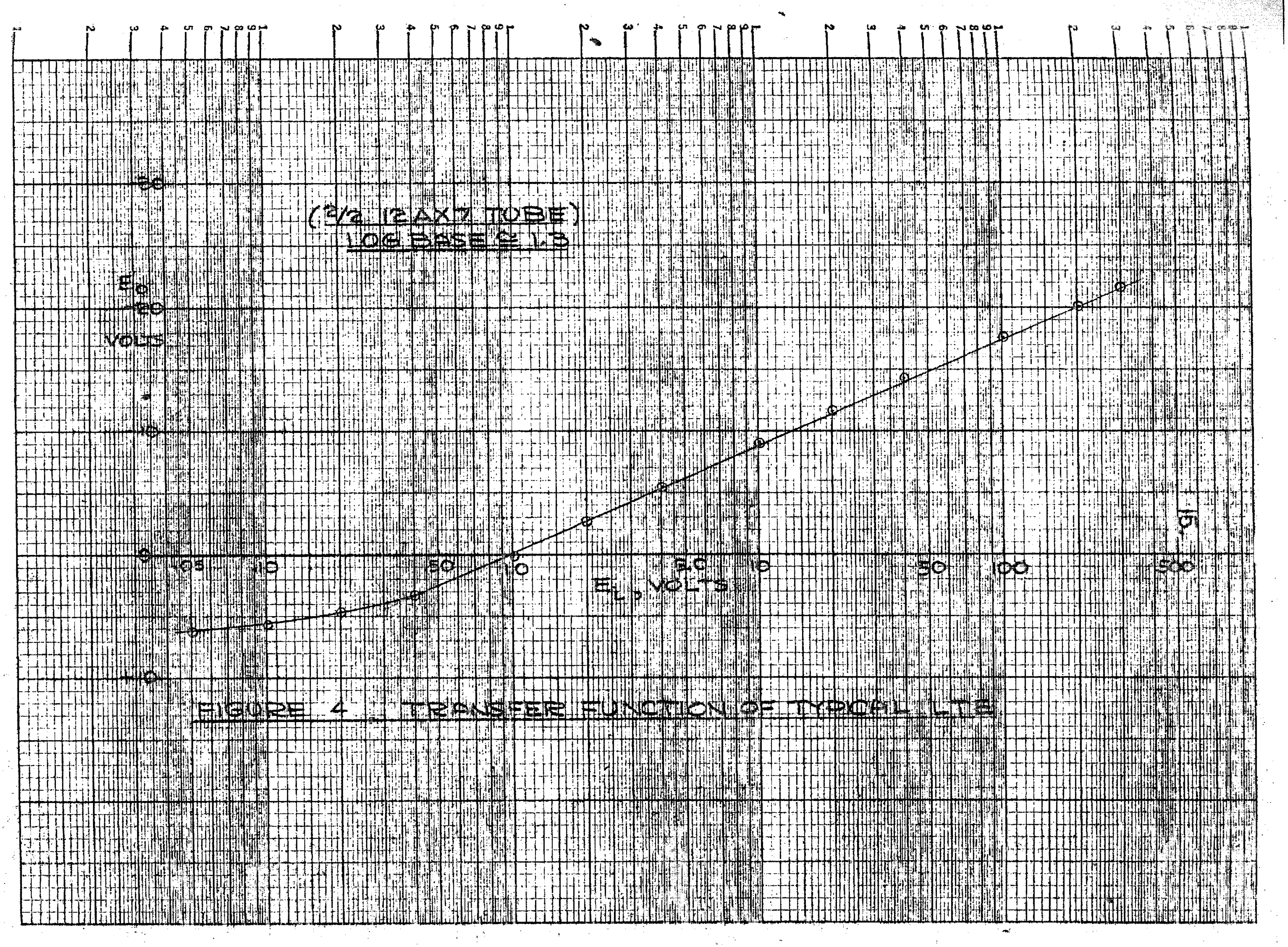

FIGURE 4 TRANSFER FUNCTION OF TYPICAL LTE

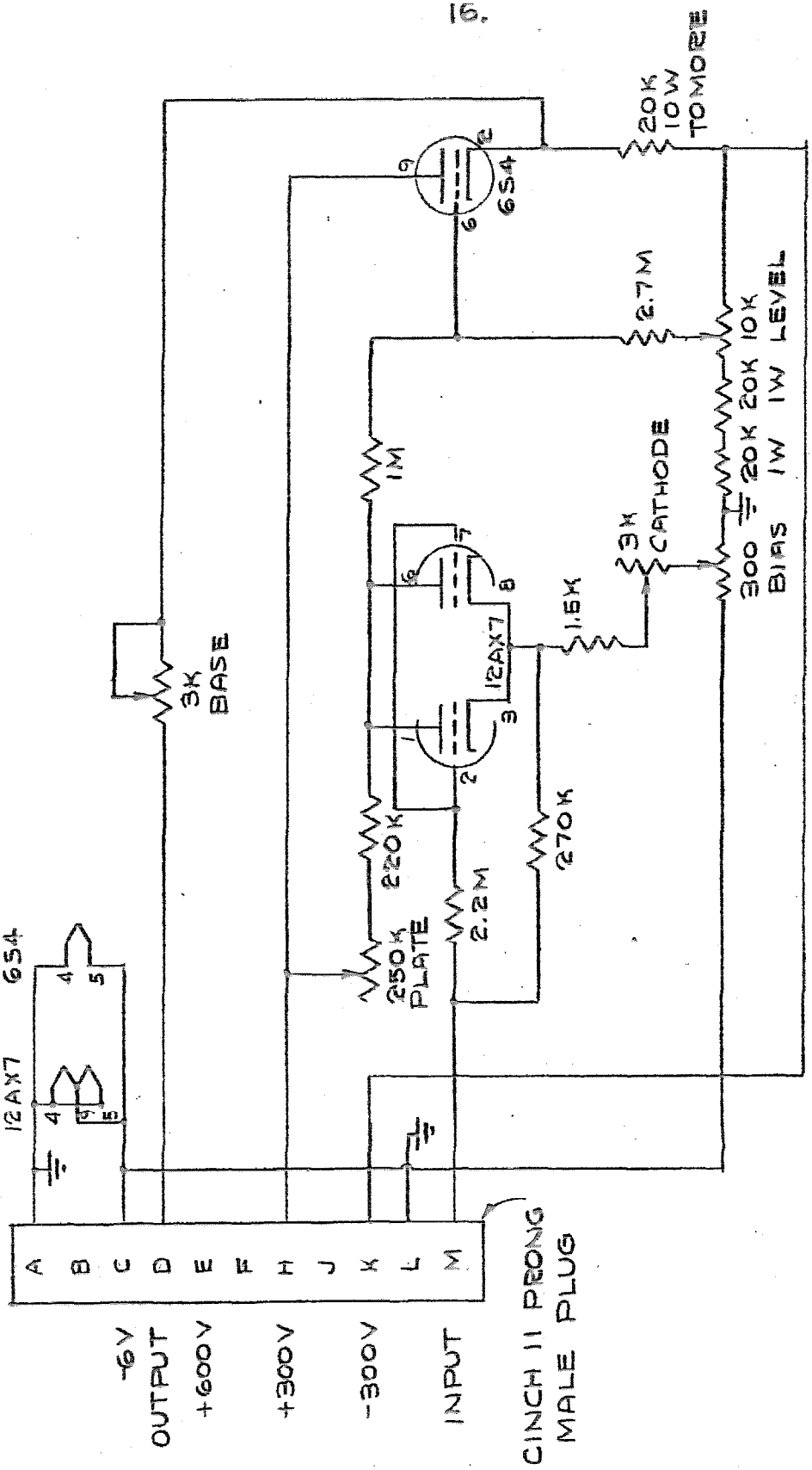

LOGARITHM TAKING ELEMENT

FIGURE 5

in Figure 6.

Although a very definite application was in mind when this converter was developed, i.e., a computer requiring a low logarithm base and zero dc level, this same circuit, with slight modifications in parameter values, has many possibilities. In order that these possibilities be best demonstrated, Table I was prepared to show the variety of logarithm base and output voltages available with the following tubes: the 12AT7, 12AU7, 12AX7, and the 12AY7.

TABLE I

Case	Tube	E_{bb}	E_f	R_L	R_K	R_f	R_g	E_k	Base	E_o
1	1/2 12AY7	300	5.8	450K	12.4K	470K	2.5M	-3.0	1.30	60
2	1/2 12AY7	300	5.8	320	14.0	470	2.5	-8.5	1.38	33
3	1/2 12AU7	280	5.8	100	14.0	5,000	2.5	-13.6	1.78	25
4	1/2 12AU7	280	5.8	27	150	5,000	2.5	-3.4	1.78	72
5	1/2 12AT7	290	5.8	36	5.6	1,000	2.5	-24	1.18	113
6	1/2 12AX7	290	5.8	18	5.3	150	2.5	-19	1.14	231
7	1/2 12AX7	290	5.8	160	6.3	400	2.5	-5.9	1.13	110
8	2/2 12AX7	300	6.0	350	3.0	270	2.2	-3.0	1.20	30

E_{bb} = plate supply voltage.

E_f = filament supply voltage.

R_L = load resistor.

R_K = cathode resistor in plate circuit.

R_f = feed-through to cathode resistor.

R_g = grid input resistor.

E_k = cathode return voltage.

E_o = output voltage.

Base refers to the logarithm base.

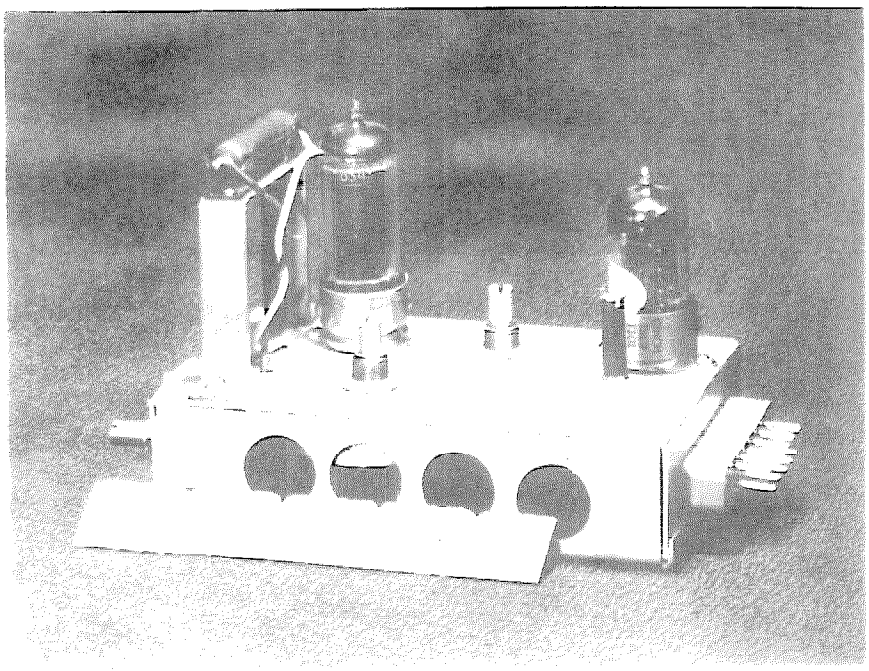

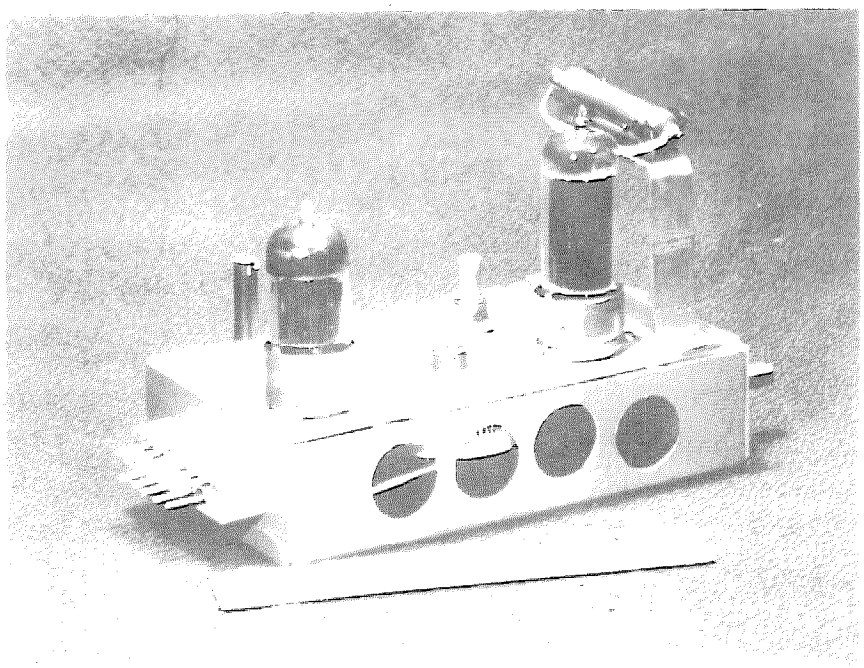

Figure 6. Two Views of Log Taking Element (LTE)

In the practical application of this logarithmic converter, an extremely useful, time-saving auxiliary device should be mentioned, the exponential test generator (Cf. Figure 7 for a schematic diagram). The generator produces periodic, exponential, time-decay voltage discharges, 300 volts initial to a fraction of a volt final (Cf. Figure 8). When this cycled test voltage is applied to a properly adjusted logarithmic converter, the converter output is a linear function of time (Cf. Figure 9) and can readily be checked by an oscilloscope.

The setup procedure for the converter is thus quite simple: (a) With an exponential test-voltage input, the bias voltage and the converter's cathode and plate resistors are adjusted until a linear output is displayed on the oscilloscope screen. (b) The slope of the linear output is adjusted by the logarithm base adjust to some predetermined value. (c) E_{offset} is subtracted out by inserting a known dc input voltage in the converter, and adjusting the E_{offset} adjust to obtain a predetermined output voltage. (d) When a precise converter characteristic is required, the procedure is repeated using accurately measured static input and output voltages at several points between 1 and 300 volts and checking conversion with a semilogarithmic plot.

Further LTE Details

As outlined in the magazine article, the heart of the computer is a three-terminal converter which has the property that the output voltage is the negative logarithm of the input.

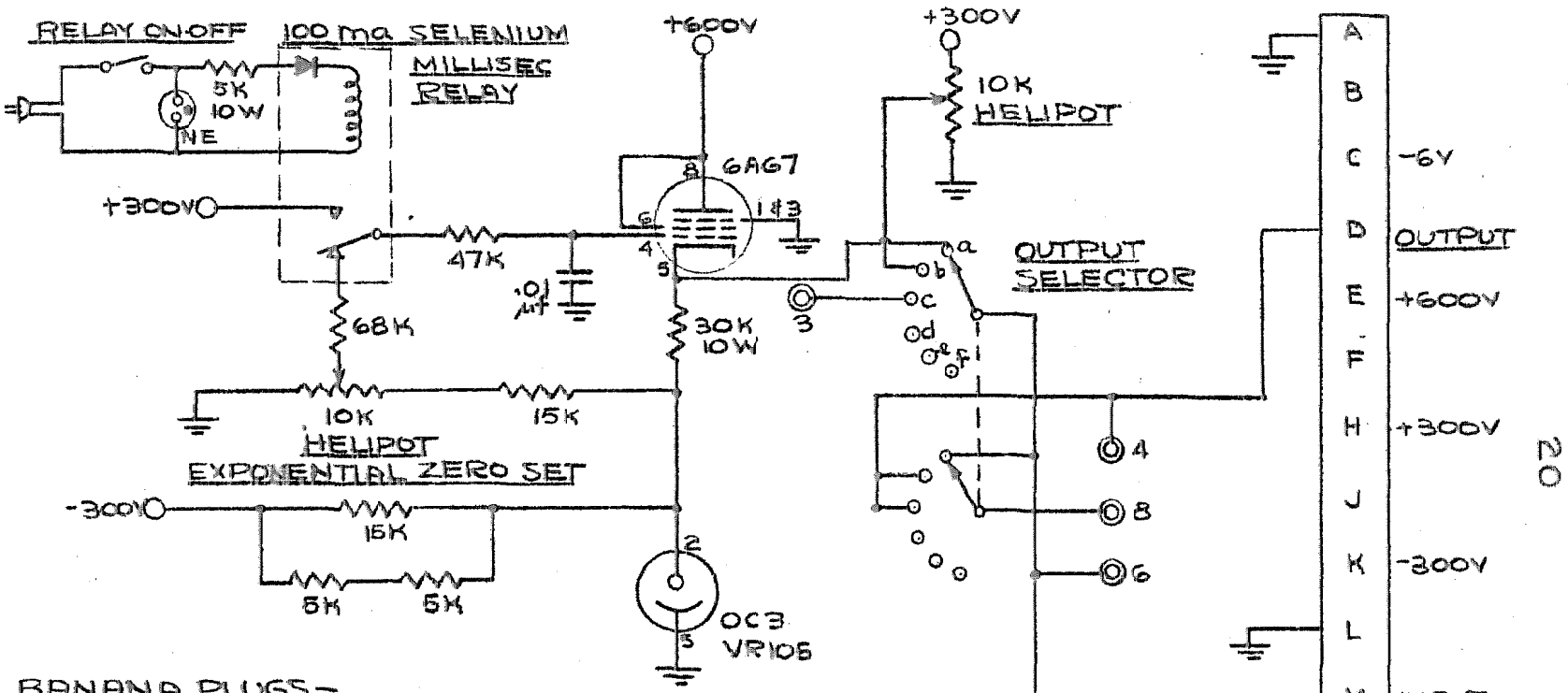

BANANA PLUGS –

3 3,9,30,90,180,300 V. INPUT
4 LTE OUTPUT
6 LTE INPUT
8 VOLTMETER
9 CHASSIS GND.
10 CHASSIS GND.

SWITCH POSITIONS –

a. EXPONENTIAL
b. 0-300 V. CONTINUOUS
c. 3,9,30,90,180,300 VOLTS.

L.T.E. TEST & SET UP UNIT

FIGURE 7

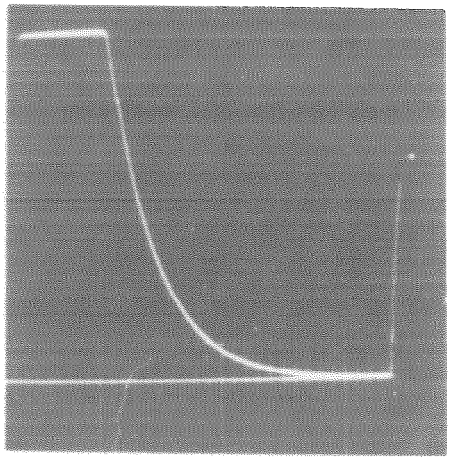

Figure 8. Output of Exponential Generator

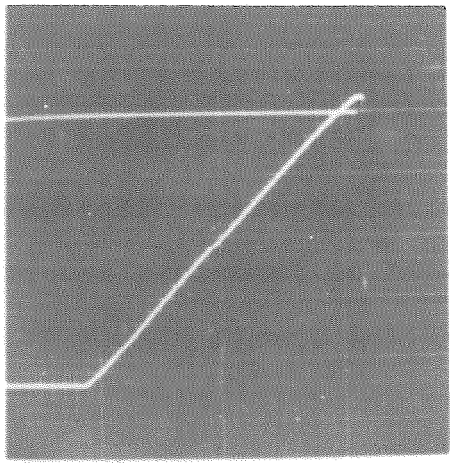

Figure 9. Output of LTE with Exponential Applied

This converter is shown in the block diagram of Figure 10 where the abbreviation LTE is used which throughout this report represents log-taking element. Although the finished version of the LTE is described in the preceding joint article, a more complete description of the LTE is included for the benefit of the reader who desires to do further work with this converter.

When the vacuum-tube triode was first considered, the circuit shown in Figure 11 was set up to test the following vacuum tubes: 6SN7, 6SL7, 12AT7, 12AU7, 12AY7, and 12AX7. All of these tubes showed linearity over a limited range and good drift stability referred to the output. Since miniature tubes were desired in the final circuit, the investigation was narrowed to miniature twin triodes. Figure 12 shows a typical curve for the response of a 12AY7 with the final circuit parameter values of Figure 5 given on the curve. These curves were taken statically by applying constant voltages and measuring the output with a null-type voltmeter. In setting up the logarithmic characteristics, one should note that the oscilloscope presentation has limited accuracy and is intended primarily as a first, easily adjustable approximation. The static test, although obviously slower and more cumbersome, offers the advantage that the response can be determined to a higher degree of accuracy.

The LTE of Figure 11 was limited in its usable range. Since the output voltage began to drop at the low voltage end, it was reasoned that the curve could be corrected by

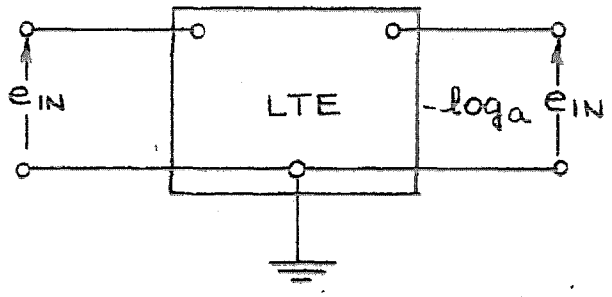

FIG.10 BLOCK DIAGRAM OF LOG TAKING ELEMENT

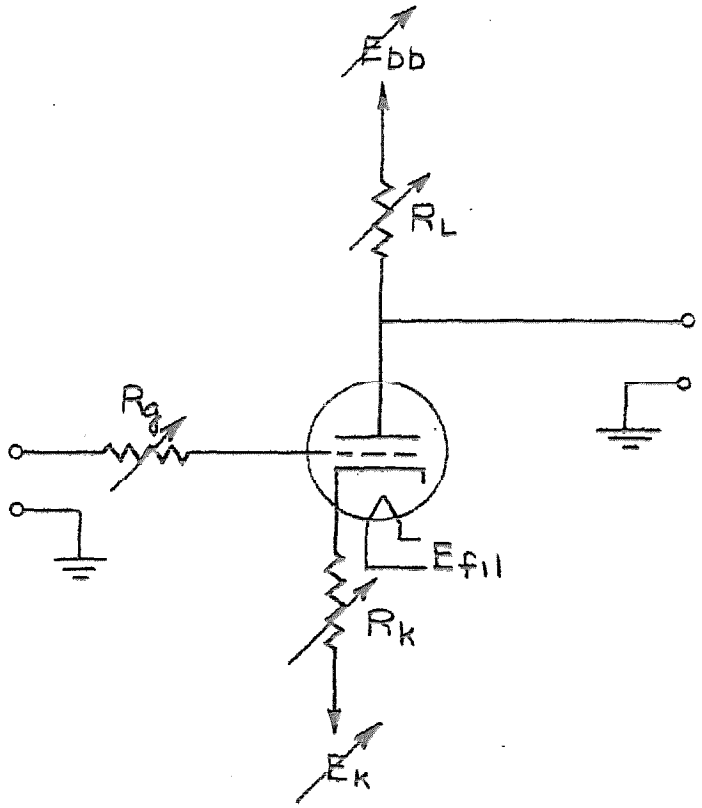

FIG. 11 FIRST TRIODE LTE CIRCUIT

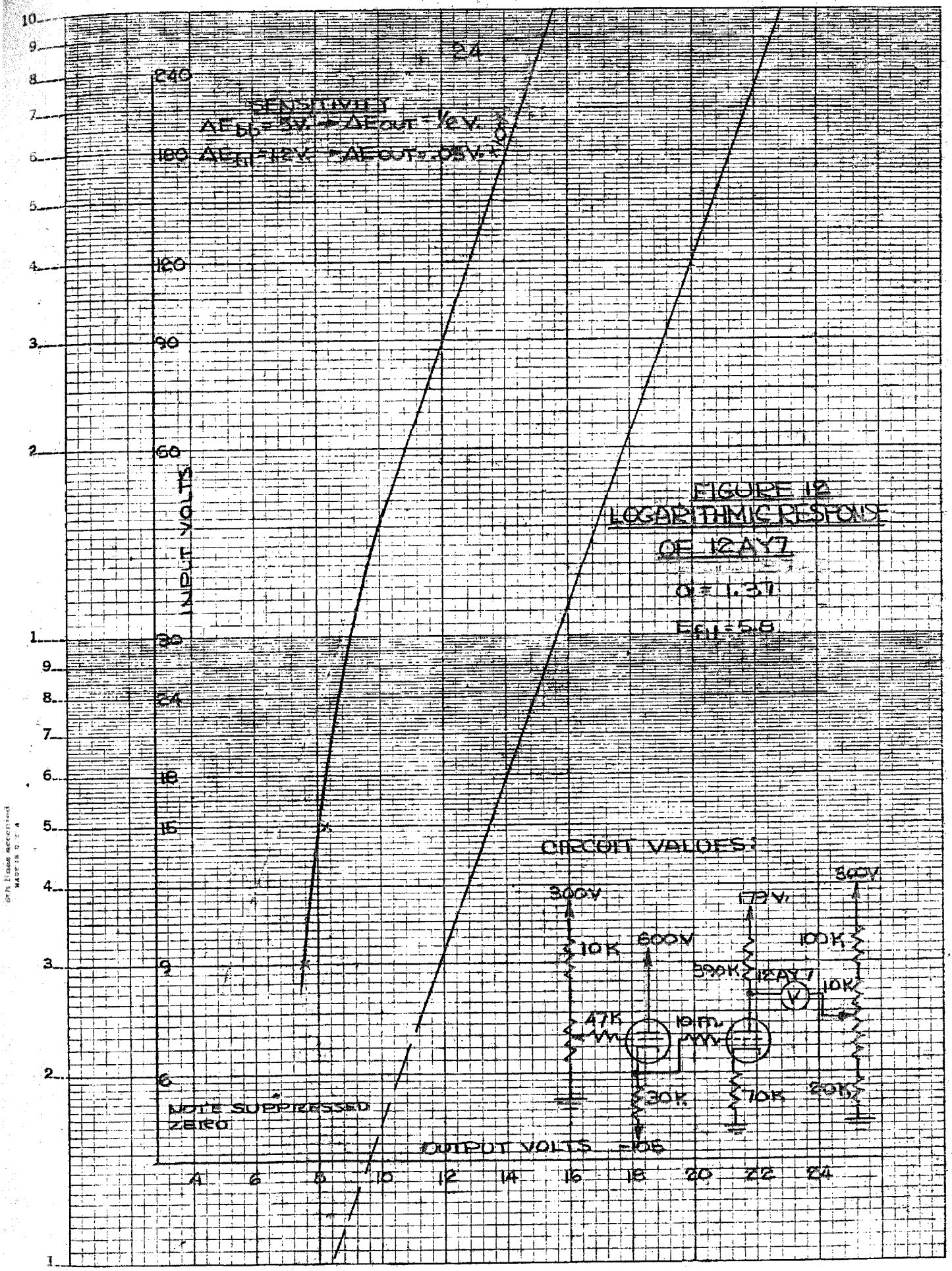

FIGURE 12
LOGARITHMIC RESPONSE
OF 12AY7

$\alpha = 1.37$

$E_{c11} = 5.8$

introducing the input signal on the cathode as well as on the grid. This thought proved to be successful. With an exponential decay as input, the LTE parameter values were appropriately varied; and with a 12AX7 twin triode, the LTE was found to be linear from 0.3 to 300 volts. Typical curves for several 12AX7 tubes from different manufacturers are included in Figure 13. The characteristics are quite linear; however, there is some variation in slope between the tubes, and there exists a slight variation from tube to tube of one manufacturer. The variation difficulty was obviated by means of an attenuating potentiometer on each LTE.

The LTE described thus far was quite satisfactory except for the fact that the output is not $-\log_a E_{in}$ but is

$$-\log_a E_{in} + K \qquad (2)$$

where K is a constant voltage. Although it is not difficult to cancel this constant voltage at the computer output, a serious difficulty arises when the input voltage is to be raised to a power m. Consider the schematic diagram of Figure 14 where the quantity E_{in}^m is desired. The computer is to be used primarily for nonlinear servomechanism synthesis. In this case the pattern on an oscilloscope presentation will be observed while the power m of the nonlinearity is changed. Unless the constant is zero (K = 0), then as m is varied, the voltage inserted to cancel mK must be varied. Since this double adjustment would naturally lessen computer flexibility, further time was invested to provide a zeroing adjustment

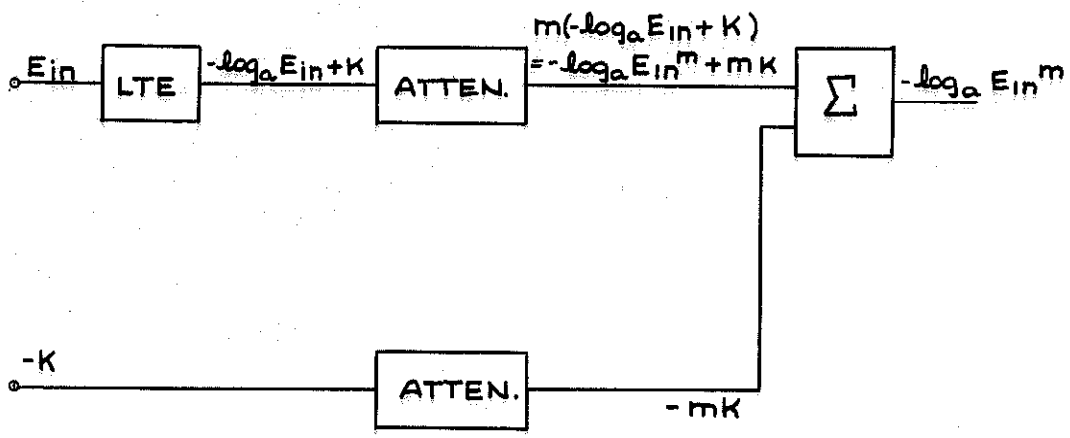

Figure 14. Block Diagram Showing Method of Removing E_{offset}

such that with a 1-volt input, the output can be adjusted to 0 volts. Hence variation of exponent can be obtained with one knob adjustment. This work led finally to the circuit of Figure 5, which allows three adjustments:

1. A dc level adjust.
2. A logarithm-base adjust.
3. A linearity adjust (accomplished by the combined variations of plate, cathode, and bias potentiometers).

The effect of varying these adjustments can most readily be seen from Figures 15 through 20, where representative oscillograms are exhibited. Explanations of the adjustments are given in Table II.

The finally accepted LTE is shown in the photographs of Figure 6. The circuit diagram is included as Figure 5, and the response of the LTE with calibrated dc input voltages is shown in Figure 4.

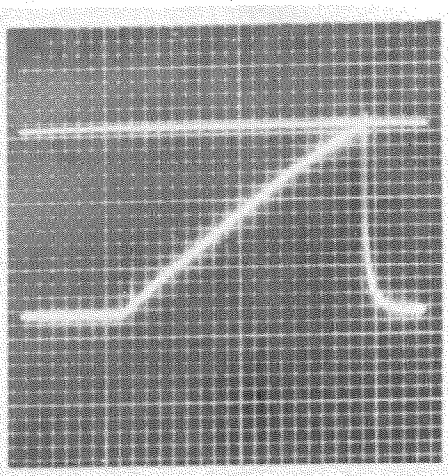

Figure 15

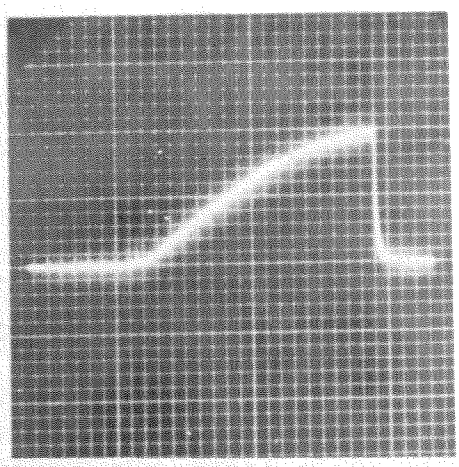

Figure 16

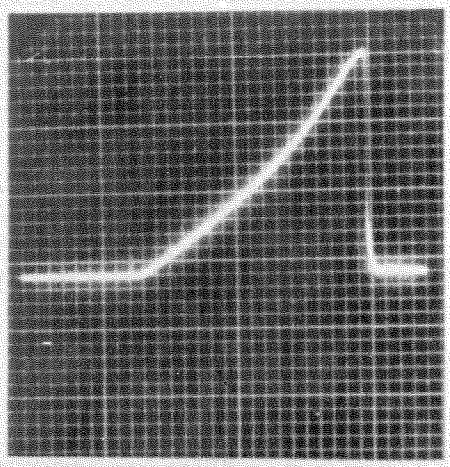

Figure 17

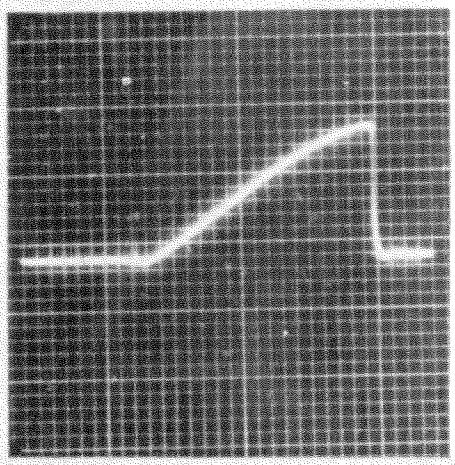

Figure 18

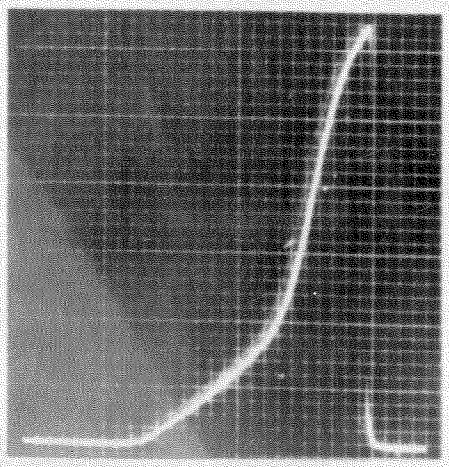

Figure 19

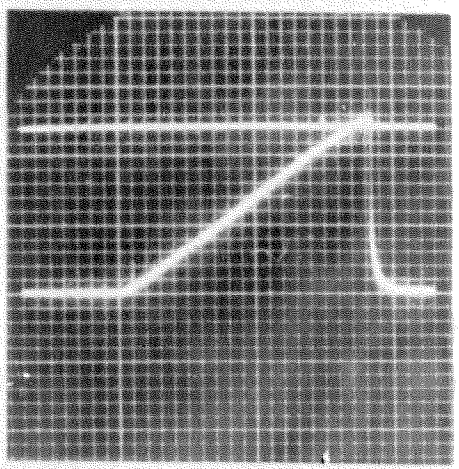

Figure 20

Table II

Oscillogram Number	Explanation
Fig. 15	LTE without feed-through resistor to cathode
Fig. 16	cathode return voltage too large
Fig. 17	cathode return voltage too small
Fig. 18	plate voltage too small
Fig. 19	plate voltage too large
Fig. 20	properly adjusted LTE

The successful operation of the LTE's depends to a large extent on having regulated power supplies and aged tubes. The details of the power supply design are described in Appendix A of this thesis, but the aging problem is discussed here.

In order to discover the effect of time variation of tube parameters, an aging rack, shown schematically on Figure 21, was constructed. This device applies normal voltages to all elements of the vacuum tube. With six new 12AX7 tubes, two each from Sylvania, RCA, and Raytheon, the output voltage was measured for a fixed input voltage with a type K potentiometer. These readings were taken regularly, and although the results are somewhat random, it was concluded that the tubes should be aged about 500 hours before being used in the LTE.

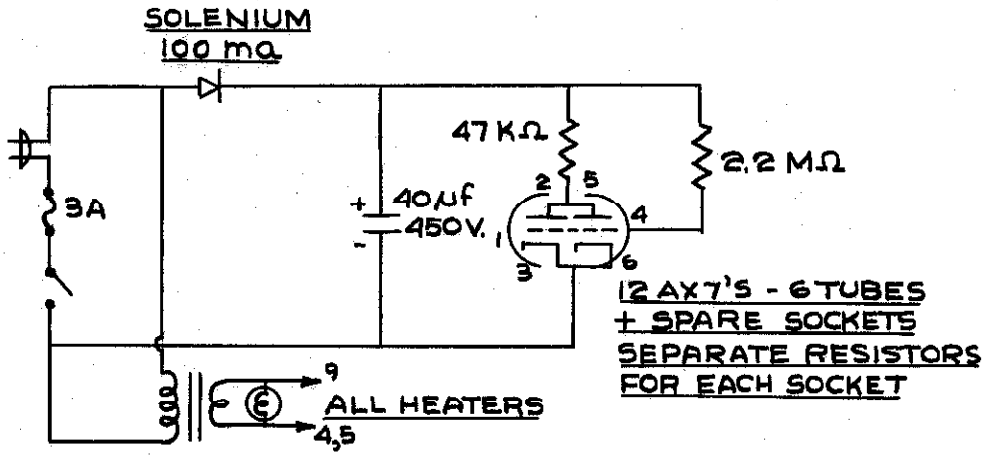

Figure 21. Schematic Diagram of the Aging Rack

Inverse-Log-Taking Element

The underlying concept governing the operation of the inverse-log-taking element, hereafter known as the ILTE, is simple, namely, use of a high-gain amplifier with a LTE in the feedback loop. The operation can best be understood

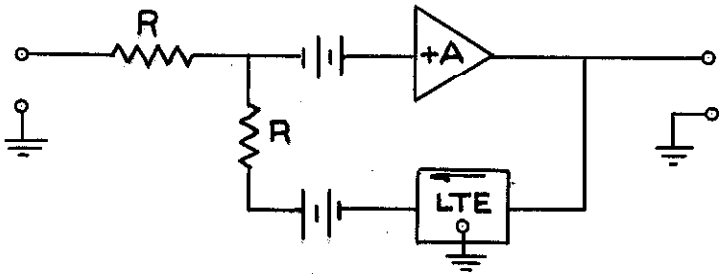

δ = drift voltage introduced in amplifier

Δ = drift voltage introduced in the LTE

Figure 22. Mathematical Treatment of ILTE

from a consideration of Figure 22. With the symbols defined on the Figure, one can readily write the following basic equations of the circuit:

$$\frac{e_f + e_{in}}{2} = \varepsilon \tag{3}$$

$$(\varepsilon + \delta) A = e_o \tag{4}$$

$$-\log_a e_o + \Delta = e_f \tag{5}$$

Combination of Equations (3), (4), and (5) results in the following system equation:

$$e_o = \exp_a (e_{in}) \left[\exp_a (\Delta + 2\delta - \frac{2e_o}{A})\right] \tag{6}$$

This last expression demonstrates that the output of the ILTE is proportional to the product of two factors, the first of which is the desired result, and the second of which is the combined error term. Since the polarity of these errors is unknown, the most pessimistic case (i.e., when δ , Δ , and e_o all have the same sign) is considered. Expanding the second term in a series (Cf. Ref. 10), one obtains the following approximate expression:

$$e_o \approx exp_a(e_{in}) \left\{[1+(\Delta+2\delta)\ln a]\right\}\left\{1+\frac{2}{A} e_o \ln a\right\} \qquad (7)$$

From Equation (7) approximate percent-error expressions resulting from drift and insufficient gain can be obtained as follows:

$$\text{Percent error from drift} \triangleq E_d \approx 100(\Delta+2\delta)\ln a \qquad (8)$$

$$\text{Percent error from lack of gain} \triangleq E_q \approx 100\frac{2}{A} e_o \ln a \qquad (9)$$

With normal values (Δ = 50 mv, δ = 25 mv, a = 1.2, e_o = 300 v, A = 8000) substituted in Equations (8) and (9), the maximum possible errors are

$$E_d = 2.3\% \qquad E_g = 2.1\% \qquad (10)$$

One must realize, however, that with appropriate adjustment of the final unit, E_d can be reduced considerably, and E_g can be eliminated completely.

Although this theory is relatively simple, the system was unstable when a plug-in LTE was used in the feedback path of an analysis laboratory dc amplifier. Crude static multiplications were possible only with the addition of large lumped capacity, which reduced the frequency response

of the ILTE to about 5 cyc/sec. Since the LTE is an attenuator which has a value varying as a function of the amplitude level, the system is stable for large input signals (resulting in large feedback) but unstable for small input signals. Considerable effort was expended in the stabilization of this system, and, as a step in eliminating stray capacitance, the ILTE was built as a single compact unit. A photograph of the completed unit is shown in Figure 23, and a schematic diagram is given in Figure 24. In addition to this consolidation onto one chassis, phase-correcting networks between all stages were found to be necessary. Removal of a Helipot which was formerly included in the output circuit of the LTE was also necessary. Although the Helipot provided easy adjustment of the base of the ILTE, it introduced considerable phase shift which was a function of the knob setting.

The circuit details of the final ILTE can best be understood by a consideration of Figure 24. Three inputs to the ILTE provide summing of three channels. The 10,000-ohm resistor from the summing point to ground reduces the effective gain of the amplifier and assures a base which is insensitive to changes of output impedance of the driving devices. The positive-gain amplifier is of standard design except for two items. The first stage which operates at low screen voltage and large plate resistor has a gain of approximately 1000. The second deviation is the large ratio between the cutoff frequencies of the two amplifier stages. The first coupling circuit cuts off at about 400 cyc/sec, whereas

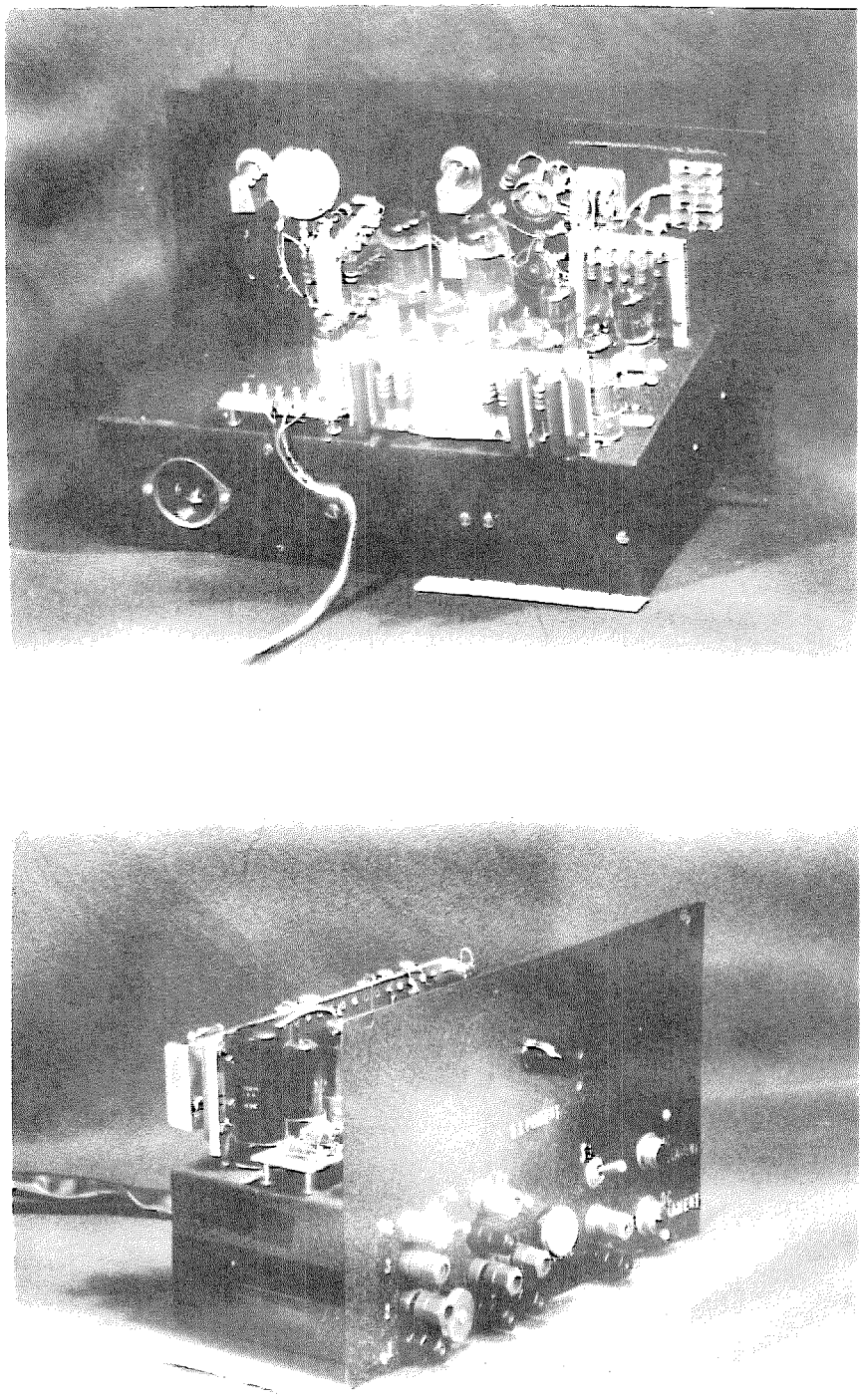

Figure 23. Two Views of Inverse Log Taking Element (ILTE)

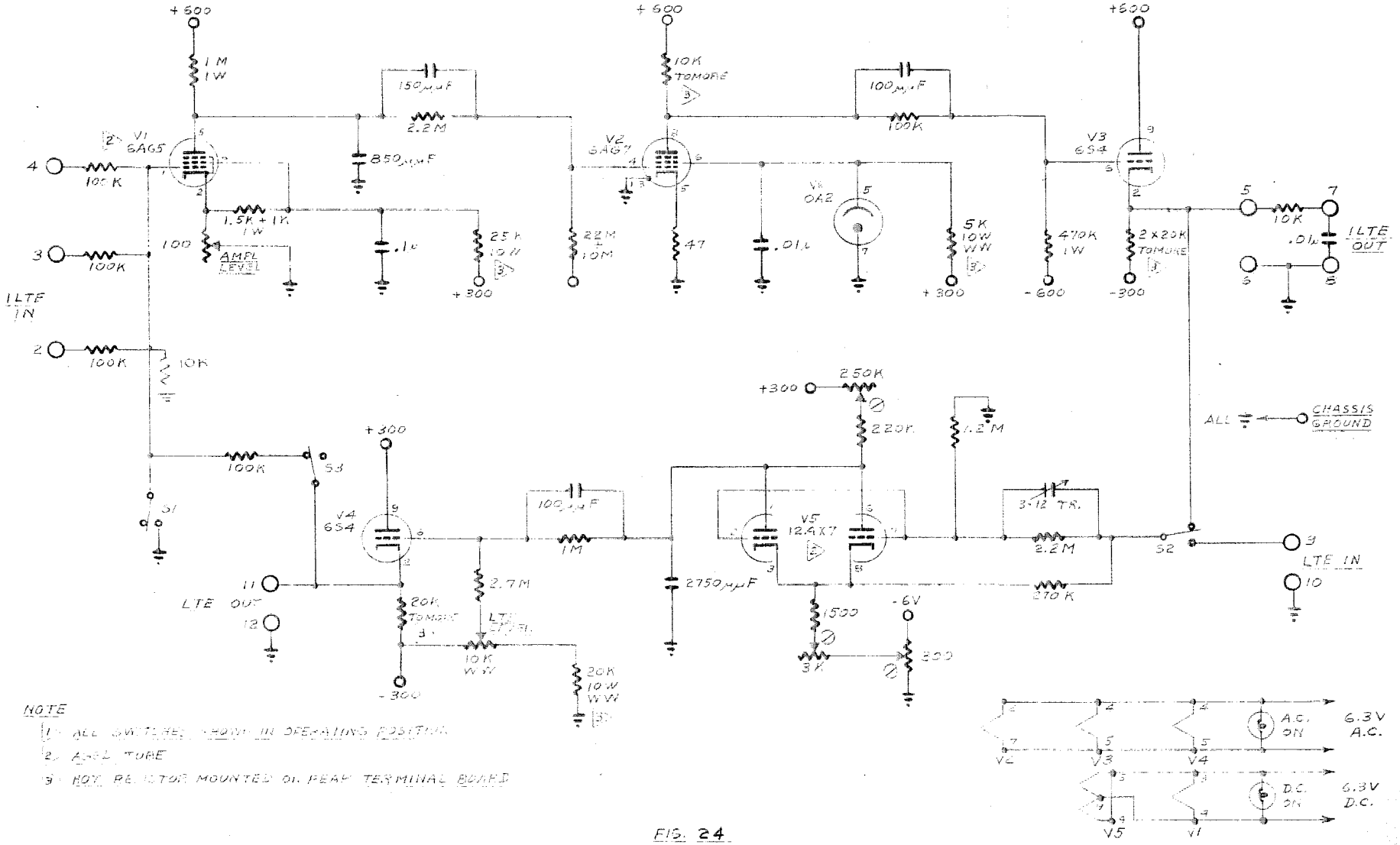

FIG. 24

INVERSE LOG TAKING ELEMENT

the second stage drops off at 500 kc. The 6S4 cathode follower provides a low output impedance, and the phase-lag network provides a second output which has a reduced high-frequency response. Except for modifications required to stabilize the loop, the LTE in the feedback path is similar to the unit described earlier in the magazine article.

The initial adjustment of the ILTE was simple, and after service of approximately 6 months, only the level requires further attention. Switches and terminals which are located on the front panel make the LTE input and output terminals readily accessible. If the LTE is adjusted in the normal manner, only minor changes are necessary when the loop is closed. With static input voltages applied, the response (Cf. Figure 25) can be determined accurately. The log base of this response curve is computed from the straight line to be a = 1.2. The drift of the ILTE has been observed in operation to be about 1 volt/hr with 3.0 volts out and 3 volts/hr with 300 volts out.

Since both LTE and ILTE are unidirectional devices, and since the outputs are not sinusoidal for sine wave outputs, discussion of the frequency response of these units separately is meaningless. The frequency response with the input and output polarity inverters included, however, has meaning. The frequency response of the complete system consisting of input inverter, LTE, ILTE, and output inverter is shown in Figure 26. From this curve, an approximate cutoff frequency (frequency at which the amplitude is reduced to 70.7 percent

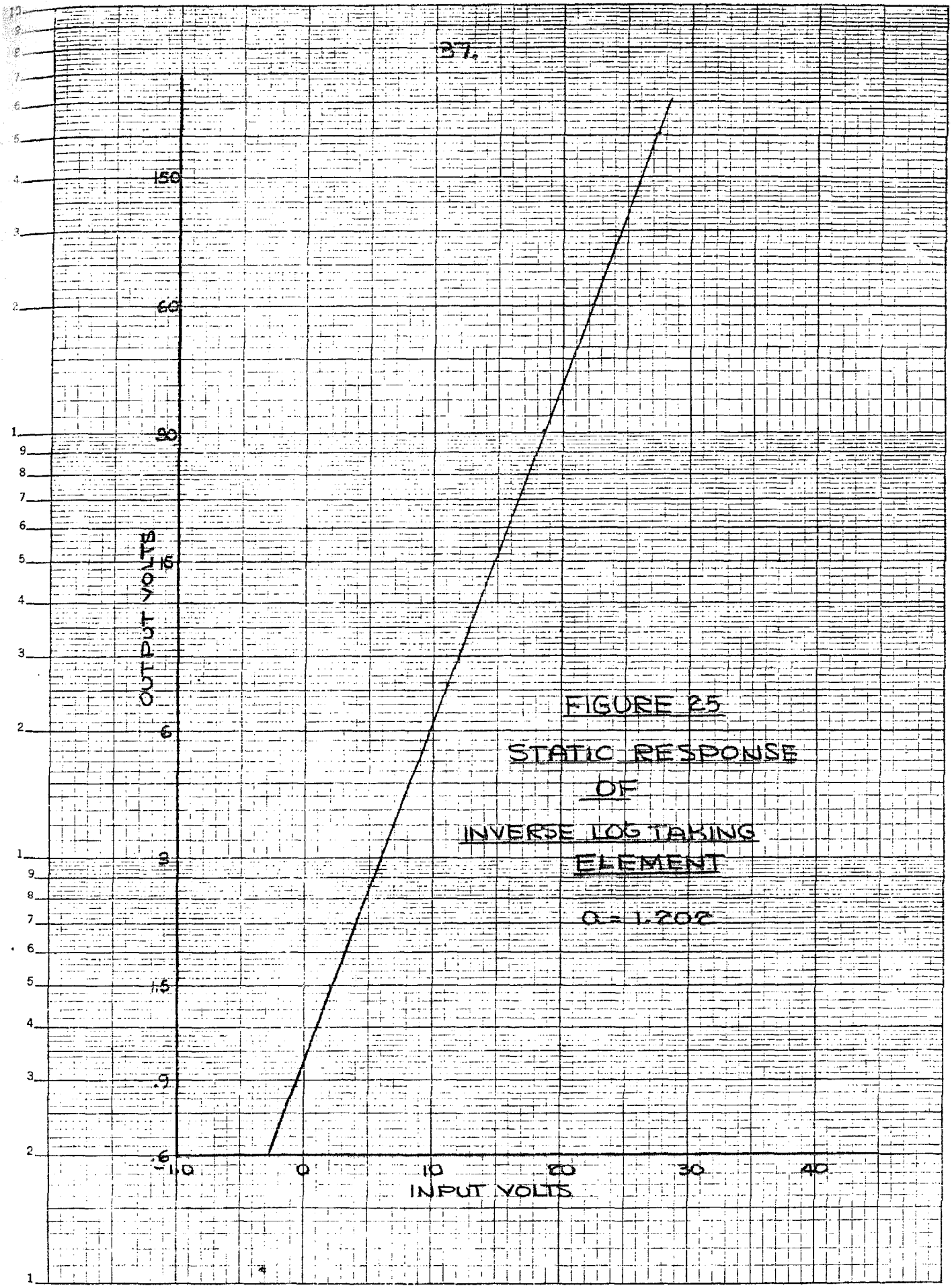

FIGURE 25

STATIC RESPONSE

OF

INVERSE LOG TAKING

ELEMENT

$\alpha = 1.202$

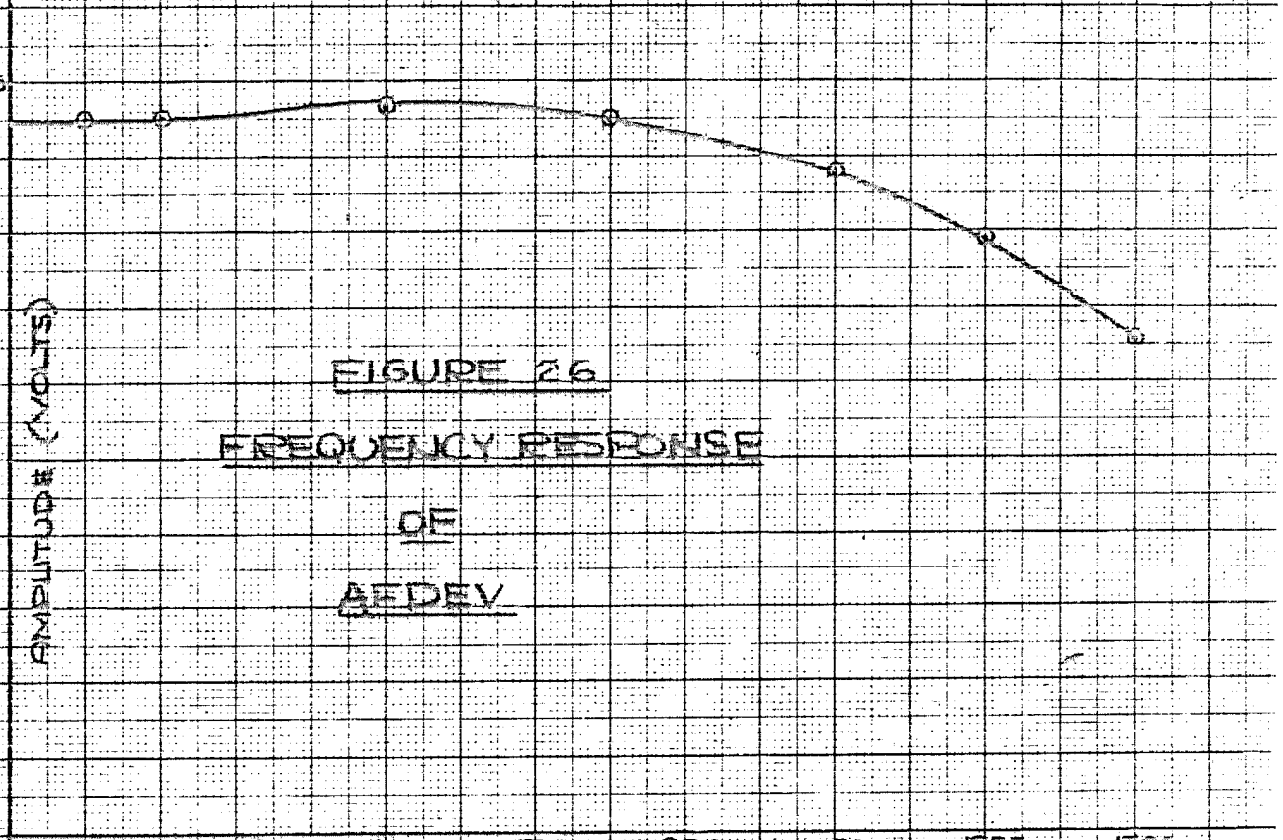

FIGURE 26

FREQUENCY RESPONSE

OF

AEDEV

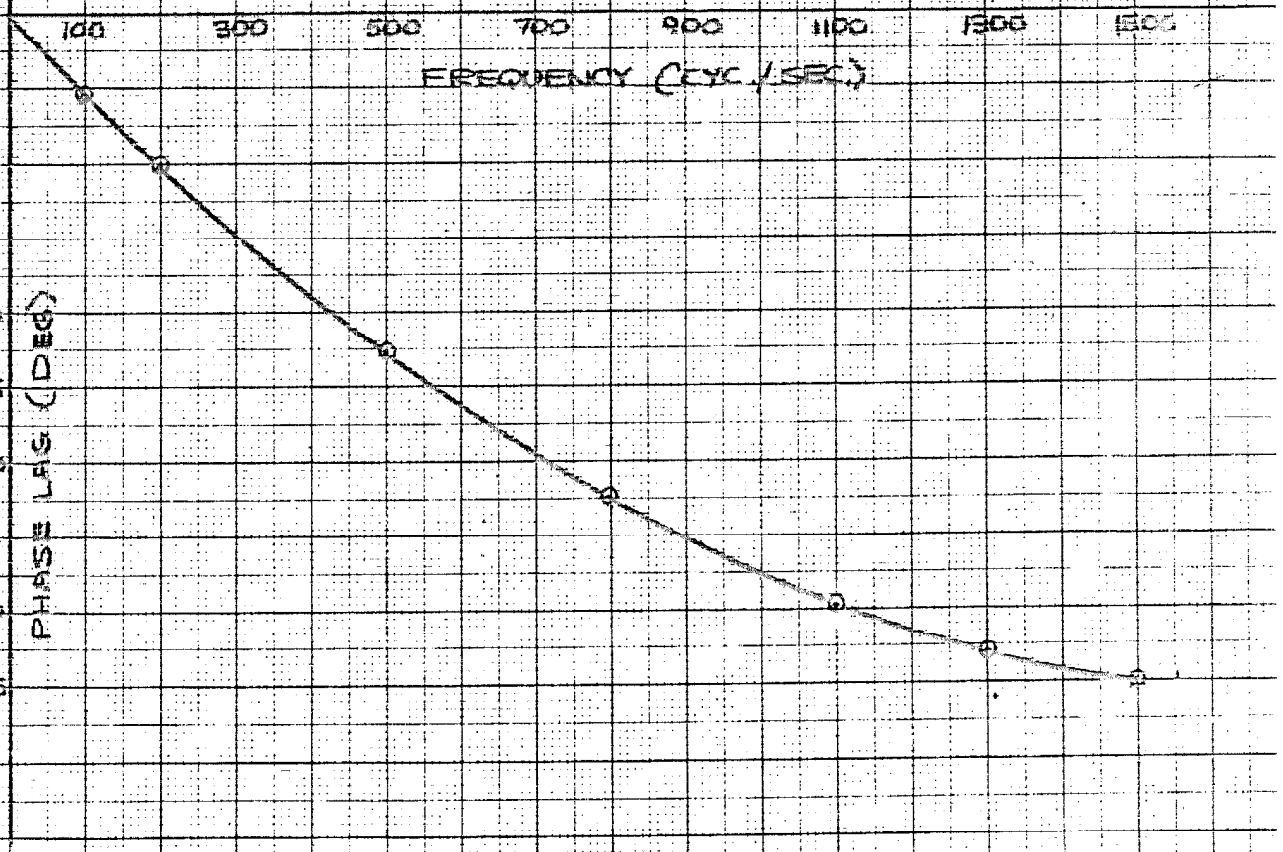

of its dc value) of 800 cyc/sec is found.

Polarity Inverting Problem: Input

From a purely mathematical point of view, the logarithm of a negative number is complex. When presented with negative input signals, the electronic LTE, however, produces extraneous output voltages which seriously affect the satisfactory performance of the complete system. The response of the LTE is proportional to the logarithm of the input voltage for positive applied voltages from 0.3 volt to +300 volts (Cf. Figure 4). For values less than 0.3 volt, the response assumes an undesirable form. To avoid the negative signal difficulty, considerable time was spent on developing the system shown in the block diagram of Figure 27. The signs of all input signals are converted to a positive sense and in this form are sent through the LTE and the remainder of the computer. At the output of the computer, the all-positive signals and all-negative signals which are obtained at the output of a negative-gain amplifier are sent into the output polarity inverter. A polarity senser is used to measure the sign of the input and to switch electronically the positive or negative signal to the output, depending on the input polarity. The appropriate sign of the resulting output has thus been restored. The details of the circuits shown in Figure 27 are included in the remainder of this section.

The input inverter unit, which is shown as the first block in the diagram of Figure 27, operates much the same as a full-wave rectifier. Hence, for varying input voltages

in the range -150 to +150 volts, the output voltage is positive, ranging from 0 to +105 volts. The gain is approximately 0.7, with a gain stability $\Delta A \leq 1/2$ percent. The drift voltage of the output is less than 0.3 volt.

The circuit consists of a positive channel which employs a cathode follower (1/2 12AU7 twin triode) and a negative channel which provides the necessary negative signal with the aid of a starved pentode amplifier (1/2 6U8 pentode-triode). Large degeneration in both of these channels reduces the gain to 0.7 with a corresponding reduction of the drift to the value stated and a gain stability of 0.5 percent. Both negative and positive channels are amplified through a cathode follower stage for the following reasons:

1. The cathode follower supplies the necessary current through a negligible output impedance.
2. The cathode follower reduces input loading from the negative-gain stage.
3. The cathode follower isolates the bias potentials of the positive-gain stage from the input.

A 5651 voltage reference tube is used in the cathode circuit of the negative-gain channel cathode follower to provide the appropriate level change. Reference to Figure 28 shows the operation of this circuit. If the input voltage varies from 100 volts to 250 volts, the output, measured across R, varies from 0 to 150. For rated operation of the 5651 reference tube, the voltage is held fixed at 84 volts, which subtracts from the applied voltage. This circuit trick has thus changed

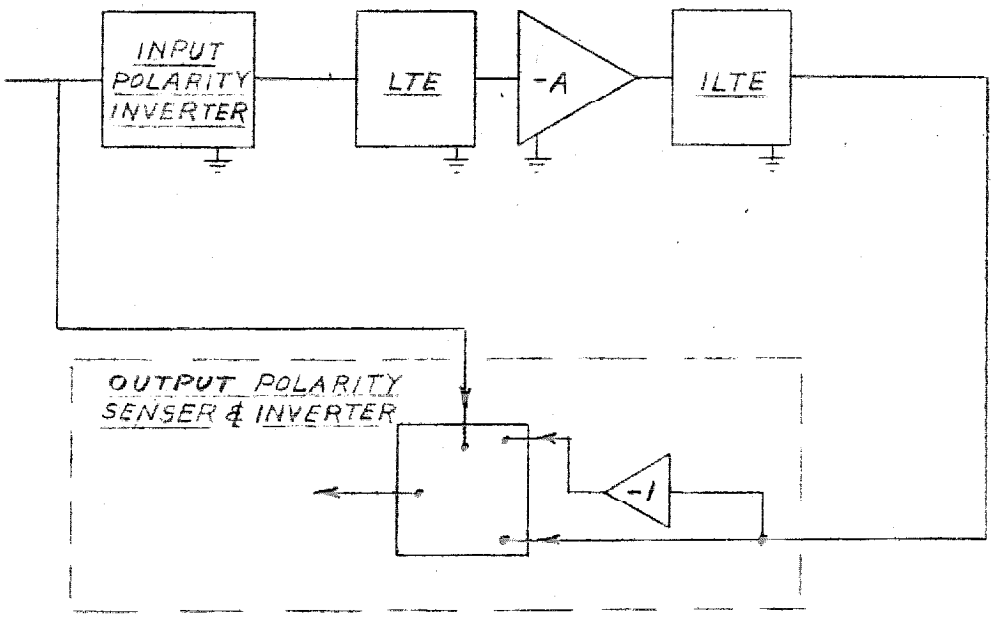

FIGURE 27 BLOCK DIAGRAM OF COMPLETE COMPUTER INCLUDING POLARITY SWITCHING

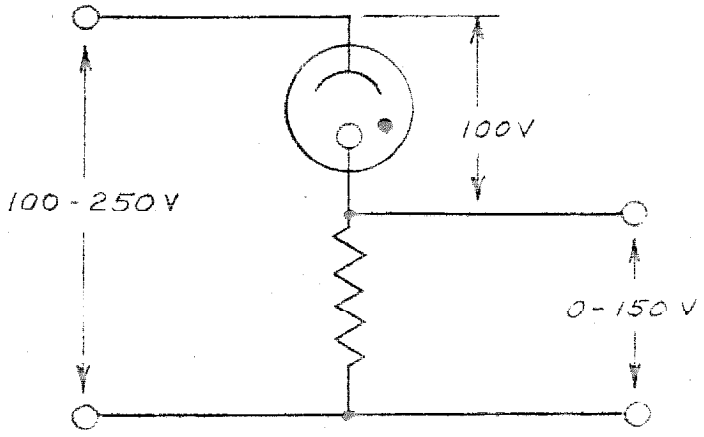

FIGURE 28 USE OF VOLTAGE REFERENCE TUBE TO CHANGE LEVEL

the level of the output signal to zero.

The schematic diagram of the inverter is shown in Figure 29. The 6AL5 twin diode selects the output from the proper amplifier and rectifies it in the conventional manner. Switches in the diode plate circuits allow the selection of one or both channels.

Three potentiometers are provided for the proper adjustment of the inverter. The following detailed alignment procedure is presented for those using this device in future work:

1. Turn on the input polarity inverter, and allow it to warm for 10 minutes.
2. Short the input.
3. Connect the voltmeter to the output terminals.
4. With the positive input switch in the "on" position (up), set the output to 50 mv by means of the positive zero control.
5. Apply 45 volts to the input, and measure the output voltage.
6. With the negative input switch in the "on" position (up), set the output to 50 mv by means of the negative zero control.
7. Apply -45 volts to the input, and adjust the negative gain control until the output voltage corresponds to that obtained in step 5.

Operation of the inverter for the past few months has proved it to be a valuable device with characteristics that

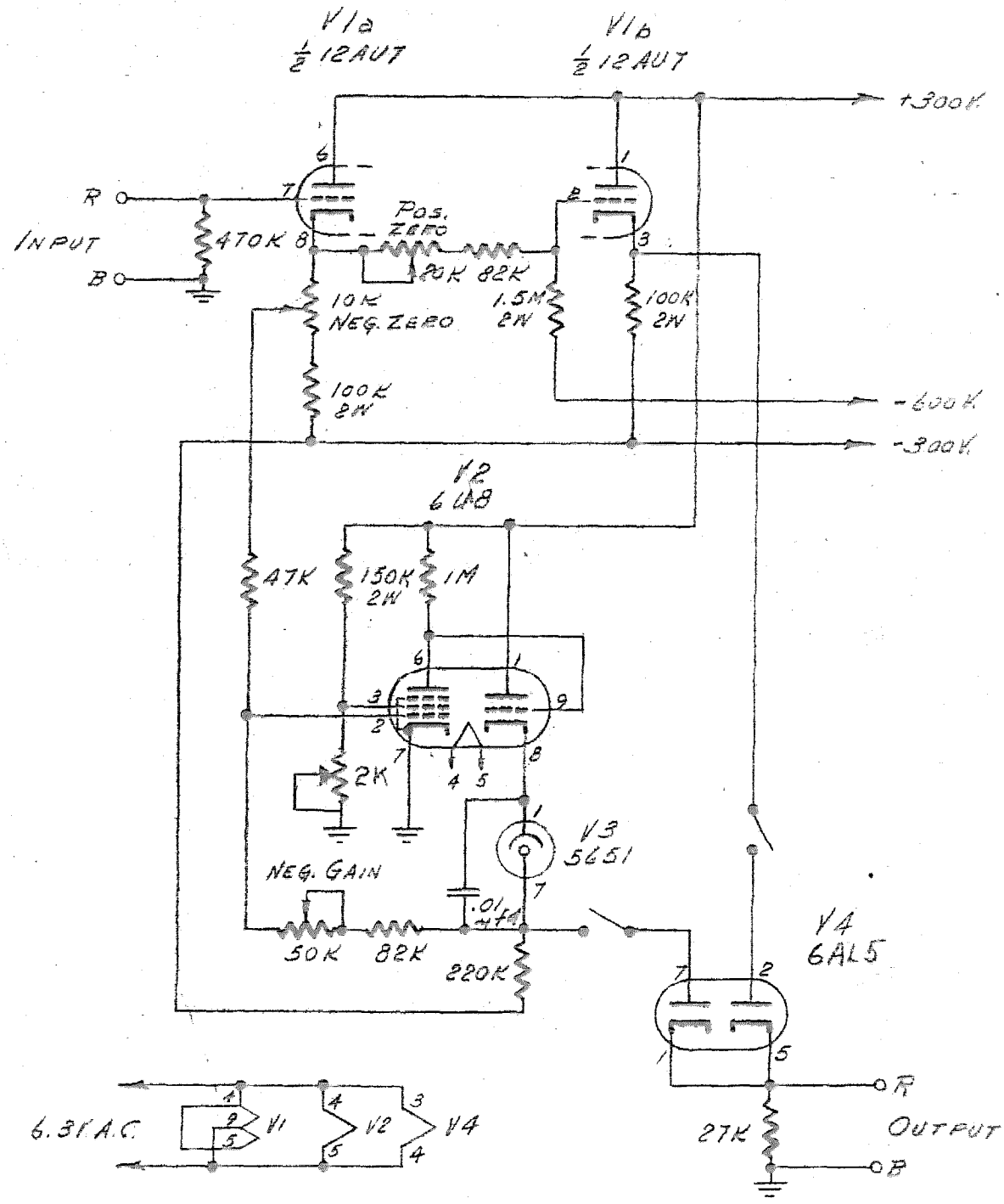

SWITCHES SHOWN IN OFF POSITION (DOWN)

FIG. 29

INPUT POLARITY INVERTER

are well within the values specified. Figure 30 shows a photograph of the inverter.

Polarity Inverting Problem: Output

The output polarity inverter includes all equipment enclosed in dashed lines on Figure 27 and, because of its logical system, is more complicated than the input inverter. The heart of the inverter is a pair of amplifiers; one inverts the input signal, and the other does not. The sensing part of the inverter allows only one amplifier to operate at a time, thus controlling the polarity of the output. Input signals applied to the sensing input terminals control the sensing circuit in such a manner that the correct algebraic sign is restored to the output. Consider, for example, the multiplication of two voltages. If both input voltages have the same polarity (i.e., both negative or both positive), then the output voltage should be positive. If, however, the two input signals have opposite signs, then the output voltage should be negative.

Since the ILTE, like the LTE, operates only on positive signals, the input to the output polarity inverter is always positive. In testing, one always applies a positive voltage because the device will give meaningless outputs for negative inputs. The sensing input terminals of the output inverter are connected at points in the circuit where the signals to be multiplied have proper signs (i.e., before the input polarity inverter), and the correct signs of the signals passing through the output inverter are again restored.

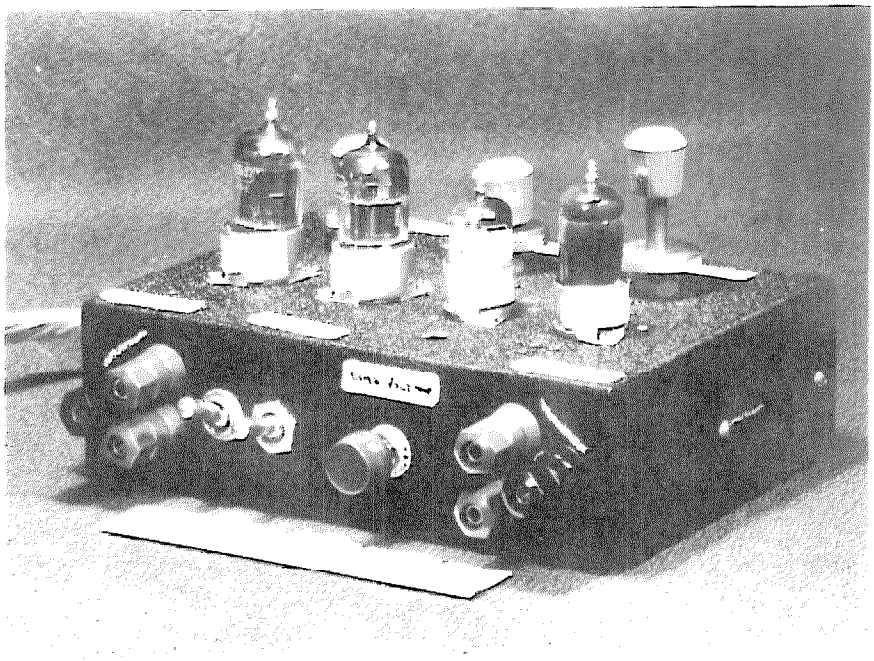

Figure 30. Photograph of Input Polarity Inverter

The complete schematic diagram of the inverter is shown on Figure 31. Three dual-purpose vacuum tubes and eight germanium diodes are required in the sensing section. Tubes V1 and V2 constitute two parallel high-gain amplifiers, the outputs of which are at either of two voltage levels, depending on the polarity of the voltage appearing on the input sensing terminal. The succeeding bridge rectifier and differential amplifier compare these two voltages and produce signals at the plates of V3 which convey the input polarity information. The cathode follower V6 and the associated voltage reference tubes V10 through V16 transfer the result of this polarity comparison to the grids of the positive and negative clamping amplifiers V5a and V7. The grid voltage swing available for these tubes is of such magnitude and level that the tubes are completely cut off or are operating with positive grid voltage. This latter operation results in only one of the two triodes being in a state of conduction at any given time. The plates of the clamping triodes are coupled to the two amplifier channels with diodes V8 and V16.

In the switching section, the positive-gain amplifier consists of one simple cathode follower circuit and an input attenuator, which includes the positive level control. The negative-gain channel is similar except for the addition of a highly degenerated sign-changing amplifier.

Since clamping of both amplifiers is identical, only one circuit is described. When the channel is open, the controlling clamp tube is cut off, and the coupling diode

has no effect. However, when the channel is clamped, the cathode of the diode is lowered to a voltage controlled by the appropriate positive or negative clamp. The grid potential is unable to change with the signal applied and hence cuts off the channel. A balance control permits adjustment of the summing ratio of the two signals, and when the gains of the two channels are equalized, symmetrical outputs result. The transients developed during switching are removed by the filtering action of the 0.01-μf capacitor, together with the resistance of the balance potentiometer.

Because analysis laboratory negative-gain amplifiers, set to -1, saturate with 100 volts applied, and since the ILTE output does not saturate until +360 volts is reached, a quarter attenuation is built into the polarity inverter for satisfactory operation. The negative-gain amplifier at the output supplies the switched signal at a desirable low impedance level.

Figure 32 shows a photograph of the polarity senser and output inverter. Two switches, labeled input bias, are mounted on the front and permit the use of the inverter with only one applied signal. When only one voltage is to be inverted, a positive or negative constant voltage is applied to the other sensing channel with the input bias switch.

The alignment procedure of the output polarity inverter is more involved than that of the other equipment. A detailed step-by-step procedure has been developed as follows:

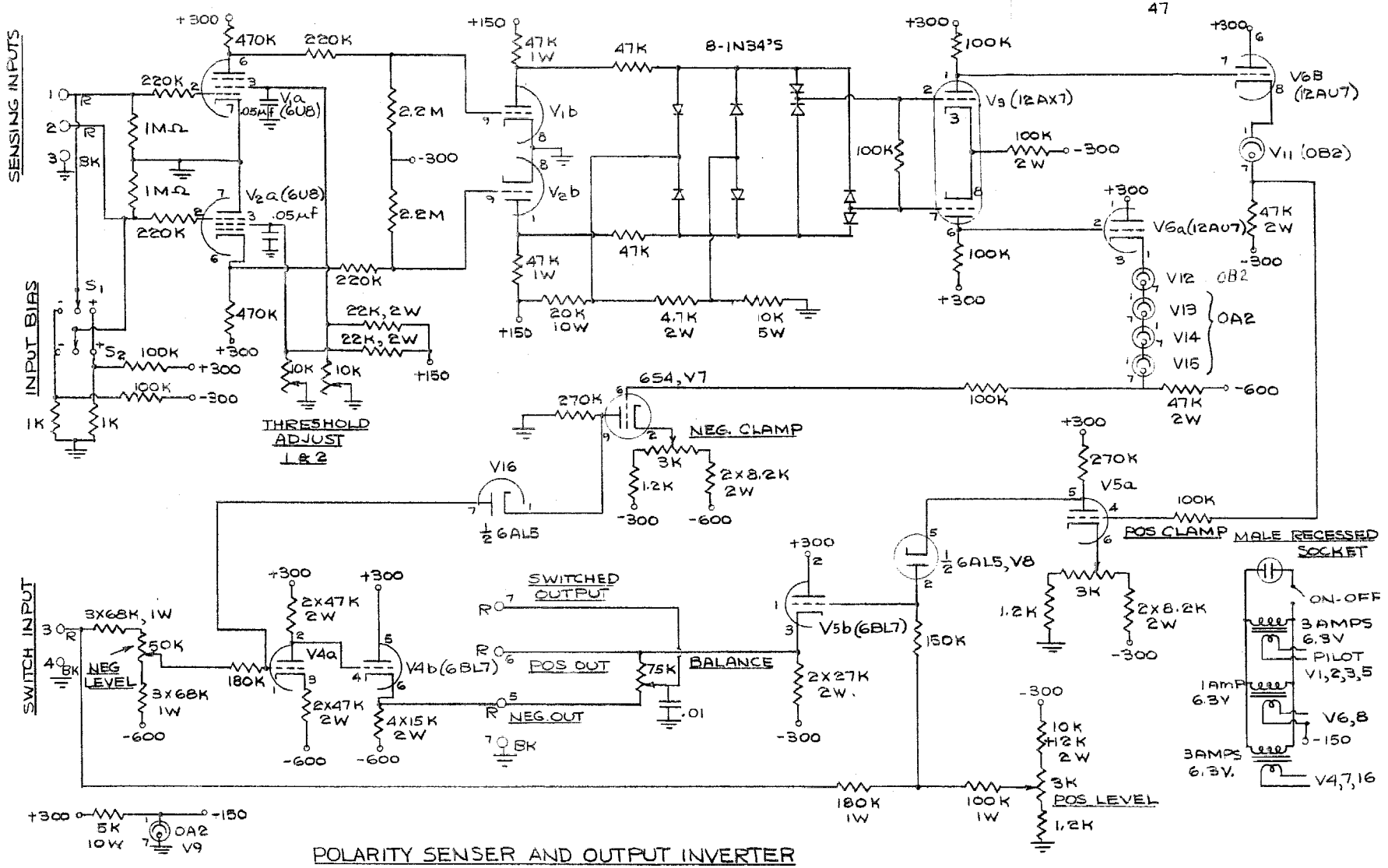

POLARITY SENSER AND OUTPUT INVERTER

FIGURE 31

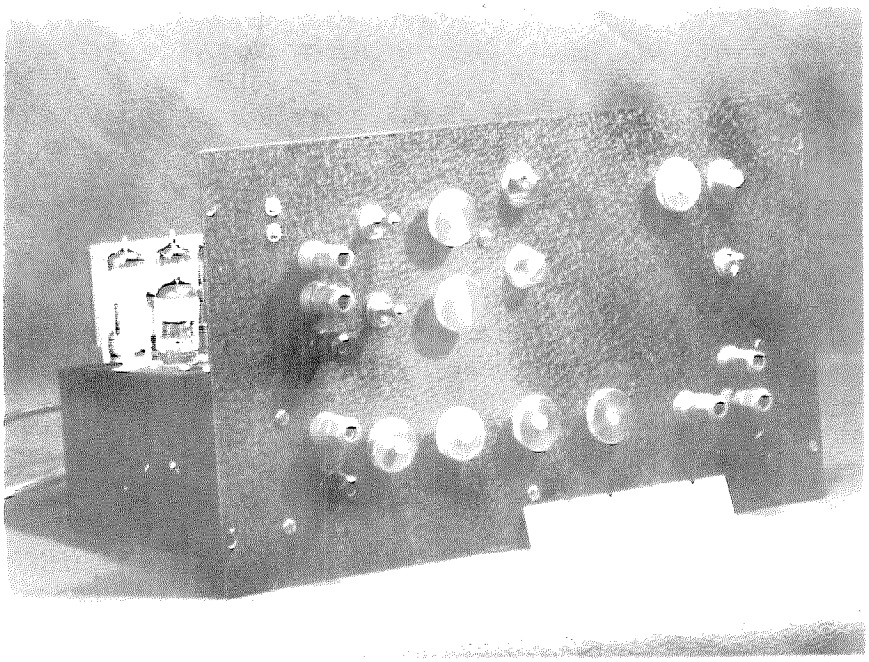

Figure 32. Photograph of Output Polarity Inverter

1. Operate for 1 hour.
2. Short the input.
3. Connect a voltmeter on the positive output terminal.
4. With input sensing switches opposite, turn the positive clamp clockwise.
5. Set the positive level to zero.
6. Set the input sensing switches in the same position.
7. Set the positive clamp just to zero. Be careful here not to overshoot.
8. With a voltmeter on the negative output terminals, turn the negative clamp counterclockwise.
9. Set the input sensing switches in the same position.
10. Set the negative level potentiometer to zero.
11. Set the sensing input switches opposite.
12. Set the negative clamp to zero, again being careful not to overshoot.
13. Connect the input to a positive low impedance voltage source of 100 to 200 volts. Connect a sine wave of amplitude at least 50 volts to one sensing input.
14. Adjust the balance controls until the output is symmetrical about zero.
15. Reduce the sensing input to 0.5 volt rms, and adjust the threshold control for symmetry of output.
16. Repeat this process on the other sensing input.

A further discussion of the equipment in this section and

in the appendices is given in Reference 10.

Complete System

Figure 33 shows a photograph of the complete computer, and Figure 34 presents a typical connection of the four basic elements in a complete system. To demonstrate the shape of the function at the intermediate points of the arbitrary function generator, Figures 35 to 40 were prepared. Figure 35 demonstrates the input to the AFDEV which is obtained from the linear sweep generator. The oscillogram of Figure 36 presents the output of the input polarity inverter. Notice that in this and all other photographs of this group, the zero trace was established by means of a double exposure. Figures 37 and 38 show the output of the LTE and the negative-gain amplifier, respectively. The gain of the amplifier was set to unity so that a direct comparison, input vs output, is possible. Figure 39 shows the output of the ILTE, and Figure 40 presents the output of the polarity inverter and hence the output of the AFDEV. In this last demonstration an exponent of 1 was established. Use of a gain other than unity, together with an attenuating potentiometer, provides the possibility of a range of exponent (1/5 to 5). In Section III this system is used to generate other arbitrary functions of an independent variable.

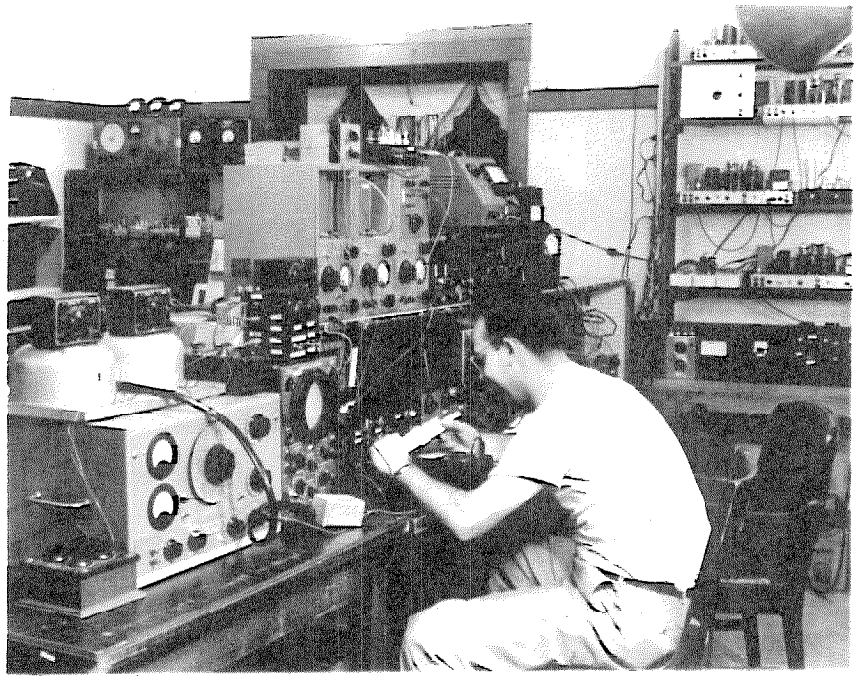

FIGURE 33.

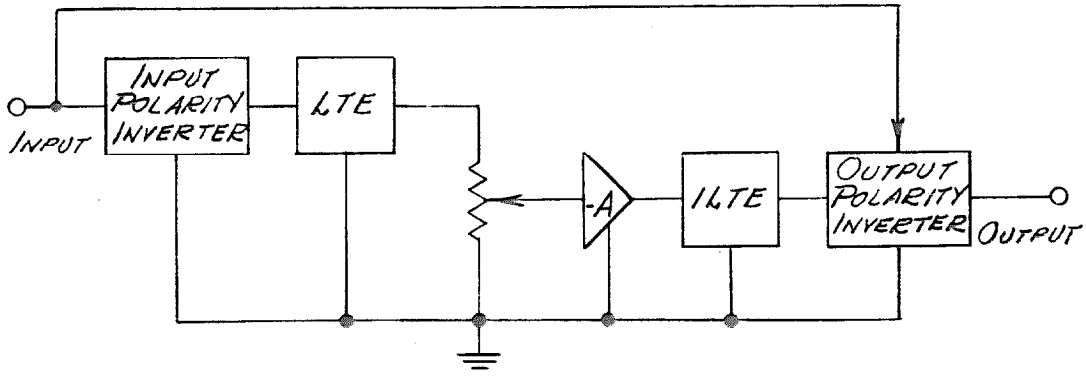

FIGURE 34. TYPICAL COMPUTER CONNECTION DIAGRAM

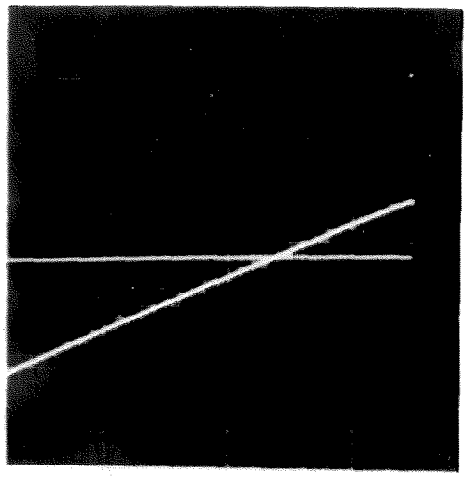

Figure 35

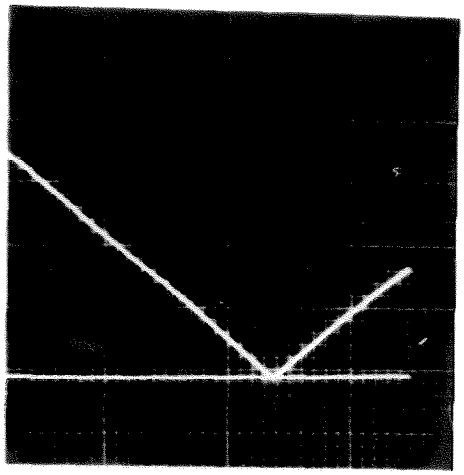

Figure 36

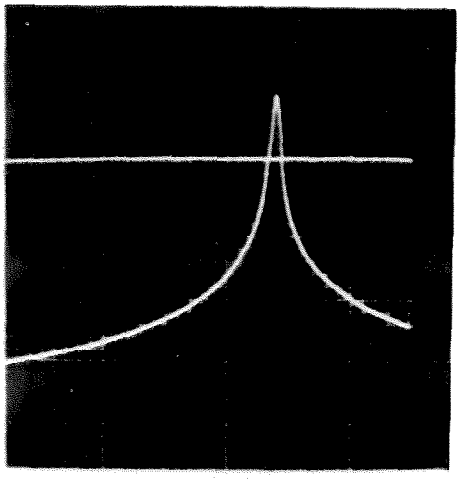

Figure 37

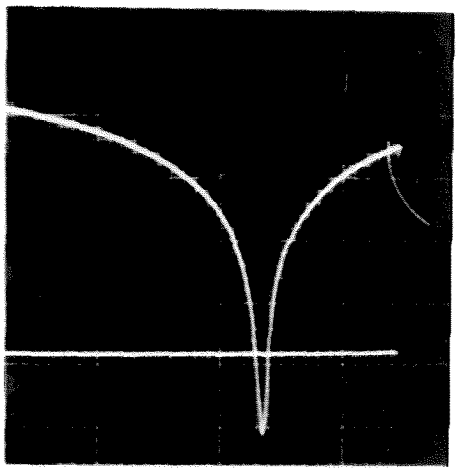

Figure 38

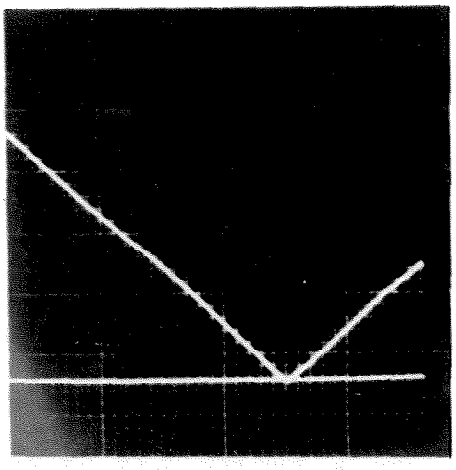

Figure 39

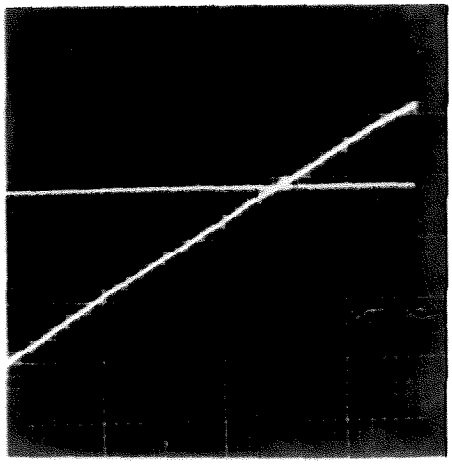

Figure 40

III. ARBITRARY FUNCTION OF AN INDEPENDENT VARIABLE

Although the nonlinear computer finds its primary use as an arbitrary function generator of a dependent variable (AFDEV), the multiplier also can act as an arbitrary function generator of an independent variable (AFINV). In this latter application, the nonlinear computer competes both in accuracy and in versatility with the existing arbitrary function generators. To demonstrate a few of the driving functions obtainable with the AFINV, the system shown in the block diagram of Figure 41 was set up. With this arrangement the output of three log-taking elements are summed and fed to the LTE. A linear sweep, provided by the generator described in Appendix C and added to a constant voltage E_1 and E_2, drives two LTE's yielding functions of the form

$$y_1 = A(x+a) \quad \text{and} \quad y_2 = B(x+b) \tag{11}$$

The third LTE is driven with an audio oscillator which provides a function

$$y = C \sin kx \tag{12}$$

To prevent the LTE signal from going negative, the input polarity inverters are appropriately inserted. Only two inverters are necessary since one signal is always positive. An output polarity inverter is used to restore the correct sign to the output signal which is displayed on an oscillo-

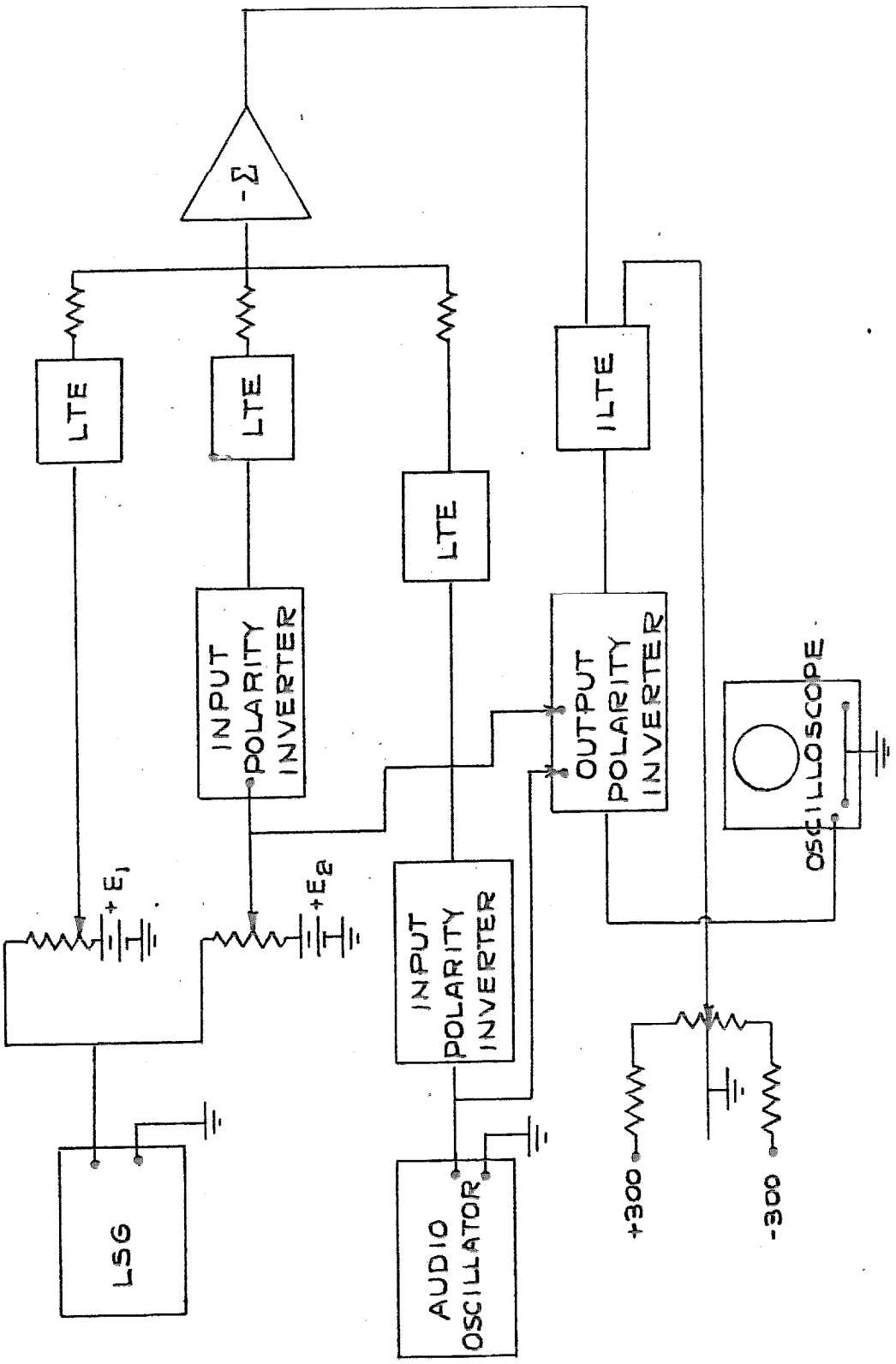

FIG. 41 USE OF COMPUTER AS AN ARBITRARY FUNCTION GENERATOR

scope.

As connected, the nonlinear computer provides multiplications of the form

$$y = A(x+a)^{\alpha}(x+b)^{\beta}(\sin kx)^{\gamma} \tag{13}$$

If other functions, g(x), h(x), and f(x), are supplied to the LTE units, the more general function

$$y = A[g(x)]^{\alpha}[h(x)]^{\beta}[f(x)]^{\gamma} \tag{14}$$

is possible. Various functions of the form of Equation (13) are demonstrated in the photographs of Figures 42 to 47 with the explanation included in Table III. A cursory glance at

Table III

Oscillogram Number	Explanation
Fig. 42	$x \sin kx$
Fig. 43	$x^n \sin kx \quad n<1$
Fig. 44	$x^n(\sin kx)^m \quad n>1 \quad m<<1$
Fig. 45	(x-a) input to system
Fig. 46	$(x-a)^n (x-b)^m$
Fig. 47	$x(x-a)(x-b)$

the available possibilities should convince the reader of the

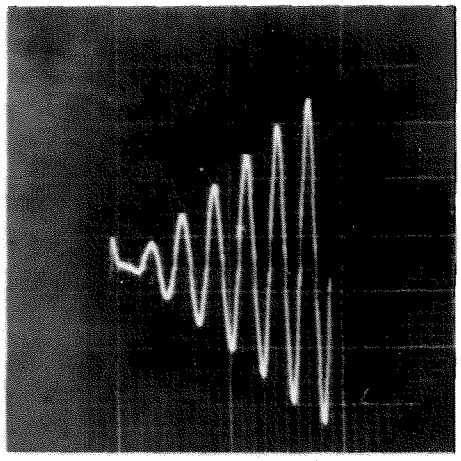

Figure 42

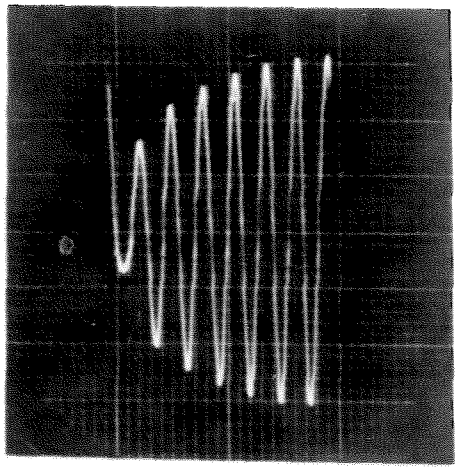

Figure 43

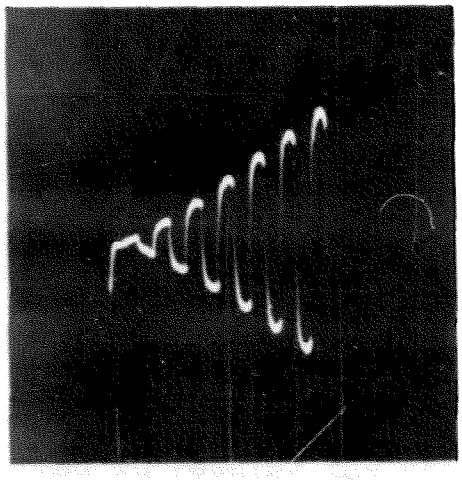

Figure 44

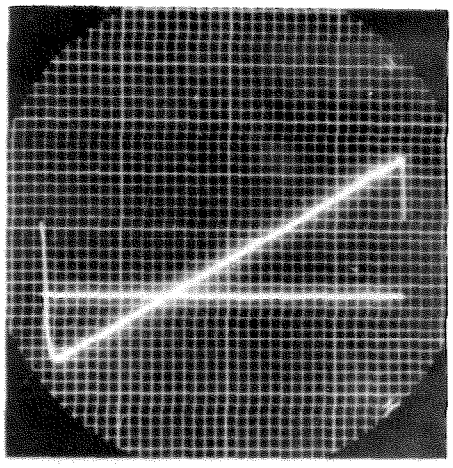

Figure 45

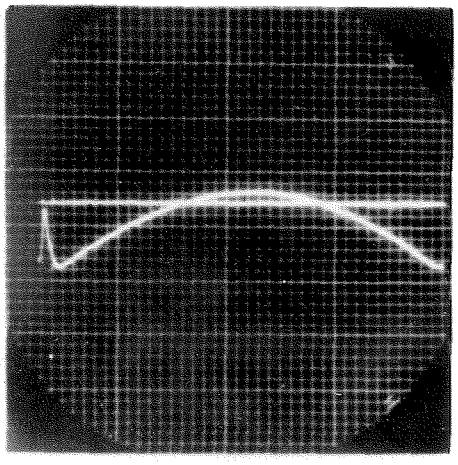

Figure 46

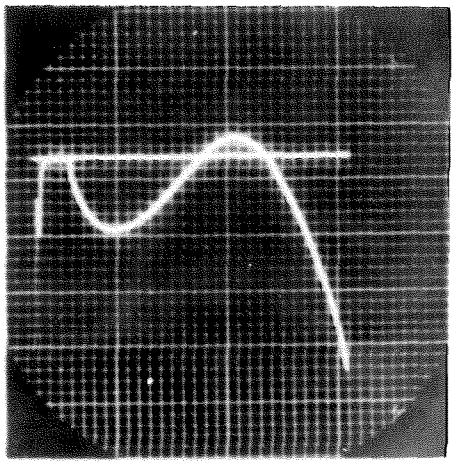

Figure 47

versatility of the nonlinear computer.

In an effort to ascertain the accuracy of the computer, the function $y = Ax^n$ ($A = 3$ and $n = 0.5$) was set up on the computer. This step was accomplished by removing all but one LTE in Figure 41. From an enlarged copy of the oscillogram shown on Figure 48, the points were plotted on log-log paper (Cf. Figure 49). From the resulting straight line, the curve was determined to be

$$y = 2.98 \times^{0.488} \qquad (15)$$

Comparison of the exponent yields a discrepancy of 2.4 percent between the two expressions, with the constant multiplier in error by 0.7 percent. From the scatter of the points the error is estimated to be 3 percent. Since judgment is required in reading the oscillogram, this last value probably could be improved with practice.

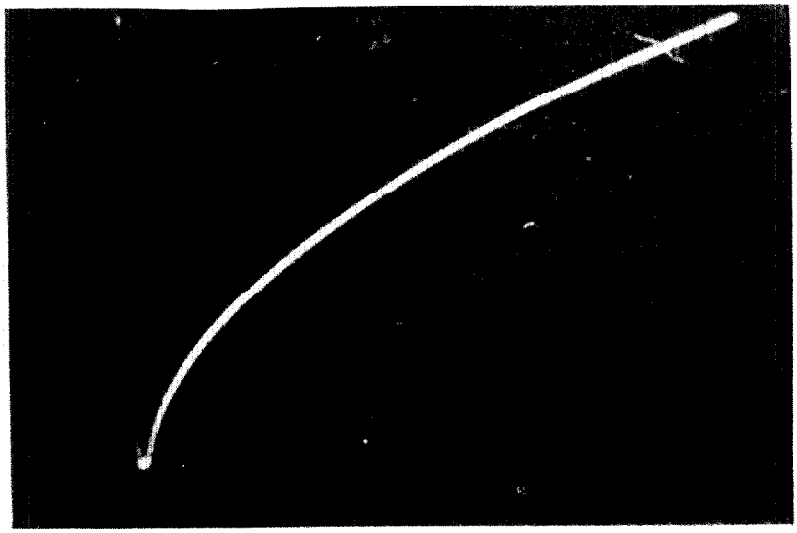

Figure 48. Oscillogram of the Function $y = 2.98\ x^{0.488}$

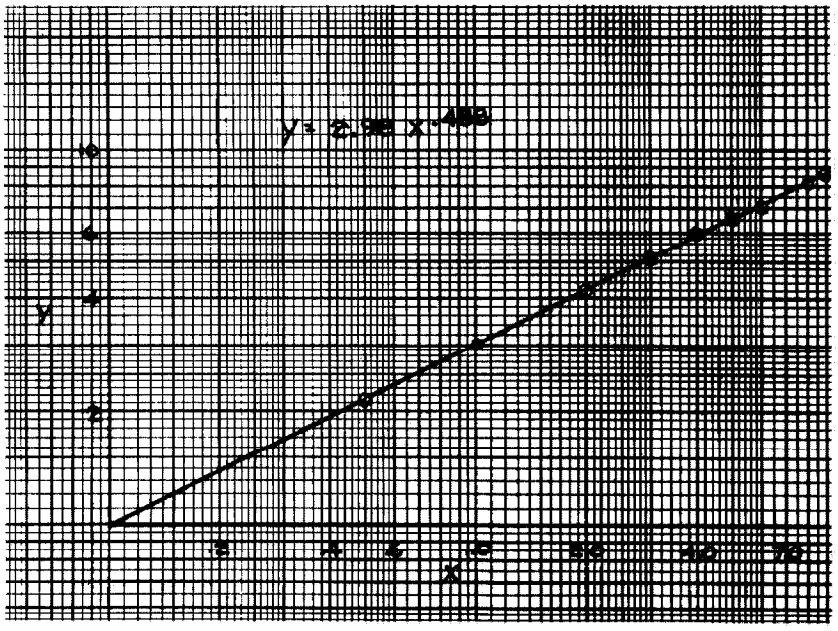

Figure 49. Log-log Plot of the Function $y = 2.98\ x^{0.488}$

IV. SOLUTION OF CLASSICAL NONLINEAR EQUATIONS

Duffing's Equation

In this section the differential equation of the form

$$\ddot{x} + c\dot{x} + (\alpha x + \beta x^3) = F \cos \omega t \qquad (16)$$

is studied. This equation occurs in several different types of physical problems, for example, the pendulum with an external periodic force applied. The problem of a mass subjected to a spring restoring force leads in general to an expression of the form of Equation (16). Saturation effects in iron core inductances and in rotating machinery are other examples of physical problems which lead to this same expression. Equation (16) is often called Duffing's equation since it was Duffing who first made significant contributions to the harmonic solutions of this equation.

Explicit solutions of an elementary character are not known for the Duffing equation. In fact, this simple-looking equation has a great variety of periodic solutions alone for which the mathematical theory has been investigated only slightly. Almost nothing is known about the nonperiodic solutions to this equation.

Because the restoring force is a function of the variable x, the resonance curve is no longer typically symmetrical and bell-shaped. The curve of Figure 50 demonstrates the following linear system:

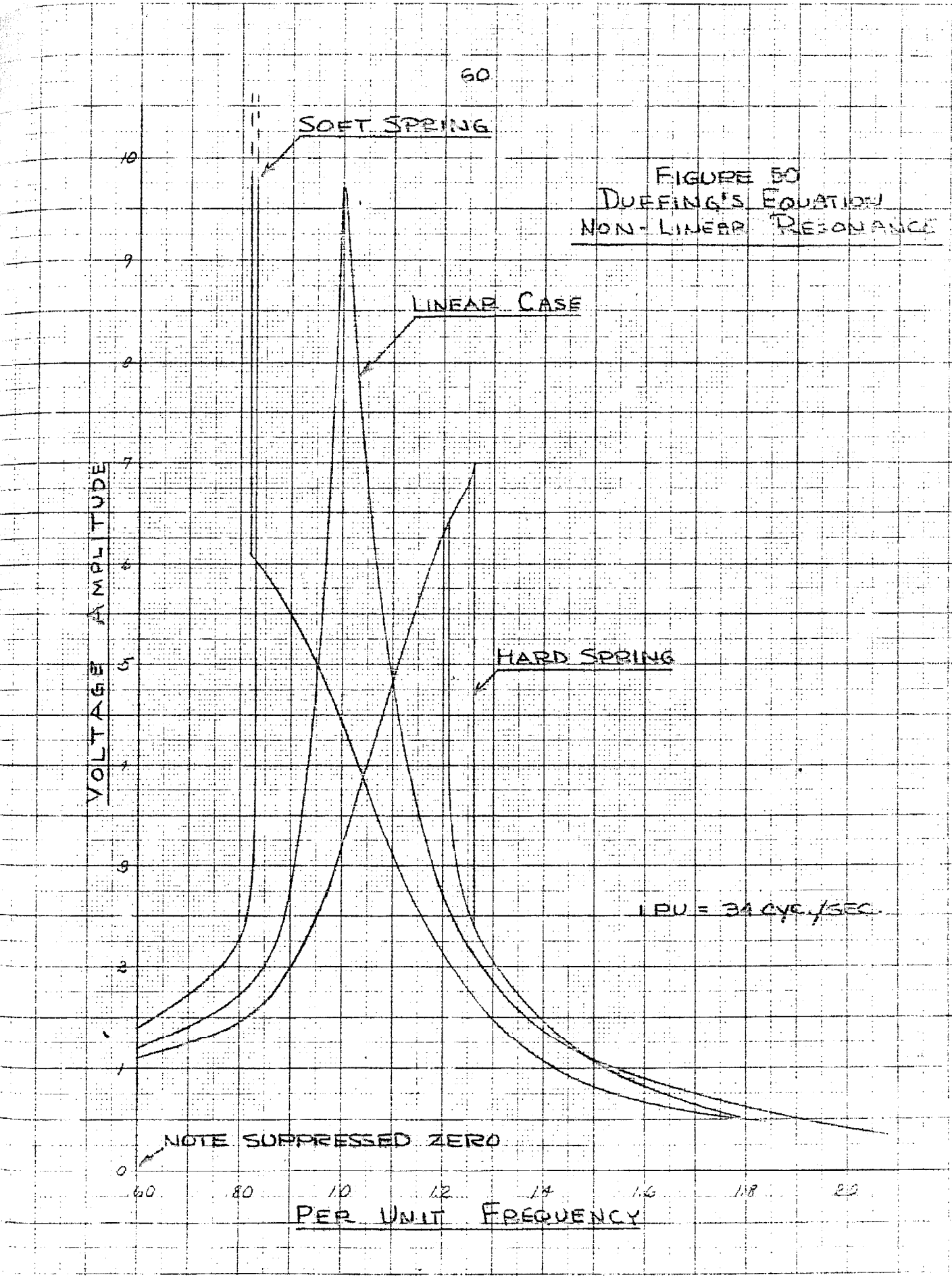

FIGURE 50
DUFFING'S EQUATION
NON-LINEAR RESONANCE

$$\ddot{x} + c\dot{x} + \alpha x = F \cos \omega t \qquad (17)$$

When the nonlinearity is introduced, the resonant frequency begins to change as the amplitude increases; as a result the resonance curve is tipped to the right or left depending on whether the spring is hard ($\beta > 0$) or soft ($\beta < 0$). Since the response cannot follow down an inverse curvature, a jumping phenomenon, sometimes called a drag loop, occurs. The shape of the amplitude vs frequency curve depends upon whether the critical frequency is approached from the low end or the high end of the spectrum.

The computer solution of Duffing's equation is demonstrated in Figure 51, where the loop analysis yields the analogous electric equation

$$L\ddot{q} + R\dot{q} + \frac{1}{C} q + kq^n = E \cos \omega t \qquad (18)$$

Appropriate variation of the exponent adjustment permits the choice of any desirable n. The classical equation dictates an n of 3, but any $n > 1$ demonstrates similar phenomena.

Oscillograms of Duffing's equation are demonstrated on Figures 52 through 57 with suitable explanation included on Table IV. The driving frequency for Figures 52 through 55 is 24 cyc/sec, and the linear natural resonant frequency for all cases is 34 cyc/sec. The driving frequency for cases 56 and 57 is 102 cyc/sec.

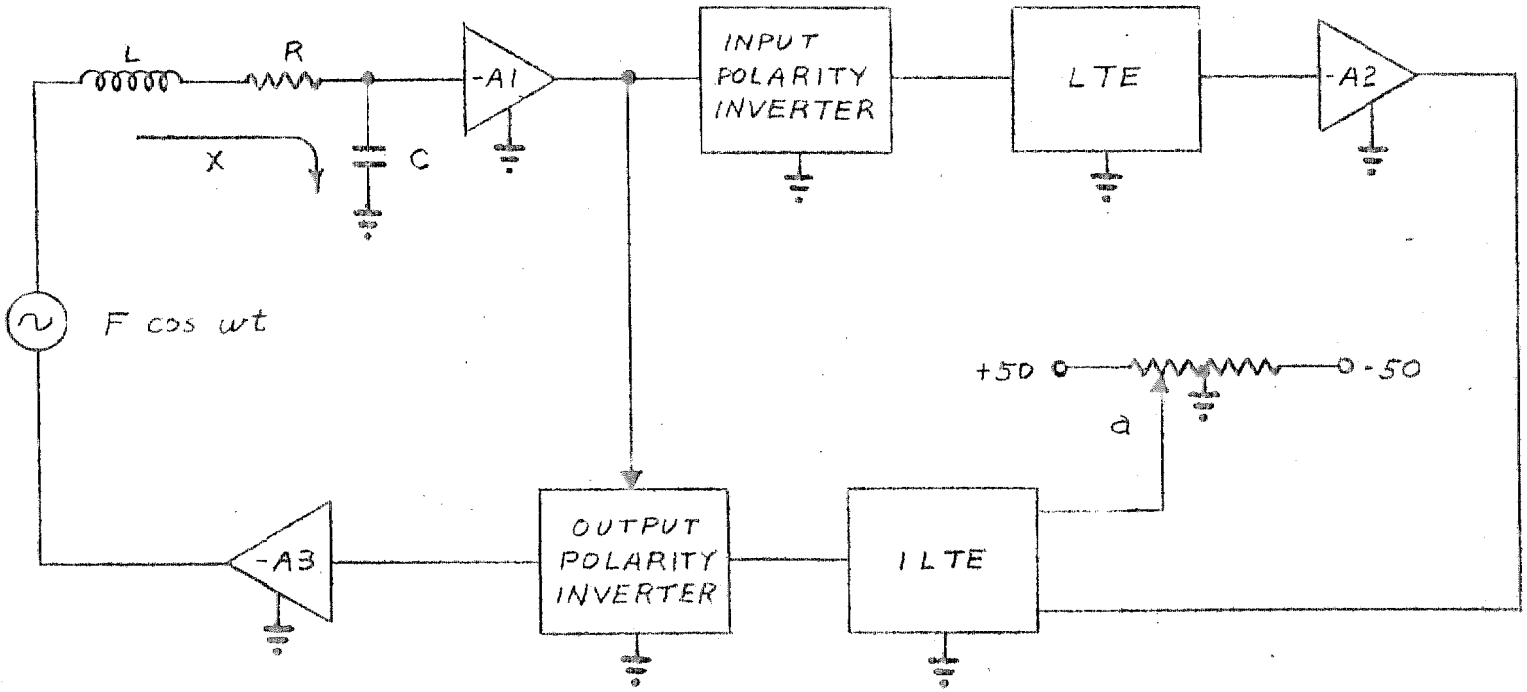

FIG. 51

BLOCK DIAGRAM

1. SOLUTION OF DUFFING'S EQUATION

$$m\ddot{x} + r\dot{x} + kx + \beta x^3 = F \cos \omega t$$

2. SOLUTION OF MODIFIED DUFFING'S EQUATION

$$m\ddot{x} + r\dot{x} + kx + f(x) = F \cos \omega t$$

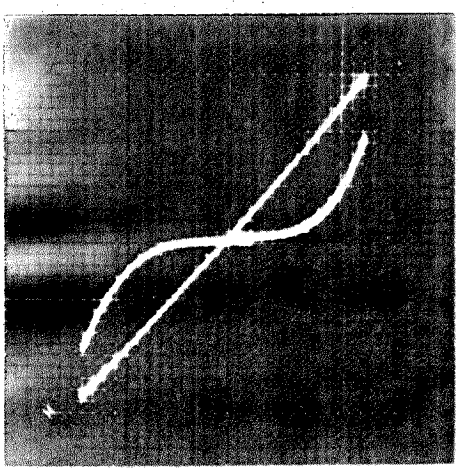

Figure 52

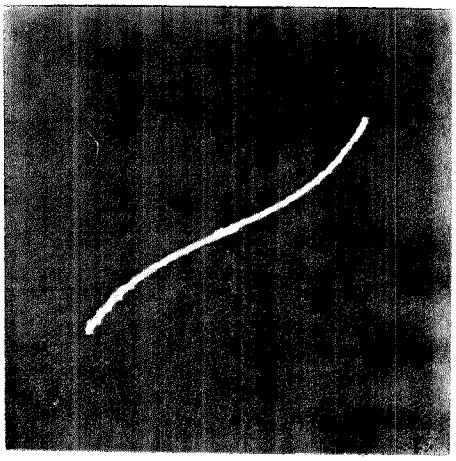

Figure 53

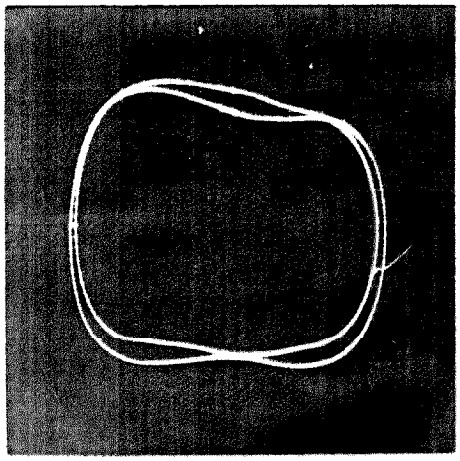

Figure 54

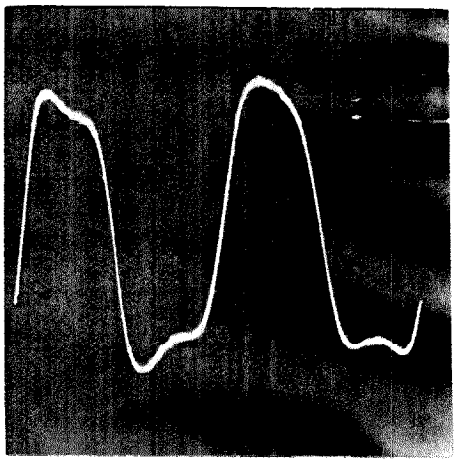

Figure 55

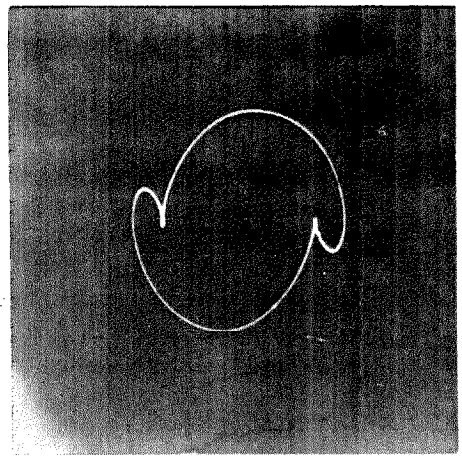

Figure 56

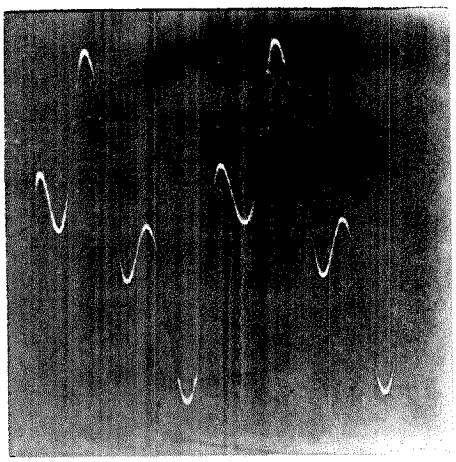

Figure 57

Table IV	
Oscillogram Number	Explanation
Fig. 52	linear (αx) and added βx^3 spring function on same oscillogram
Fig. 53	total nonlinear function (hard spring)
Fig. 54	phase trajectory of forced oscillation with function of Figure 53
Fig. 55	x vs t for forced oscillation of Figure 53
Fig. 56	phase trajectory of forced oscillation with frequency increased by 3/2
Fig. 57	x vs t for forced oscillation of Figure 56

A static amplitude vs frequency curve, shown on Figure 50, was taken for a hard spring and a soft spring. These curves demonstrate the familiar nonlinear resonance, or drag loop phenomenon. In the case of the hard spring, the system jumps from 6.8 to 2.4 at a frequency of 43 cyc/sec, and in the return scan the jump is from 3.5 to 6.4 at 41 cyc/sec. In the case of the soft spring, the jump occurs in the neighborhood of 28 cyc/sec. At the large amplitudes at which this curve was taken, the system does not return after the jump but increases without limit in the soft-spring case. This latter phenomenon results from the change in sign of the $(\alpha x - \beta x^3)$ term. When $x \geq \sqrt{\frac{\alpha}{\beta}}$, the restoring force becomes negative, and hence the system moves to its extremity.

Van der Pol's Equation

Consider as the next example an equation which arises in numerous oscillator and multivibrator applications, the equation due to Van der Pol. When normalized, this equation has the form

$$\ddot{x} - \mu (1 - x^2) \dot{x} + x = 0 \tag{19}$$

Again for comparison purposes, this expression is solved by both topological and computer methods.

In order to have a direct comparison with computer results, the phase trajectories are constructed by the method of isoclines. By taking $\dot{x} = y$ and substituting in the differential equation, one obtains

$$\dot{y} = \mu (1 - x^2) y - x \tag{20}$$

The isoclines, found by setting $\lambda = dy/dx = \text{constant}$, are given by the equation

$$y = \frac{x}{\mu (1 - x^2) - \lambda} \tag{21}$$

If μ is taken as 1, Equation (21) simplifies to

$$y = \frac{x}{(1 - \lambda) - x^2} \tag{22}$$

The equation of the family of isoclines (Equation 22) is plotted for various values of λ on Figure 58, where also is shown the phase trajectories. As in all previous graphical solutions, the construction was performed on 17x17-inch paper and was photographically reduced for this presentation. As one should expect from this equation, there exists a limit cycle (Cf. Figure 58). This cycle is due physically to the fact that the sign of the damping force changes as x is greater or less than 1. Hence for $x < 1$ the system builds up, whereas for $x > 1$ the system damps down, culminating in a stable-limit cycle or oscillation.

The solution of this problem on the computer is greatly simplified if one multiplies Equation (19) by dt and integrates from 0 to t, assuming zero initial conditions:

$$\int_0^t \frac{d}{dt}\left(\frac{dx}{dt}\right)dt - \mu\int_0^t (1-x^2)\frac{dx}{dt}dt + \int_0^t x\,dt = 0$$

$$\frac{dx}{dt} - \mu\left(x - \frac{x^3}{3}\right) + \int_0^t x\,dt = 0 \qquad (23)$$

The computer analog of Equation (23) is shown in the block diagram of Figure 59, where the loop equation yields

$$\frac{di}{dt} - \mu\left(i - \frac{i^3}{3}\right) + \int_0^t i\,dt = 0 \qquad (24)$$

As in the case of Duffing's equation, the computer is able to establish any exponent in the nonlinear term, but for the sake of comparison with the classical expression, the cubic

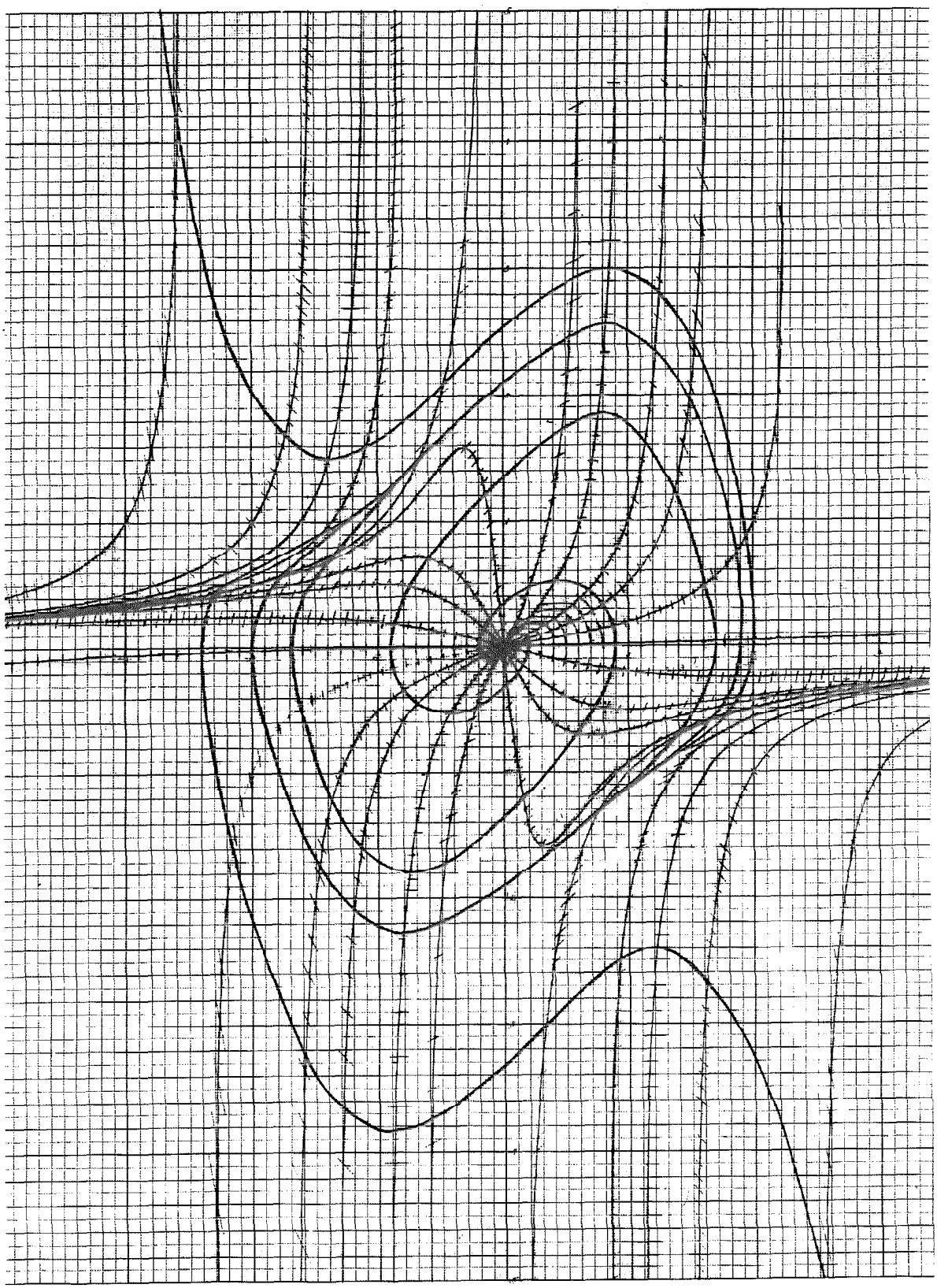

FIG. 58

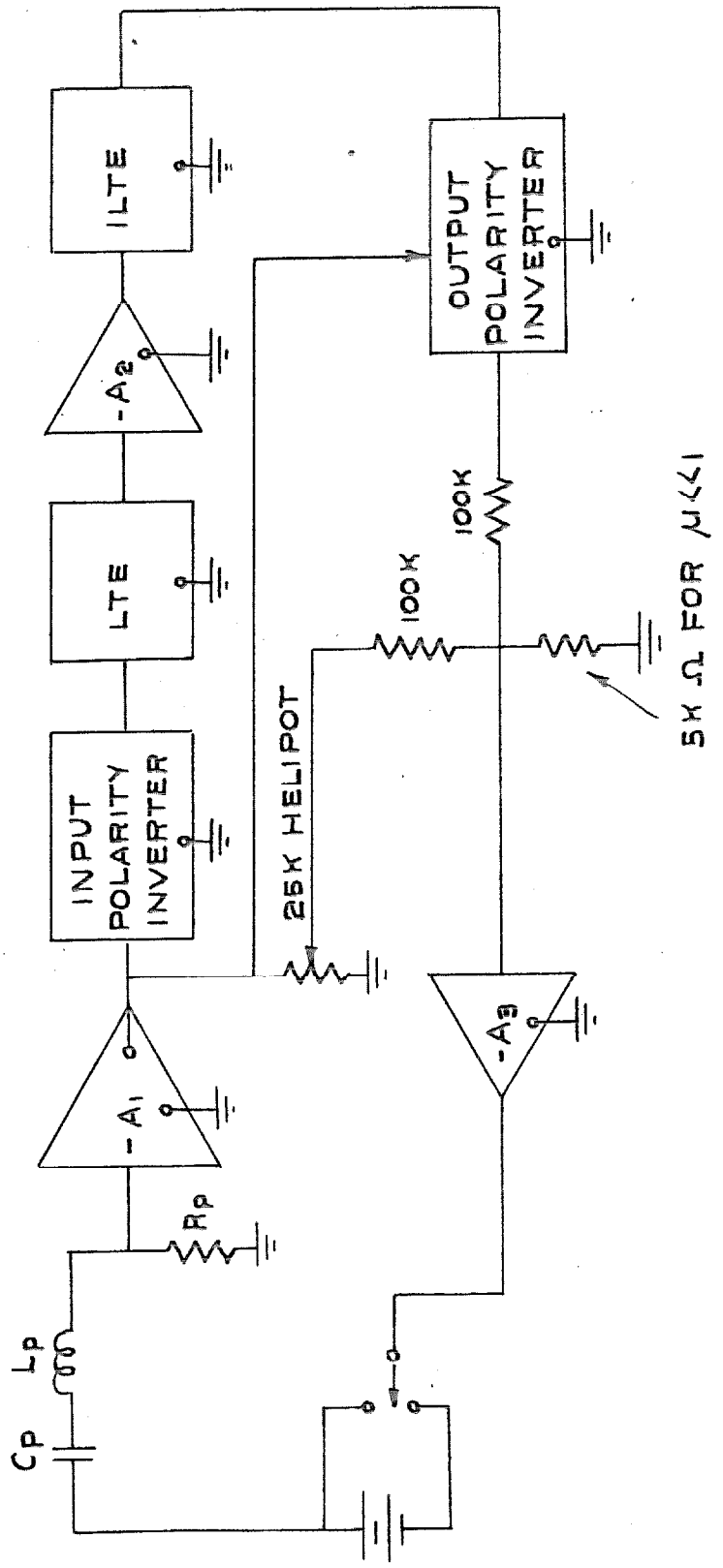

FIG. 59

SOLUTION OF VAN DER POL'S EQUATION

exponent was used. Typical oscillograms for Equation (24) are shown in Figures 60 through 65 with detailed description included in Table V. The similarity of the calculated phase

Table V

Oscillogram Number	Explanation
Fig. 60	x^3 supplied by the computer
Fig. 61	build-up phase trajectory with $\mu = 1$
Fig. 62	build-up of x vs t with $\mu = 1$
Fig. 63	build-up of $\dot{x}$ vs t with $\mu = 1$
Fig. 64	build-up of phase trajectory with $\mu = 8.4$
Fig. 65	build-up of phase trajectory with $\mu = 0.1$

trajectory of Figure 58 and the computer trajectory of Figure 61 demonstrates the good comparison between topological and computer solutions.

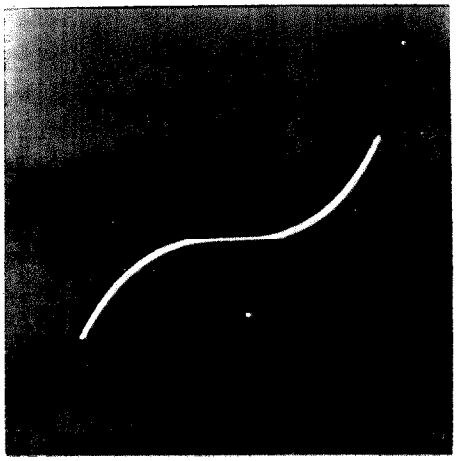

Figure 60

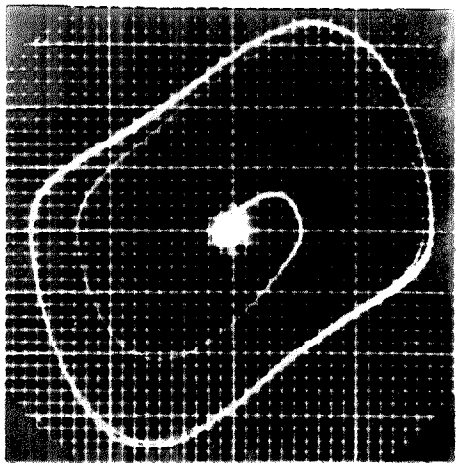

Figure 61

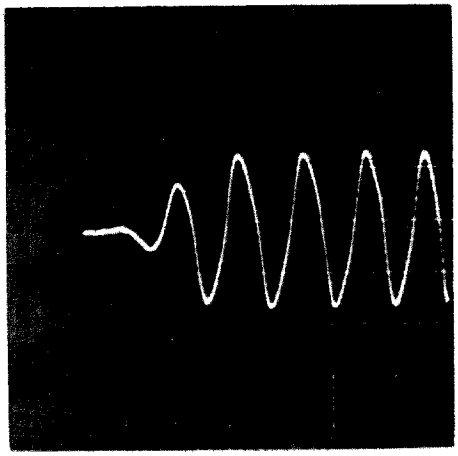

Figure 62

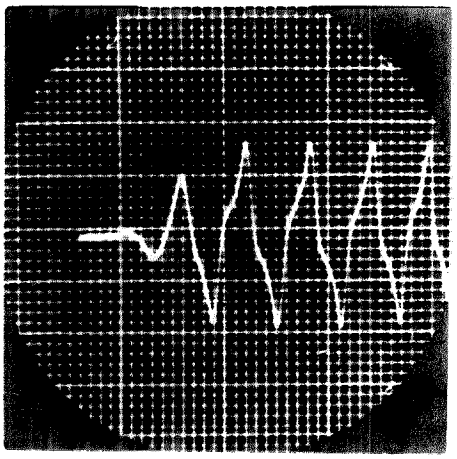

Figure 63

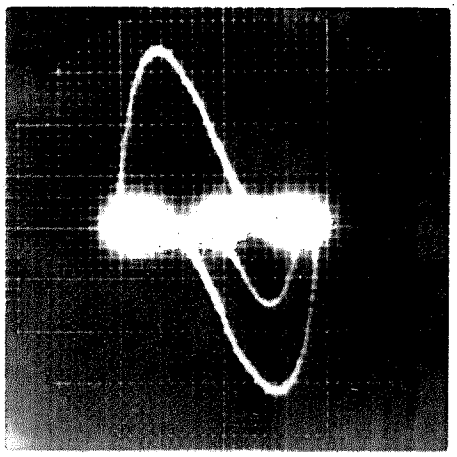

Figure 64

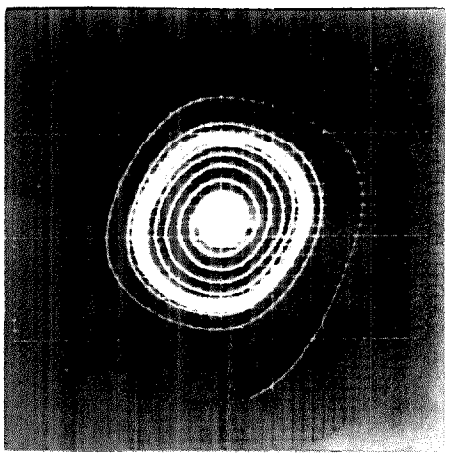

Figure 65

V. VARIOUS FORMS OF NONLINEAR DAMPING

Most engineers are familar with the exponentially damped sinuscidal response of the linear equation

$$\ddot{x} + 2\xi\omega_n\dot{x} + \omega_n^2 x = 0 \tag{25}$$

when a step input is applied. Other more interesting types of response can be obtained if the damping function is made nonlinear. To demonstrate this last thought and at the same time to show the application of the computer as a divider, the equation

$$\ddot{x} + \alpha\left(\frac{1}{\dot{x}+a}\right)^n + x = 0 \tag{26}$$

was shocked with a step function. The block diagram, which is shown on Figure 66, is similar to the multiplier circuits with the omission of the -1 gain amplifier between LTE and ILTE. The output of the LTE is

$$\begin{aligned} e_o &= -n\log_a e_{in} \\ &= \log_a\left(\frac{1}{e_{in}}\right)^n \end{aligned} \tag{27}$$

If the amplifier is omitted, the ILTE output yields a division. With the amplifier in its usual place, the input to the ILTE is

$$-\log_a\left(\frac{1}{e_{in}}\right)^n = \log e_{in}^n \tag{28}$$

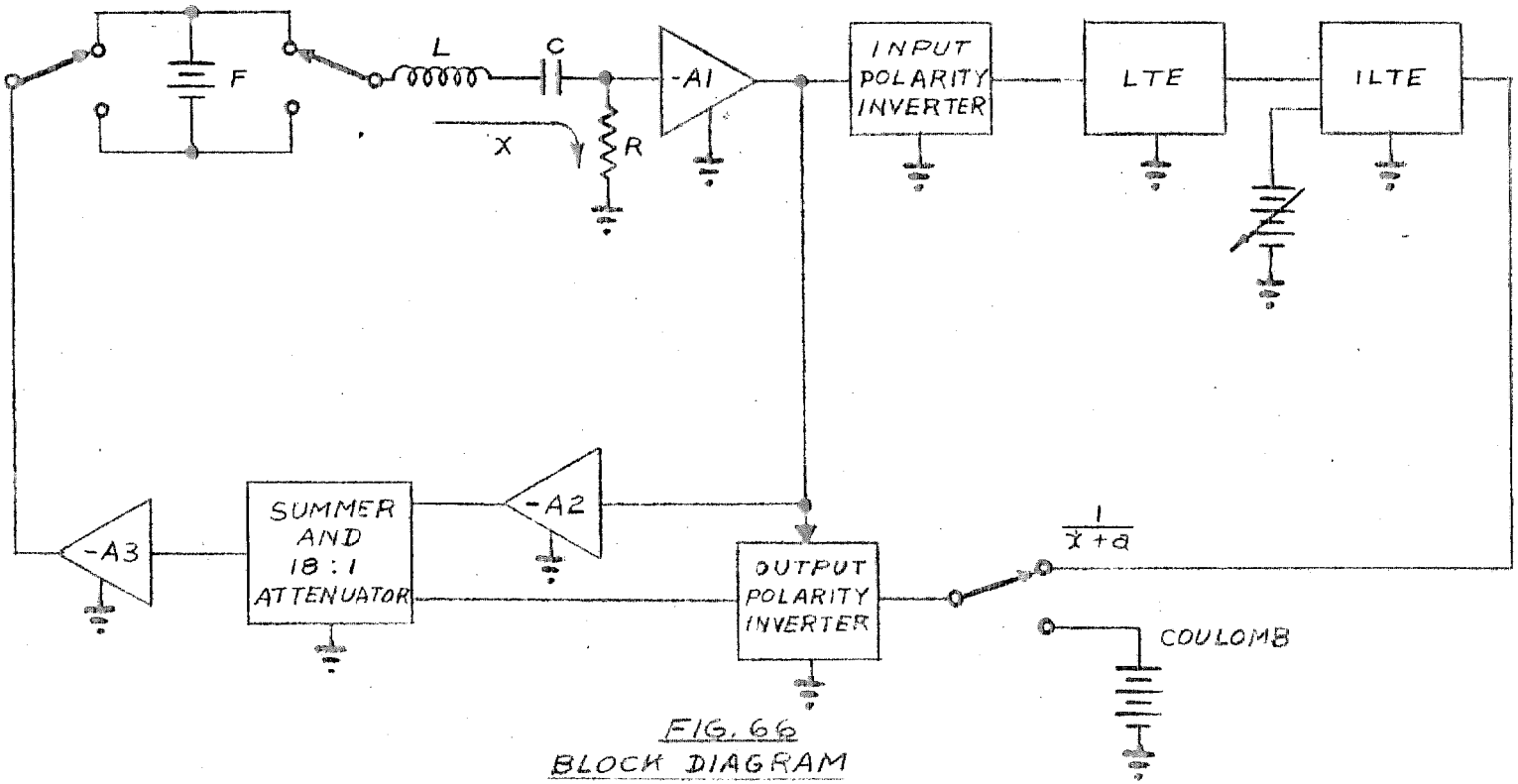

FIG. 66

BLOCK DIAGRAM

SOLUTION OF SIMPLE DYNAMIC SYSTEM

1. WITH COULOMB DAMPING

$$m\ddot{x} + r\dot{x} + C(\dot{x}) + kx = F$$

2. WITH INVERSE DAMPING

$$m\ddot{x} + \frac{b}{\dot{x}+a} + kx = F$$

and hence the equipment multiplies. On Figures 67 through 69 are demonstrated oscillograms of the response of Equation (26) to a step function of voltage. The explanations are included on Table VI. As would be expected from the form of the damp-

Table VI

Oscillogram Number	Explanation
Fig. 67	damping function $\alpha \left(\frac{1}{\dot{x}+a}\right)^n$ vs $\dot{x}$
Fig. 68	phase trajectory with damping function of Figure 67
Fig. 69	x vs t with damping function of Figure 67

ing function, only small decrease in amplitude per cycle is observed until the signal approaches zero, at which time the system damps rapidly.

A second more common type of damping which is often experienced in physical systems is Coulomb friction. The damping force is opposed to the motion ($\dot{x}$), but the magnitude is invariant with velocity. The computer solution, as shown on the block diagram of Figure 66, requires only the output polarity inverter and a battery. From the oscillograms shown on Figures 70 through 72 and explained on Table VII, the response to an applied step function is a linearly damped sinusoid. This response verifies known theory (Cf. Ref. 1, pp. 427-430).

Figure 73 demonstrates a more realistic form of damping function which defies analytic computation. For small values

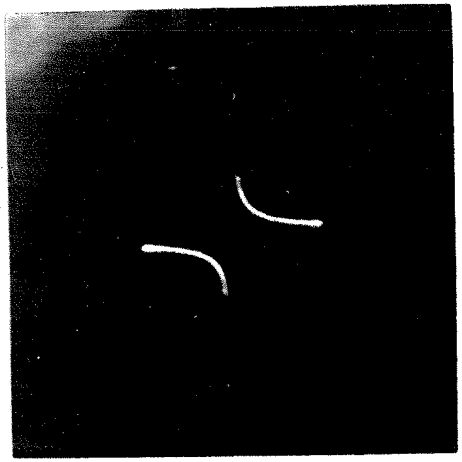

Figure 67

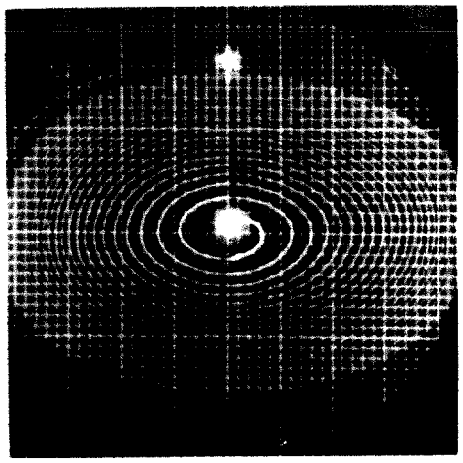

Figure 68

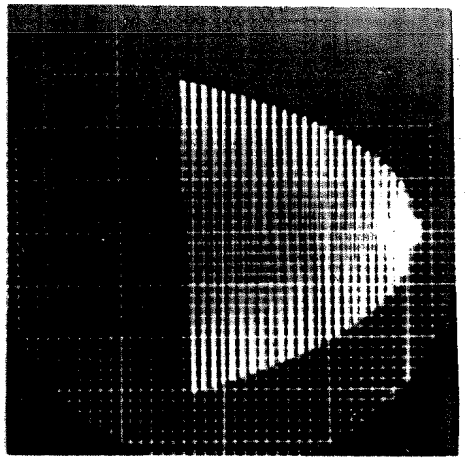

Figure 69

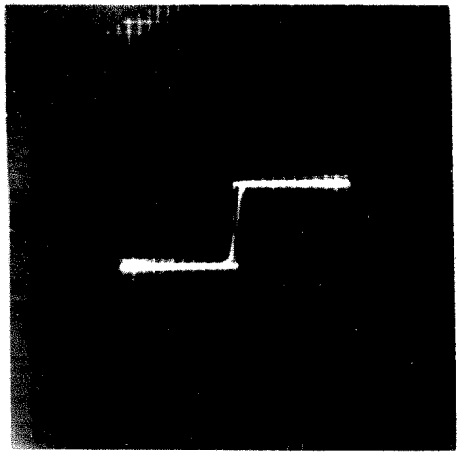

Figure 70

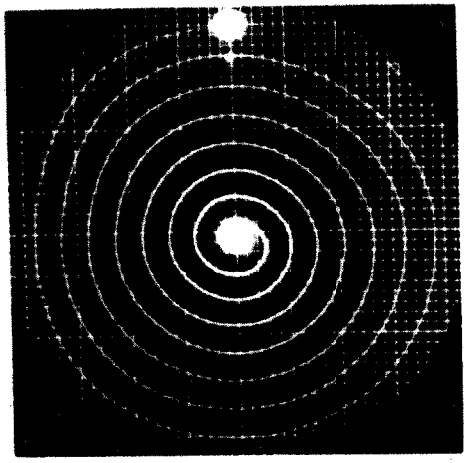

Figure 71

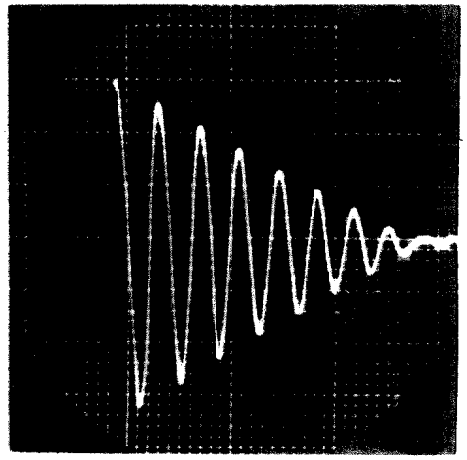

Figure 72

Table VII	
Oscillogram Number	Explanation
Fig. 70	damping function $B(\dot{x})$ vs $\dot{x}$
Fig. 71	phase trajectory with damping function of Figure 70
Fig. 72	x vs t with damping function of Figure 70

of $\dot{x}$ the phenomenon of stiction is exhibited. After the body is in motion, the damping increases with the velocity. A combination of these types, $\frac{1}{\dot{x}+a}$, Coulomb, and viscous damping, could produce a function which approximates that of Figure 73 quite closely.

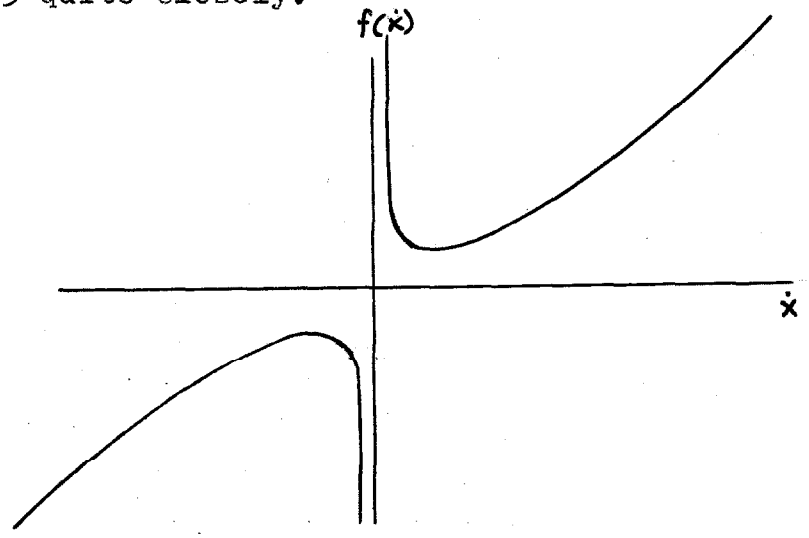

Figure 73. Common Damping Function

VI. IMPROVED RESPONSE OF A PNEUMATIC SERVO SYSTEM

Because of over-all system requirements, it is not always practical to improve the response of a control system by adding functional feedback. In these cases, improved response may result through variation of the forward-loop parameters. To demonstrate the use of the computer in this application a pneumatic autopilot was studied. The parameters of the actual system were measured, and the analog was solved on the computer. Figure 74 demonstrates a typical pneumatic autopilot which positions a control surface as a function of the applied voltage. The error signal, formed by subtracting a function of output angle ϕ from the input, is amplified with a linear dc amplifier of gain K. The amplifier is assumed to have no appreciable time delays in the frequency range of interest. The output of the amplifier drives a rotary solenoid which, in turn, positions a pneumatic valve. The position of this transfer valve directs the air into one of two cylinders of a double-acting piston. The details of the mechanical arrangement are shown in Figure 75. The actuator is connected through a series of mechanical linkages to the controlling surface of the aircraft being piloted. Feedback from the output position of the control surface is provided with a potentiometer. Since aerodynamic considerations dictate the form of the feedback β, the designer has only the forward-loop quantities at his disposal. In the particular problem at hand, the physical characteristics of the transfer valve

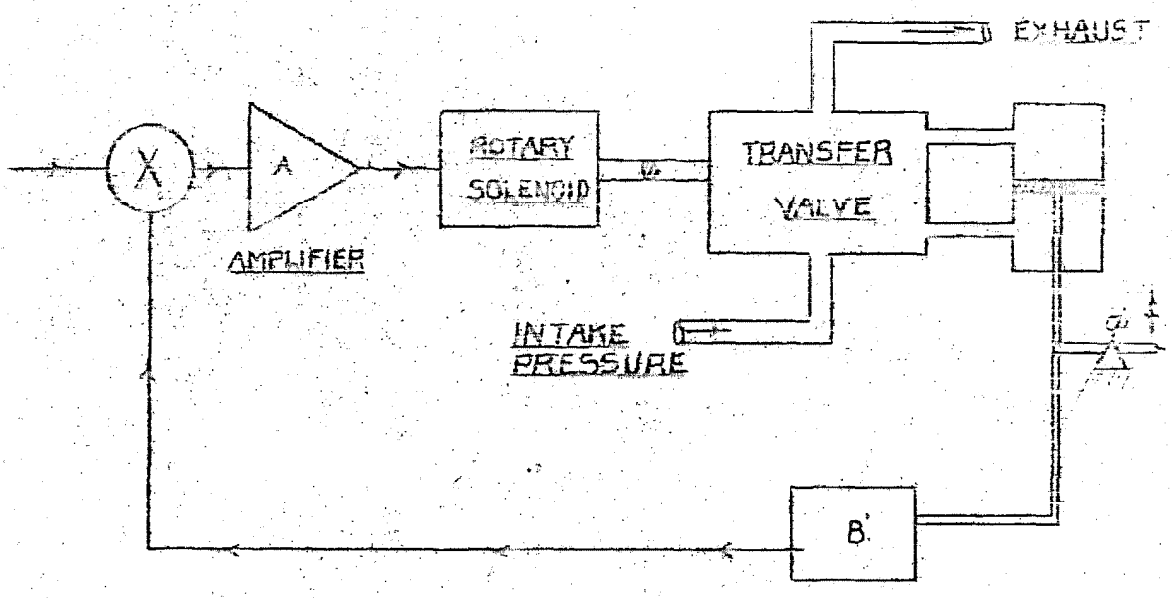

FIGURE 74 BLOCK DIAGRAM FOR PNEUMATIC AUTOPILOT

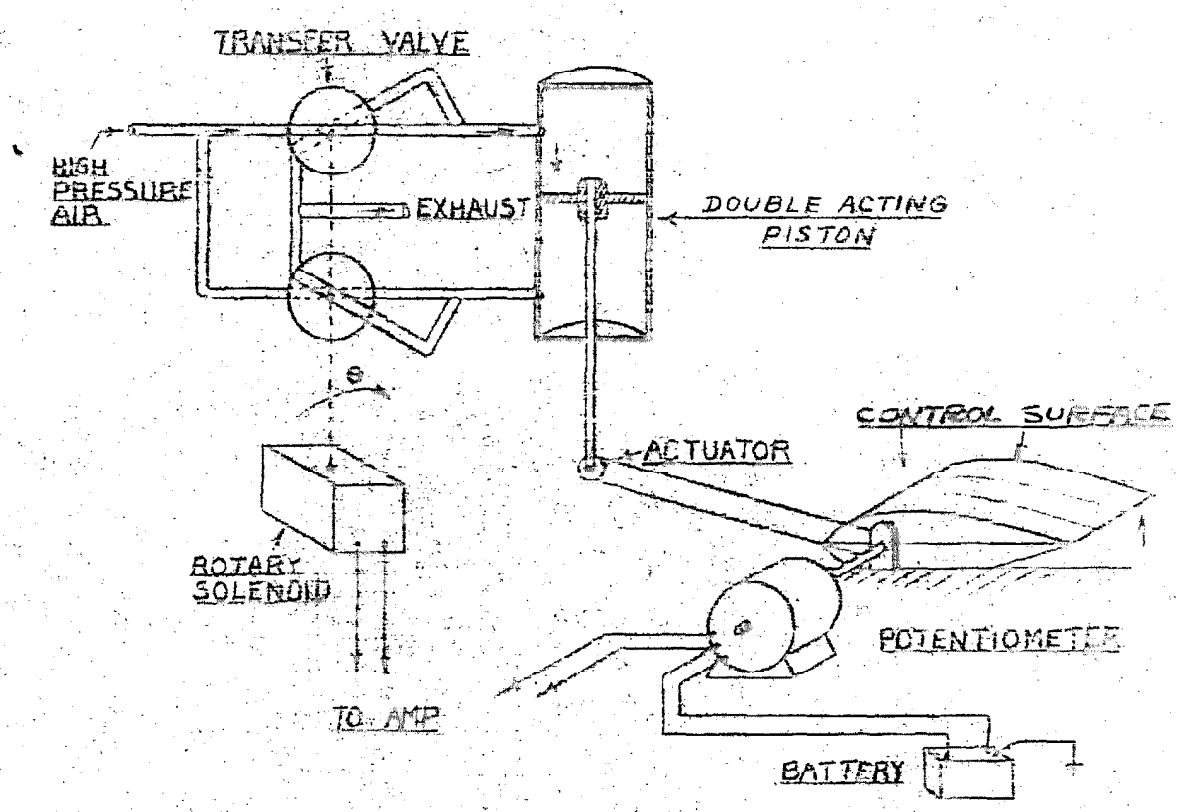

FIGURE 75 MECHANICAL ARRANGEMENT FOR PNEUMATIC AUTOPILOT

are partly available for improved response. The computer solution will determine the best values of these characteristics in terms of improved servo performance.

In most pneumatic valves, it is possible to obtain linear operation over only a relatively limited region, and for large excursions of the valve it can be shown (Cf. Ref. 12) that the restoring forces are of the form

$$F_R = aT_k(\theta) + bT_b(\dot{\theta}) \tag{29}$$

where θ is the angular position of the valve.

The characteristics of the particular system considered were measured and, following true to form, resulted in the forces given by the expressions

$$aT_k(\theta) = 3.75 \sin 8\theta \text{ oz.in.}$$

$$bT_b(\dot{\theta}) = \left[+8.725 + .1883\,\dot{\theta}^3\right] \times 10^{-2} \text{ oz.in.} \quad \dot{\theta} > 0 \tag{30}$$

$$= \left[-8.725 + .1883\,\dot{\theta}^3\right] \times 10^{-2} \text{ oz.in.} \quad \dot{\theta} < 0$$

The $T_k(\theta)$ represents the restoring torque (on the rotary part of the valve) which is caused by the flow of high-velocity air past restricted orifices. In the particular system studied here, experiments showed that for full delivered power the valve travel was limited to the linear part of the sinusoidal curve. Hence it was concluded that this torque could be linearized, with no appreciable error, to the form

$$a T_k(\theta) = 3.75\,(8)\,\theta = 30\,\theta \qquad (31)$$

The second torque $T_b(\dot{\theta})$ has the form of an energy dissipation term caused by Coulomb damping plus approximate cubic damping, both resulting from aerodynamic forces. The experimental curves for this torque are plotted on Figure 76 where the approximate analytical curve is also included. Since the important part of this problem is the method of solution, the details of testing the physical system are omitted.

Curves of electric motor and amplifier response show that as a first approximation these characteristics can be considered linear, and the transfer functions taken to be constant. The polar moment of inertia J was calculated to be 2.64×10^{-4} in. oz. sec^2. The collected data result in the following differential equation relating input voltage e to output position θ of the transfer valve

$$J\frac{d^2\theta}{dt^2} + T_B\left(\frac{d\theta}{dt}\right) + T_k(\theta) = K_A K_m e \qquad (32)$$

where K_A is the gain of the amplifier = e_{in}/i_{out} = volts/amp, and K_m is the transfer function of the electric motor = i_{in}/torque out = amp/in.oz.

Combining these expressions, one obtains

$$2.64\times10^{-4}\ddot{\theta} + \left[(\pm)\,8.725 + 0.1883\,\dot{\theta}^3\right]10^2 + 30\,\theta = K_a K_m e(t) \qquad (33)$$

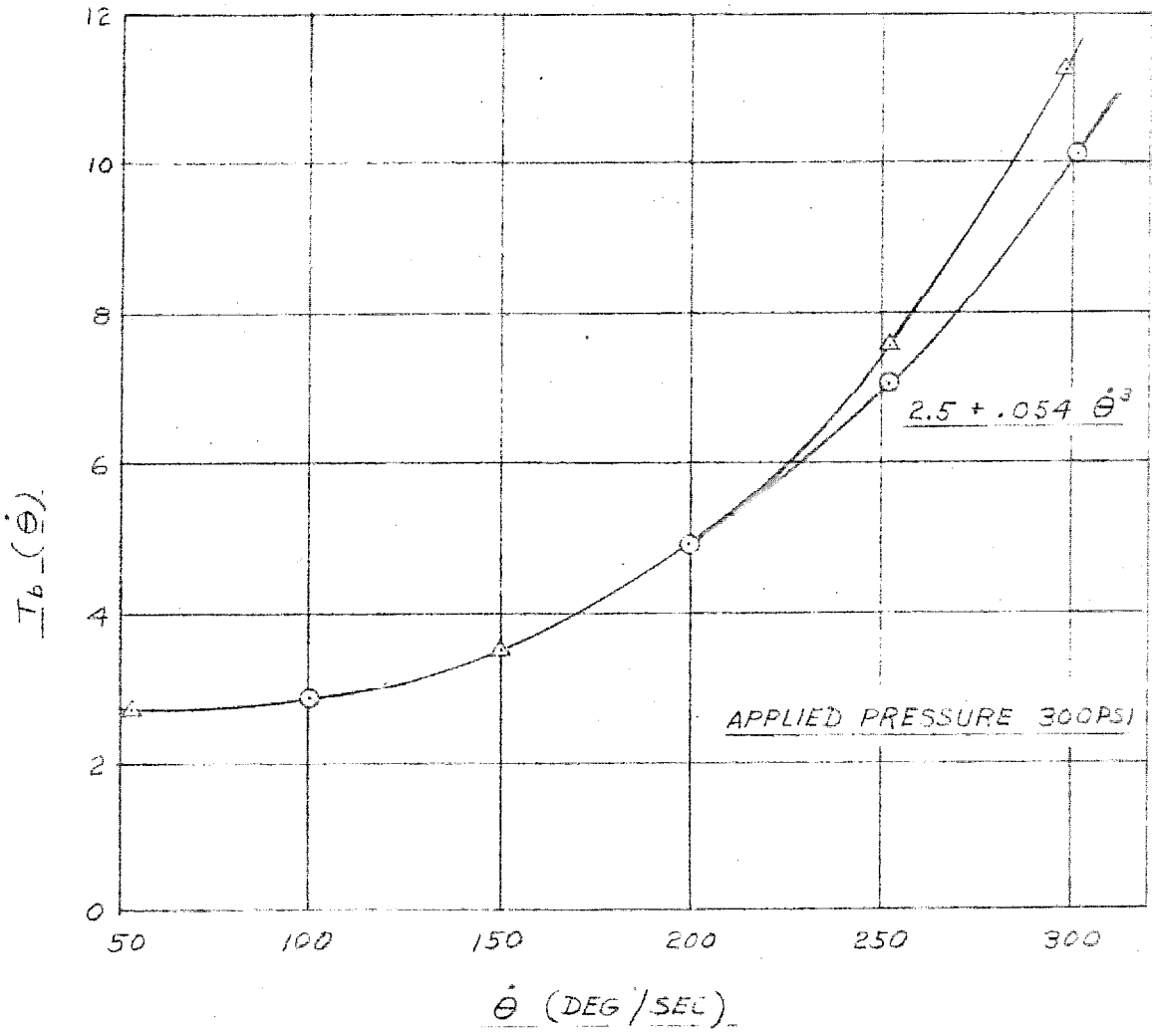

FIGURE 76 AVERAGE $T_b(\dot{\theta})$ VS $\dot{\theta}$

where the symbol ($\pm$) means to take the sign which is appropriate ($+$ for $\dot{\theta} > 0$ and $-$ for $\dot{\theta} < 0$).

Before the computer solution of Equation (32) is attempted, the transient solution is studied on the phase plane. Dividing through by 2.64×10^{-4} and setting $e(t) = 0$, one obtains

$$\ddot{\theta} + \left[(\pm)\, 3.3 + 0.071\, \dot{\theta}^3\right] 10^2 + 1.42 \times 10^4\, (8\theta) = 0 \qquad (34)$$

Defining a new variable $y = \dot{\theta}$ and solving for $\dot{y}$, the following expression results:

$$\dot{y} = -\left[(\pm)\, 3.3 + 0.071\, y^3\right] 10^2 - 11.36 \times 10^4\, \theta = 0 \qquad (35)$$

Forming the slope $\lambda = (dy/d\theta) = \dot{y}/\dot{\theta}$, one has

$$\lambda = \frac{-\left[(\pm)\, 3.3 + 0.071\, y^3\right] 10^2 - 11.36 \times 10^4\, \theta}{y} \qquad (36)$$

The isoclines, or lines of constant slope, are found by solving for θ in terms of y, with λ as a parameter. With a slight amount of algebra, Equation (36) can be rewritten as

$$\theta = \frac{+\,y\,(\lambda + 7.1\, y^2) + (\pm)\, 330}{11.36 \times 10^4} \qquad (37)$$

Following the usual procedure (except this time a sheet of 17x27-inch paper was used for the original), the isoclines

and phase trajectories were plotted. The resulting curve, which is shown on Figure 77, has some extremely interesting features. Notice that to demonstrate the interesting effects near the origin, the scale of $\dot{\theta}$ was made 500 times as large as that of θ. The system exhibits the ordinary character of damped oscillating motion for larger values of θ and $\dot{\theta}$, but the motion suddenly stops wherever a trajectory tries to pass between the two focal points. This fact is borne out also from the clockwise direction which the trajectories must travel; hence the one trajectory which appears to pass between these focal points at $\theta = -0.0005$ radian is, in reality, two trajectories both of which terminate at the same point. Physically this plot has great significance since, because of the dry friction in the region between the focal points, the restoring force is less than the dry friction. Hence, whenever the velocity passes through zero, all motion ceases, and the rotating pintle suddenly sticks.

The computer solution for this problem is shown in the block diagram of Figure 78. The equation satisfied by the computer is of the form

$$L\ddot{q} + R\dot{q} + \frac{1}{C}q + f(\dot{q}) = 0 \qquad (38)$$

Making the following substitutions

$$q = a\,\phi \text{ and } t = b\tau$$

one has

$$L\frac{a}{b^2}\phi'' + R\frac{a}{b}\phi' + f\left(\frac{a}{b}\phi'\right) + \frac{a}{C}\phi = 0 \qquad (39)$$

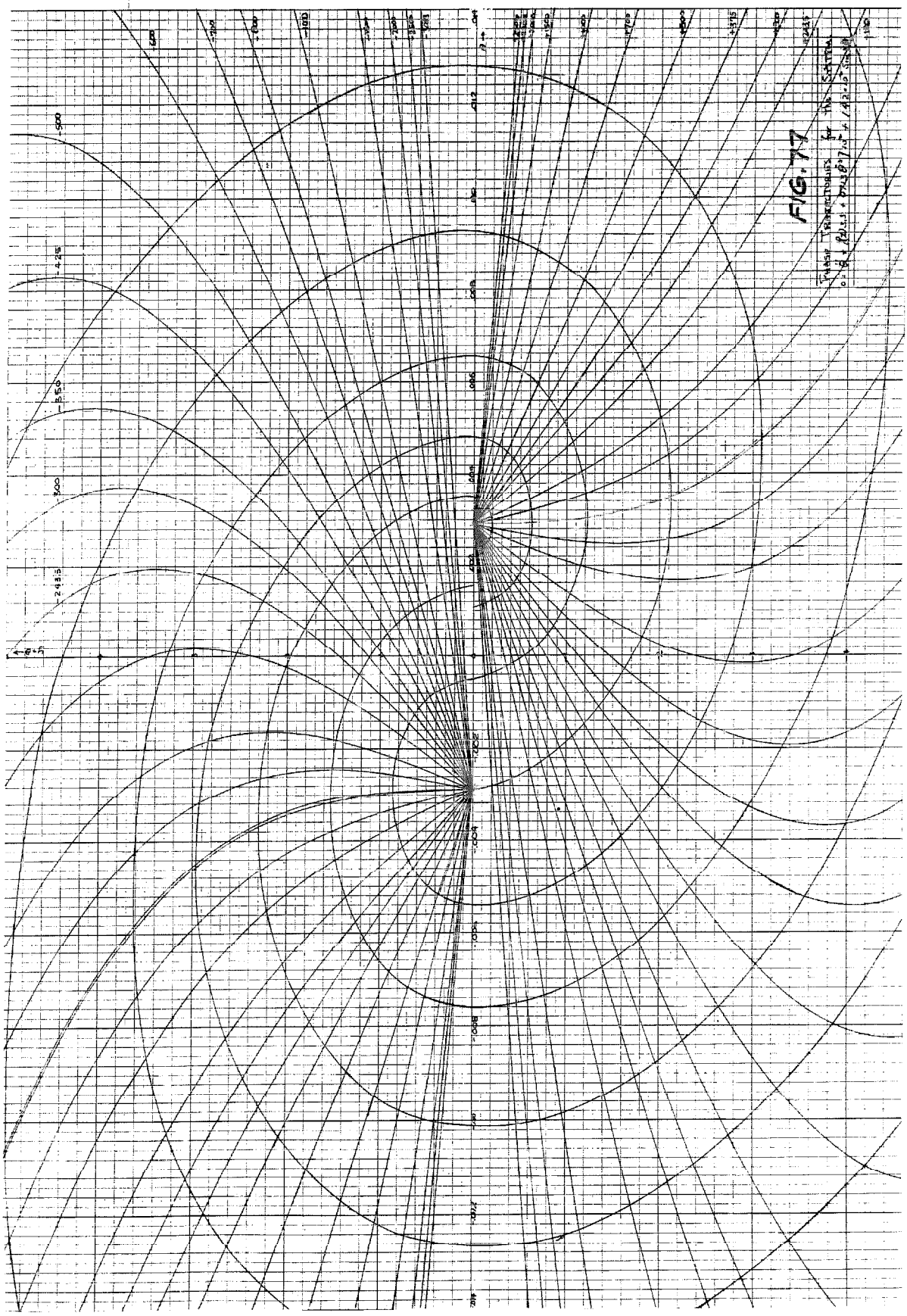

FIG. 77

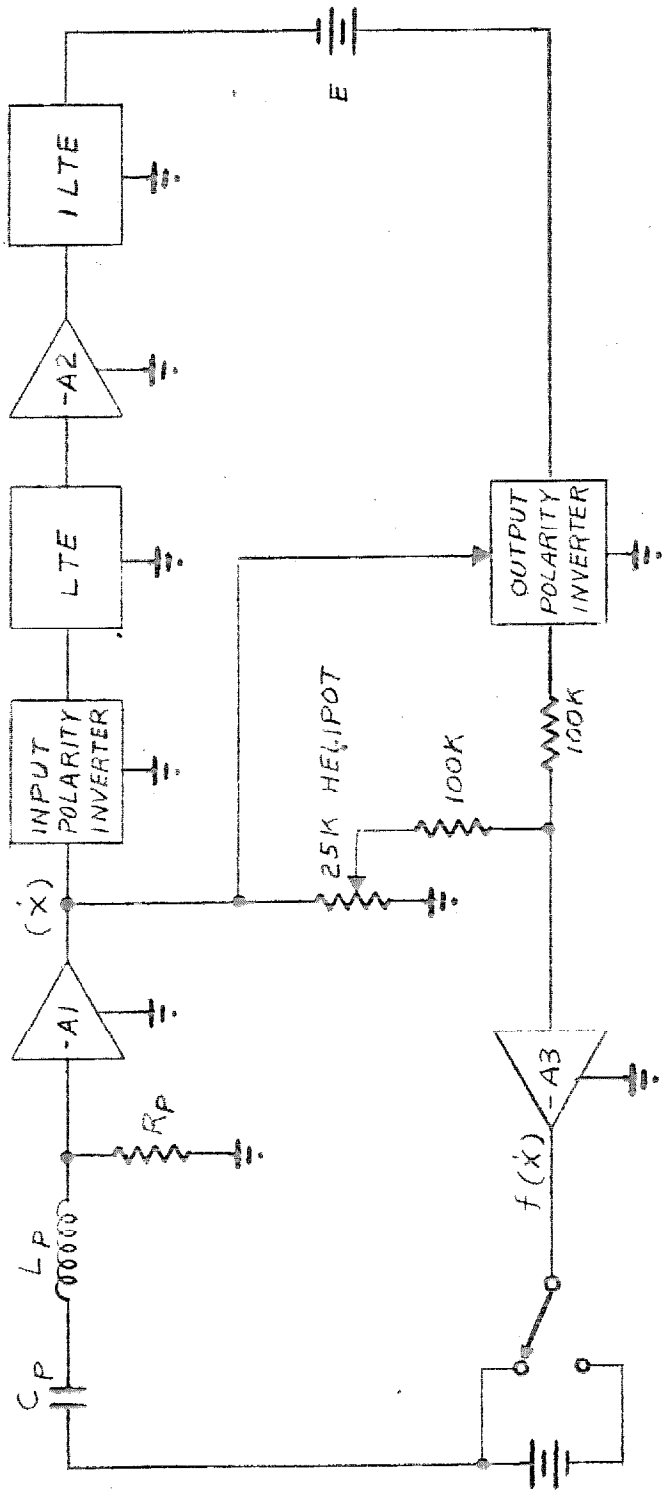

FIG. 78
BLOCK DIAGRAM
PNEUMATIC SERVOMECHANISM PROBLEM

where primes indicate differentiation with respect to τ. The function $f(a\phi'/b)$ is supplied by the computer and has the form

$$f\left(\frac{a}{b}\phi'\right) = (\pm)\alpha + \beta\left(\frac{a}{b}\right)^3 \phi'^3 \qquad (40)$$

Upon substituting Equation (40) in Equation (39), one obtains the analogous equation

$$\left(\frac{La}{b^2}\right)\phi'' + \left(\frac{Ra}{b}\right)\phi' + \left(\frac{a}{c}\right)\phi + (\pm)\alpha + \beta\left(\frac{a}{b}\right)^3 \phi'^3 = 0 \qquad (41)$$

A second negative-gain amplifier is used to insert enough negative resistance to cancel the undesirable second term of Equation (41), which operation results in the following equation:

$$\gamma\left(\frac{La}{b^2}\right)\phi'' + (\pm)\gamma\alpha + \gamma\beta\left(\frac{a\phi'}{b}\right)^3 + \gamma\frac{a}{c}\phi = 0 \qquad (42)$$

where both sides have been multiplied by γ, a third-scale factor. Equation (42) has the same form as Equation (34) and, with proper choice of constants, represents the analogy for the pneumatic autopilot.

Since the present system has been designed and existing constants have been predetermined, the scaling problem becomes more difficult. A fair number of trial-and-error computations were carried out before the problem was put on the computer since the range of the computer must be matched to the desired numerical values of Equation (42). The results of this computation are summarized in Table VIII, where numerical values of all constants are given. The

computer constants were set in on the basis of the values of Table I, but as a check the nonlinear function

$$y = m(\phi')^3 + (\pm)n \tag{43}$$

was verified, and minor additional adjustments were necessary to obtain the curve of Figure 79. This curve was obtained by applying a sinusoidal signal to the AFDEV. The output was viewed on the y axis, and the input was viewed on the x axis of the oscilloscope. On this curve the horizontal-axis gain is 10^{-3} times the vertical-axis gain. Two sample phase trajectories for a series of initial values are given in Figures

Table VIII

$\gamma\alpha$	$= 330$	$\gamma = 165$
$\frac{a}{b}^3\gamma\beta$	$= 7.1$	$\alpha = 2$
$\frac{\gamma La}{b^2}$	$= 1$	$k = 10^{-3}$
$\frac{a\gamma}{c}$	$= 11.4$	$\beta = 6 \times 10^6$
y	$= m(\phi')^3 + (\pm)\, n$	$a = 0.276 \times 10^{-2}$
	$= mk^3 \dot{\xi}^3 + (\pm)\, n$	$b = 1.43$
	$= \frac{6\times10^{-3}}{k^3}\phi^3 + (\pm)2$	$c = 4\ \mu f$
		$L = 4.5\ h$

80 and 81. Each oscillogram was exposed many times, one for each initial condition. This procedure results in an overexposure near the origin, but careful examination verifies

that, although blurred, the stiction line does exist. Good comparison results between these computer transient solutions and topological solutions of Figure 77.

With the existing closed-loop system established on the computer, the constants of the forward loop were varied so as to improve the speed of response. In this operation the x vs t transient curve was used for comparison rather than the phase trajectory because it is necessary that an accurate time base be established. The oscillogram of Figure 82 shows the response of the original system to a step-voltage input. The zero of the trace is marked by the dot at the lower right-hand corner of all x vs t photographs. By varying only the spring constant, one is able to improve the response to that of Figure 83. The reciprocal capacity is analogous to the mechanical spring constant, and the same step function was applied in both cases. Notice that the sweep time in Figure 83 is one-fourth that of Figure 82. Hence, with an increase of spring constant by 16, the speed of response is about four times as fast.

As a final variable quantity the Coulomb friction was altered. The analog of the Coulomb friction term is the battery voltage E. With the same spring constant as that of Figure 83, the Coulomb damping was increased by 3/2, and the response to the same step input is that shown in Figure 84. Again notice that the sweep time in Figure 84 is one-fourth as great as that of the original system shown in Figure 82.

The problem is concluded with the x vs t curve of Figure

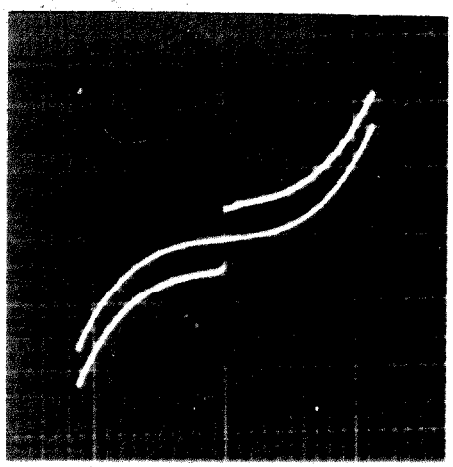

Figure 7c

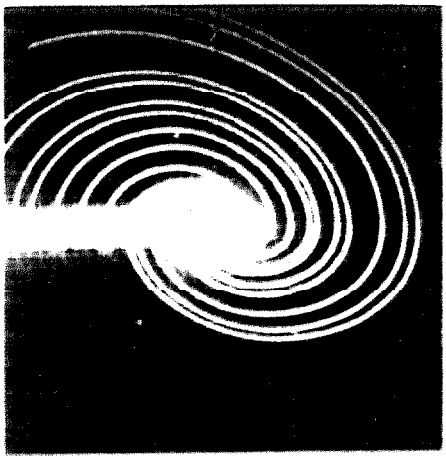

Figure 8C

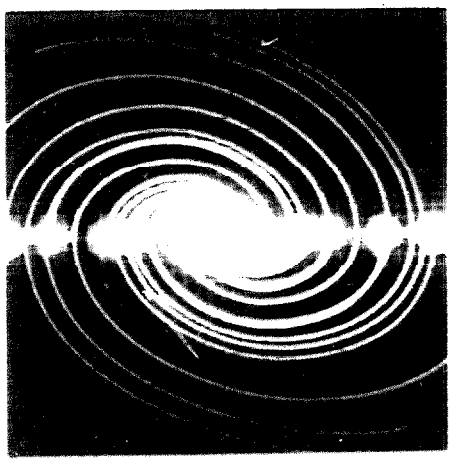

Figure 81

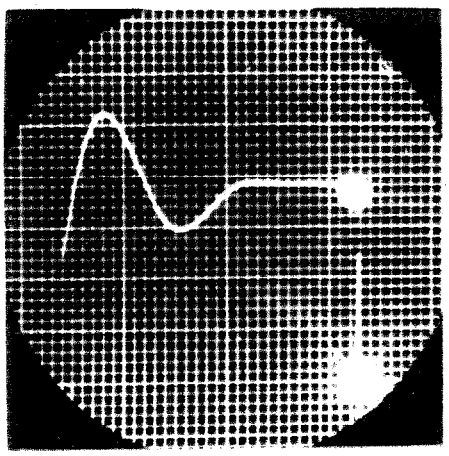

Figure 8[illegible]

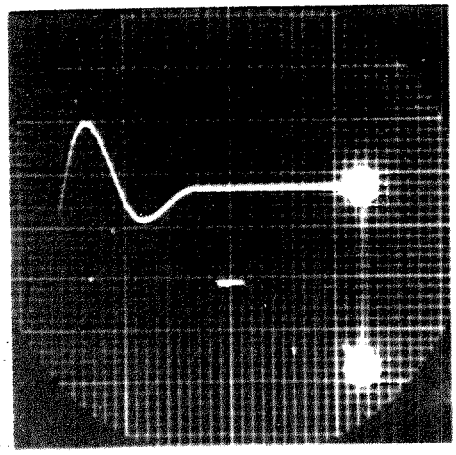

Figure 8'

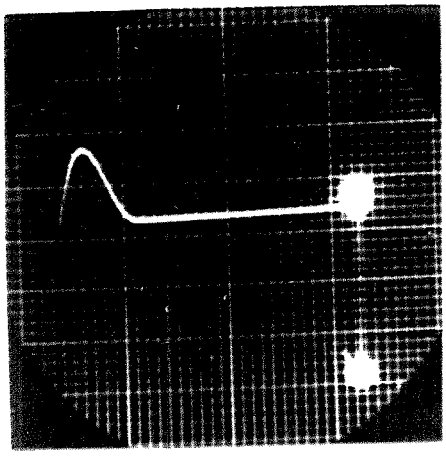

Figure 84

84 as the improved system. The author does not believe that an optimum system has been found since the number of possibilities is so large. This system has been improved in a practical manner since the improvements can be mechanized with little difficulty. Further improvement might result if nonlinear feedback be used in addition to the changes already made, but the mechanization of the resulting nonlinear expressions might prove more tedious than the design would allow. Section V uses functional feedback to obtain an improved response.

VII. IMPROVED SERVO RESPONSE THROUGH NONLINEAR FEEDBACK

In the design of closed-loop systems, one is often faced with unavoidable nonlinear operation of certain forward-loop elements. Amplifier saturation, gear-train backlash, brush-friction dead space, and controller-force saturation are just a few typical examples of undesirable nonlinearities. By using a large amount of linear feedback, one is able to improve the response; however, with the use of nonlinear feedback functions, a greater range of possibilities is made available. Improvement of system performance might be possible if a method of design of the feedback function were known. The electronic computer provides this method. An analog of the open-loop system is established, and the AFDEV supplies the feedback function. The unavoidable nonlinearities are obtained with various diode arrangements or with a second AFDEV.

To demonstrate the use of the AFDEV in this application, the simple position servomechanism of Figure 85 was considered. The system consists of two selsyns, an amplifier, a two-phase induction motor, an inertia load, and a nonlinear function generator. The performance of the induction motor driving an inertia load is approximated by the equation

$$T = k_t (e_i - k_\omega p \theta_m) \tag{44}$$

where e_i is the applied voltage, T the produced torque, and θ_m the output shaft position. For a pure inertia load, the

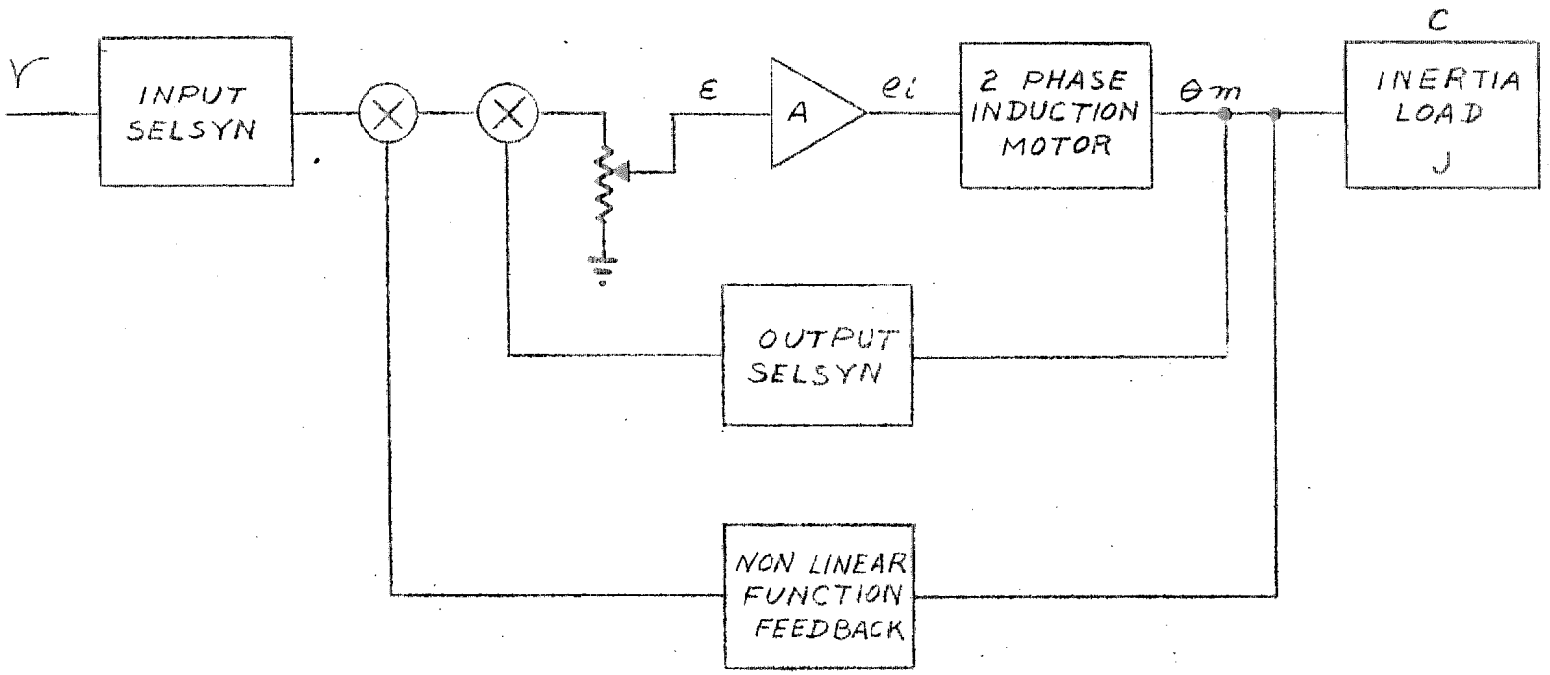

FIG. 85
BLOCK DIAGRAM
SIMPLE POSITION SERVOMECHANISM

torque can be expressed by

$$T = Jp^2 \theta_m \tag{45}$$

The amplifier transfer function is approximated by a one-delay expression of the form

$$e_i = \frac{A\varepsilon}{(\tau_a p + 1)} \tag{46}$$

The selsyns and amplifier produce a voltage at the motor terminals given by

$$e_i = \frac{k_s A (r-c)}{(\tau_a p + 1)} \tag{47}$$

where k_s is the selsyn sensitivity in volts/radian, and A is the zero-frequency amplifier gain. The performance of the system can be approximated by the differential equation obtained by combining Equations (44), (45), and (46) as follows:

$$\theta_m = c = \frac{A\varepsilon}{p(\tau_a p + 1)\left(\frac{J}{k_t} p + \frac{k_\omega}{k_t}\right)} \tag{48}$$

This expression can be simplified

$$C = \frac{K\varepsilon}{P(\tau_a P+1)(\tau_m P+1)} \tag{49}$$

where $K = Ak_t/k$ and $\tau_m = J/k_\omega$.

Figure 86 shows the electric analog of the open-loop system. Writing the circuit equations for this system, one has

$$q = \frac{+A_1 \frac{1}{PC} e}{(R_1+\frac{1}{PC_1})(LP^2+R_2P)} \tag{50}$$

which can be simplified to

$$q = \frac{K_1 e}{P(\tau_1 P+1)(\tau_2 P+1)} \tag{51}$$

where $\tau_1 = R_1C_1$, $\tau_2 = L/R_2$, and $K_1 = A_1/R_2$. Comparison of Equations (49) and (51) demonstrates the analogy. A list of analogous quantities is included in Table IX.

To provide the necessary position feedback, the voltage across $R_2(=R_2pq)$ is integrated; the result is

$$e_2 = -\frac{R_2}{R_3C_2}q = -kq$$

Additional velocity and position signals are available for the AFDEV from the designated points in the analogy. The

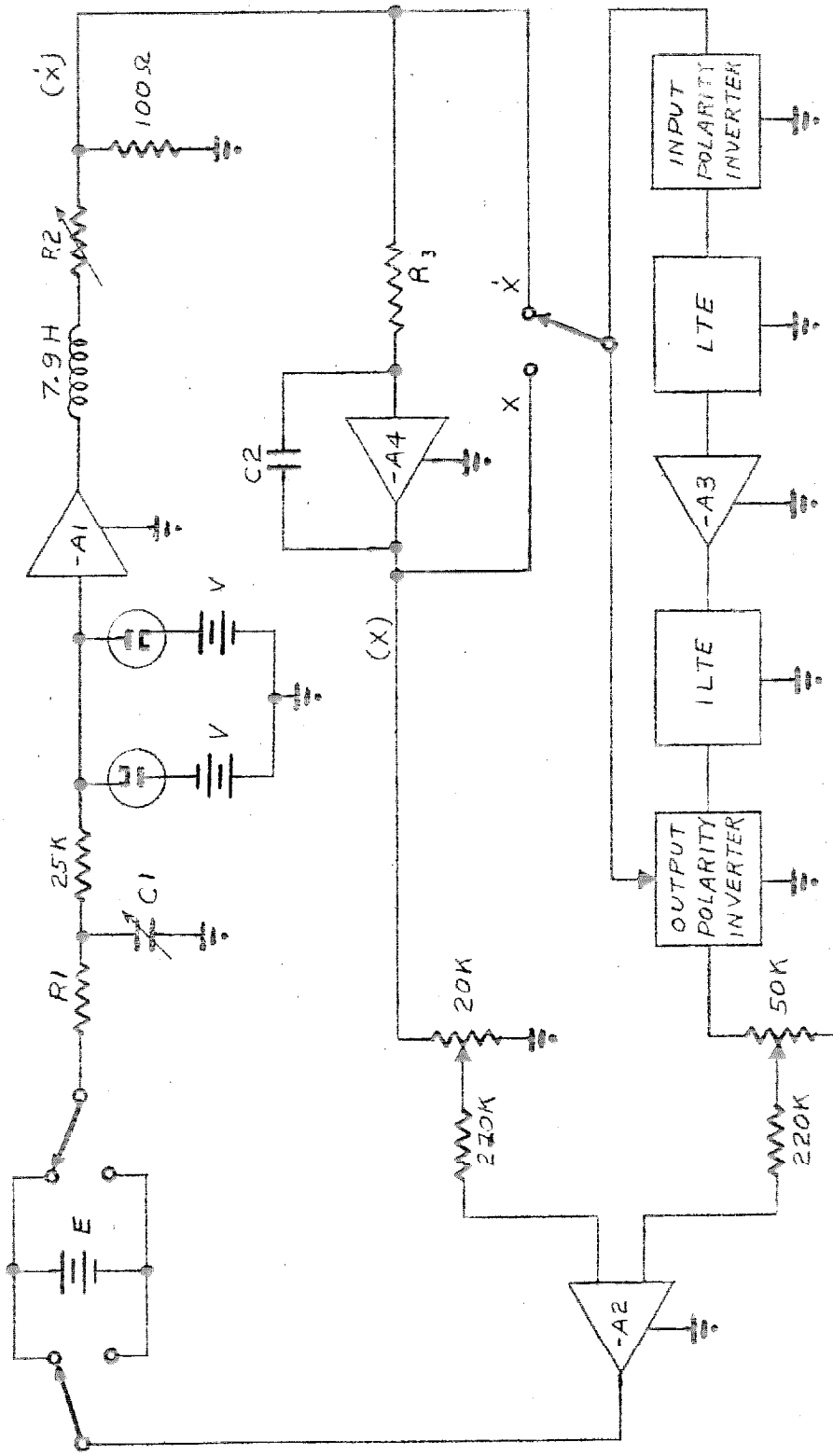

FIG. 86
BLOCK DIAGRAM
ANALOG COMPUTER SOLUTION OF CONTROL SYSTEM WITH SATURATED AMPLIFIER & NON LINEAR RATE OR POSITION FEEDBACK

position feedback plus any function feedback (of x or $\dot{x}$) are summed and supplied to the main loop through two negative-gain amplifiers ($-\Sigma$ and $-A_2$). The voltage fed back has the form

$$e = q + f(q) + g(pq) \tag{52}$$

and the system equation can be written

$$q = \frac{K_1\{V_0 - A[q + f(q) + g(pq)]\}}{p(\tau_1 p+1)(\tau_2 p+1)} \tag{53}$$

Equation (53) has the same form as Equation (47) when f = g = 0.

Table IX

Mechanical System	Electrical System
x	q
$\dot{x}$	pq
$\ddot{x}$	p^2q
$\tau_1 = R_1C_1$	τ_a
$\tau_2 = L/R_2$	$\tau_m = J/km$

Consider now that the control system has an amplifier which saturates; i.e., the gain is constant up to a certain value and then becomes zero. The characteristic is shown in Figure 87. The saturating amplifier finds its analogy in

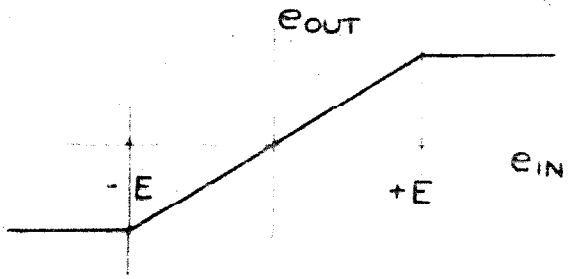

FIGURE 87 SATURATED AMPLIFIER CHARACTERISTIC

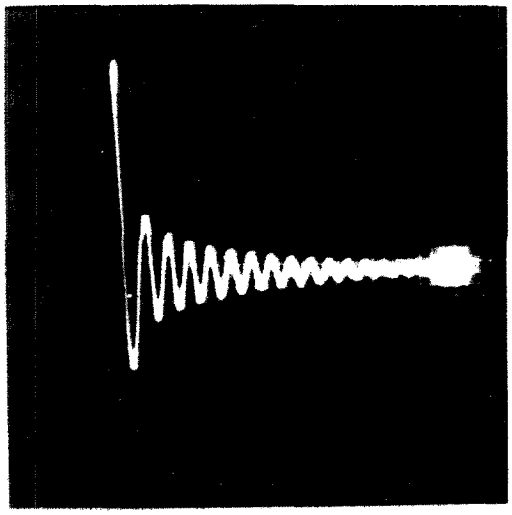

Figure 88

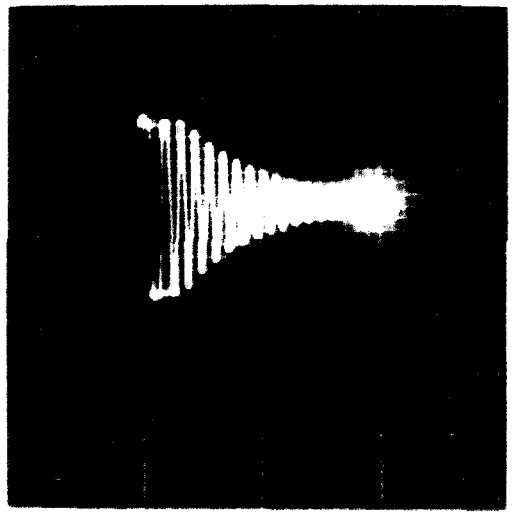

Figure 89

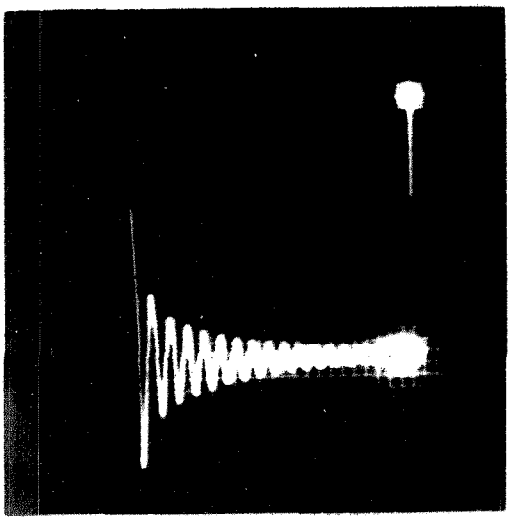

Figure 90

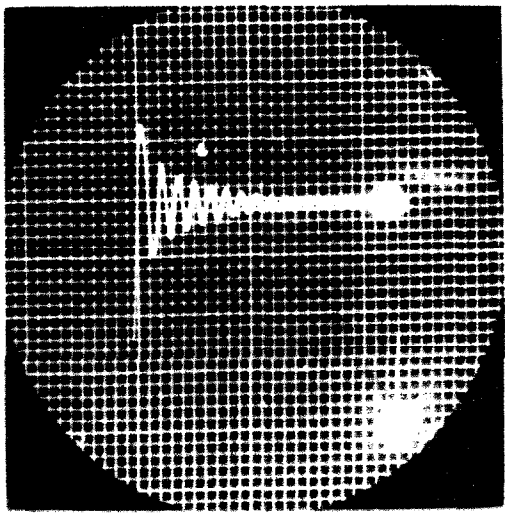

Figure 91

Figure 86 in the form of A_1, which has two diodes at its input. As long as the potential is less than V in magnitude, the gain is constant. When the amplifier voltage reaches V, one of the diodes conducts, producing the saturation curve. The oscillograms of Figures 88 through 91, explained in Table X, demonstrate the effects on the system. Notice that,

Table X

Oscillogram Number	Explanation
Fig. 88	input to saturated amplifier (top of 1μf capacitor)
Fig. 89	output of saturated amplifier
Fig. 90	position feedback signal with the loop open
Fig. 91	closed loop x vs t with only position feedback

although the output of amplifier A_1 is definitely cutting off (Cf. Figure 89), the momentum of the energy storage devices produces a fairly sinusoidal output (Cf. Figure 91).

Before the functional feedback is presented, ordinary rate feedback was used to improve the response of the system. The oscillogram of Figure 91 shows the zero feedback case, and Figures 92 through 97 list several improved curves which were obtained with increasing amounts of rate feedback. Both negative and positive rate feedback are shown, and the explanation of the photographs is given in Table XI. The amount of positive rate feedback necessary to establish zero

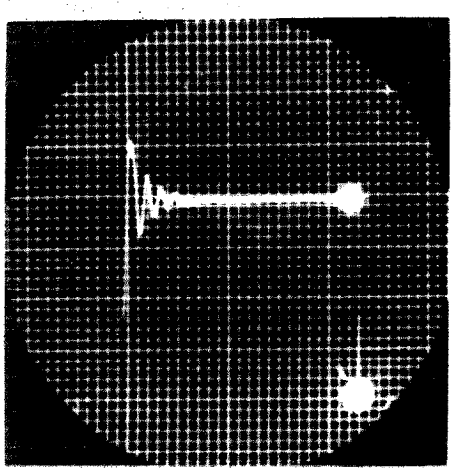

Figure 92

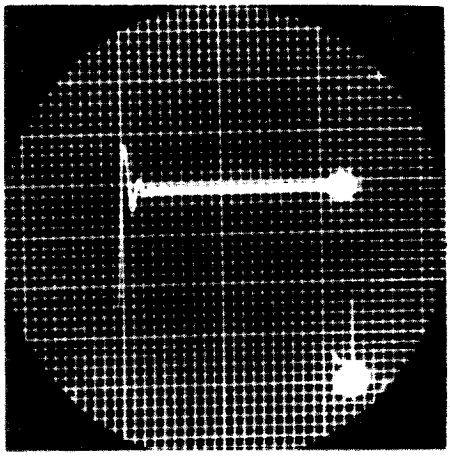

Figure 93

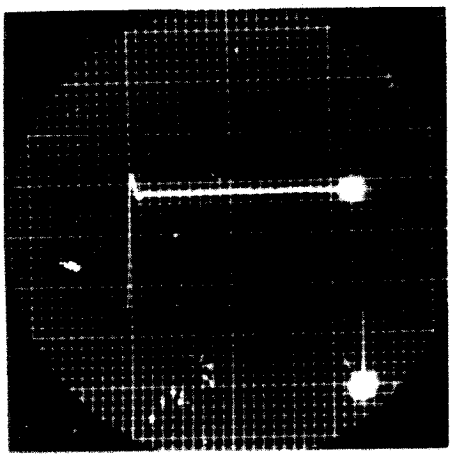

Figure 94

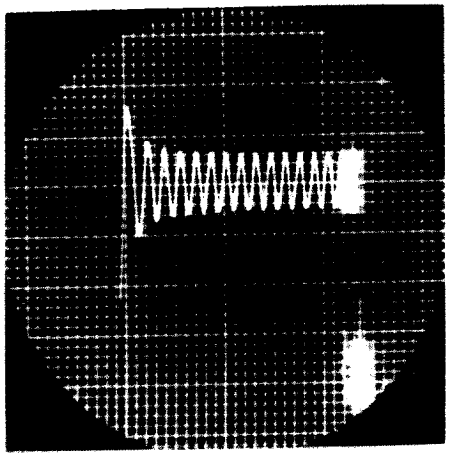

Figure 95

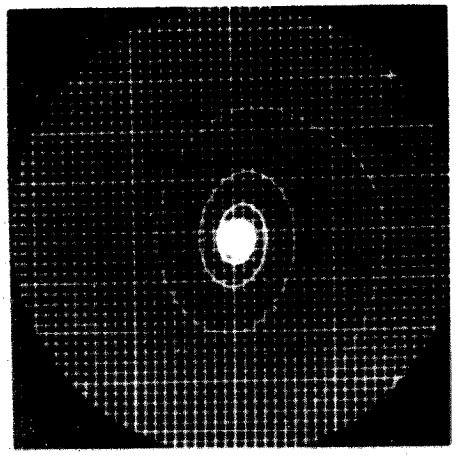

Figure 96

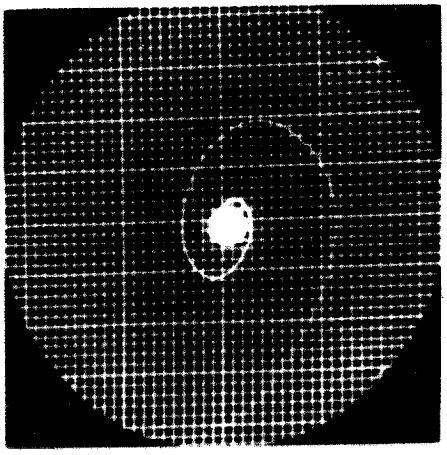

Figure 97

Table XI

Oscillogram Number	Explanation
Fig. 92	x vs t with σ = -1.6
Fig. 93	x vs t with σ = -4.0
Fig. 94	x vs t with σ = -8.0
Fig. 95	x vs t with σ = 1.0
Fig. 96	phase trajectory of Figure 92
Fig. 97	phase trajectory of Figure 93

damping is used as the base of the per unit damping system. The basic unit (σ = 1) is obtained from the zero-damped case of Figure 95.

The function $-(\dot{x})^n$ ($n > 1$) was first used in an attempt to improve the response of the control system. As n was varied, it was found, as one might reason physically, that the damping decreased with decreasing signal. The response curve damps rapidly at first but dies out slowly as the origin is approached. A typical set of oscillograms for the case n = 3.27 is shown on Figures 98 through 103 and is explained in Table XII. It is especially interesting to note the phase trajectory for the positive $\dot{x}^n$ (n = 3.27) damping shown on Figures 102 and 103. If the damping is larger than σ = 4.8, a stable oscillation results. For smaller values, perhaps, σ = 4.56, the system damps down and almost oscillates; the momentum of the system is great enough, however, to carry the trajectory through the limit cycle, and the motion dies out.

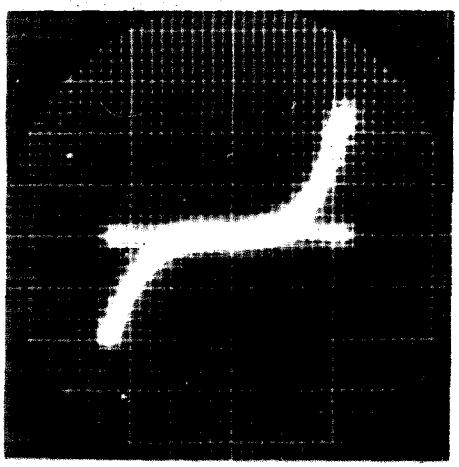

Figure 98

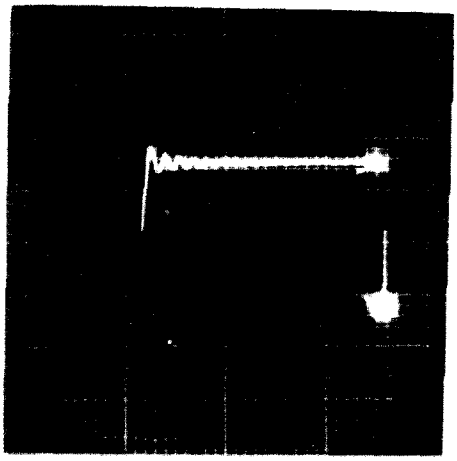

Figure 99

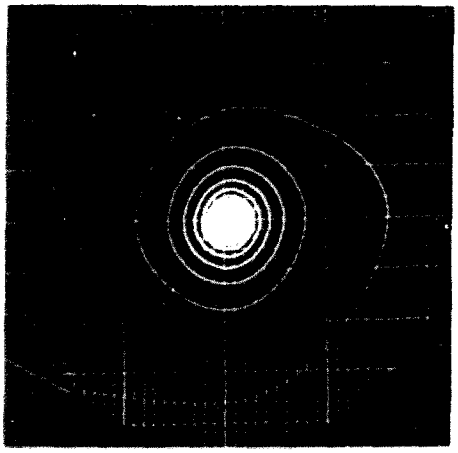

Figure 100

Figure 101

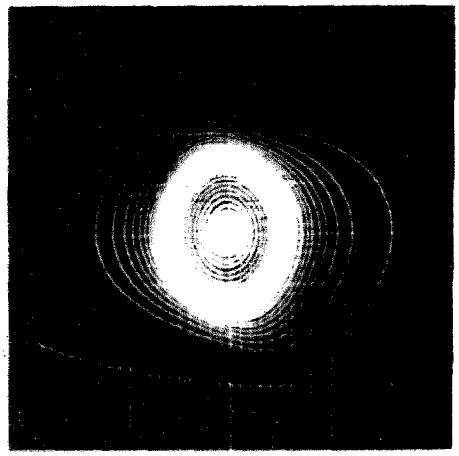

Figure 102

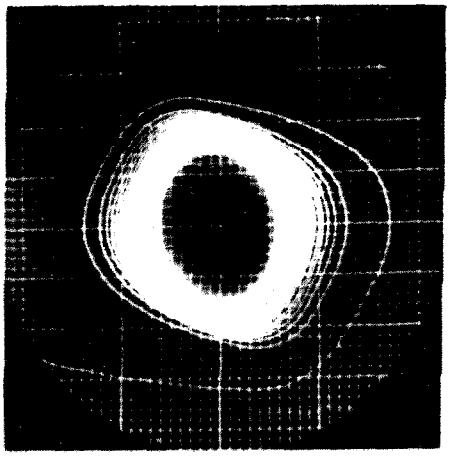

Figure 103

Table XII

Oscillogram Number	Explanation
Fig. 98	rate feedback function $(\dot{x})^n$ $n = 3.27$
Fig. 99	x vs t with $\sigma = -24$
Fig. 100	phase trajectory with $\sigma = -1.6$
Fig. 101	phase trajectory with $\sigma = -24$
Fig. 102	phase trajectory with $\sigma = 4.56$
Fig. 103	phase trajectory with $\sigma = 4.80$

More is said about this interesting phenomenon when it again appears in cubic position feedback. From these latter oscillograms one can see that in the region $n > 1$ no improvement is observed.

A search was made in the region $n < 1$ to find a more improved response. The result of this investigation yielded an improved response, in terms of rise time, with the function $y = x^{0.348}$. Oscillograms of this improved system are shown in Figures 104 through 109 and are explained in Table XIII. In terms of speed of response, a comparison of Figures 108 and 109 shows that the best response of the linear system is slower than that with the nonlinear feedback if in each case the amount of feedback is adjusted to the point of no overshoot. Notice that the same step of voltage was applied in each case and that the horizontal axis has the same gain for both oscillograms. Only the vertical gain is slightly greater

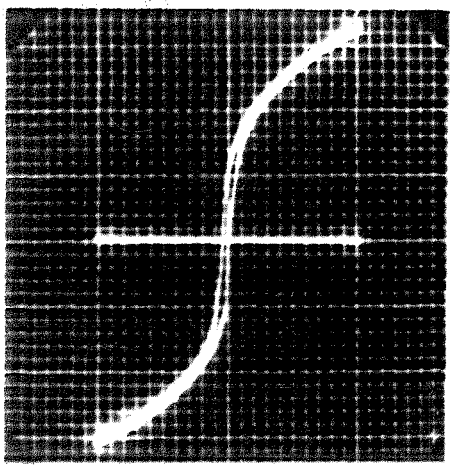

Figure 104

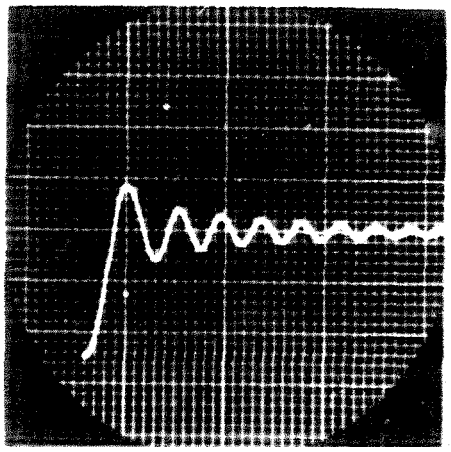

Figure 105

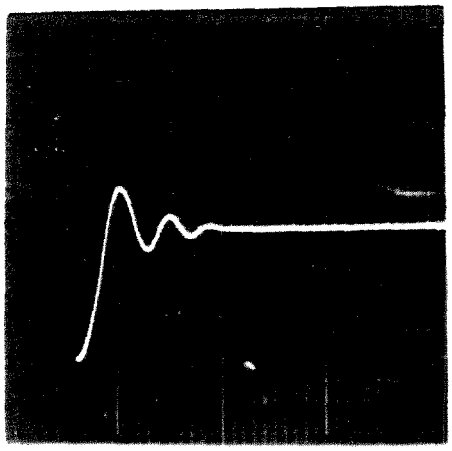

Figure 106

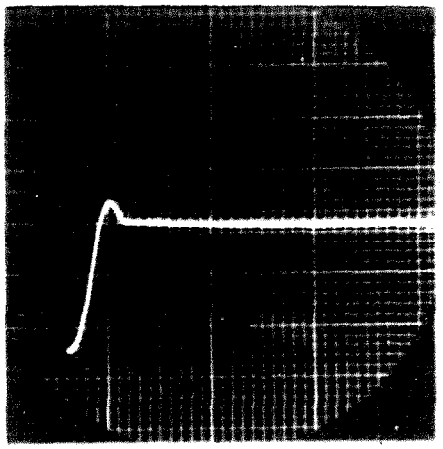

Figure 107

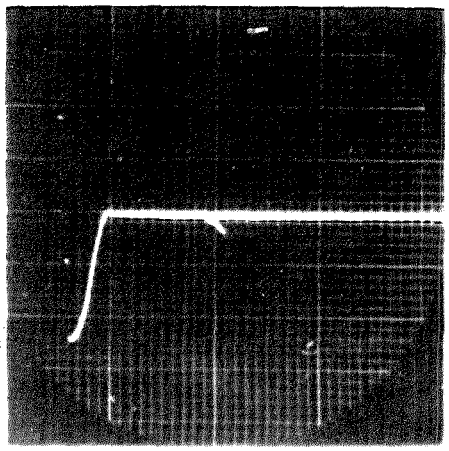

Figure 108

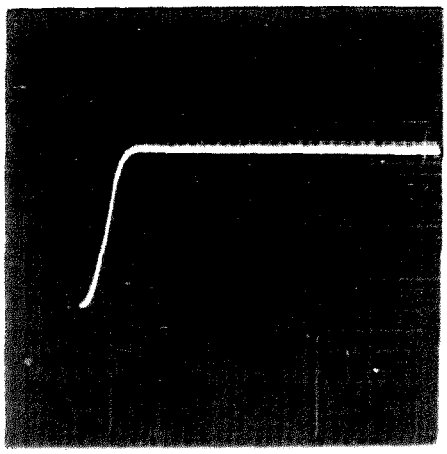

Figure 109

Table VIII	
Oscillogram Number	Explanation
Fig. 104	(*) velocity feedback function
Fig. 105	undamped natural oscillation with $\sigma = 0$ and only position feedback
Fig. 106	nonlinear velocity feedback x vs t with $\sigma = -1.6$
Fig. 107	nonlinear velocity feedback x vs t with $\sigma = -8.0$
Fig. 108	improved response curve of x vs t with $\sigma = -15.2$
Fig. 109	best response with linear velocity feedback x vs t with $\sigma = -8.8$

for the linearly damped case, an error which has no effect upon the comparison.

An investigation of various functions of position feedback showed that no improvement in response over pure linear position feedback resulted. For both cases of x^n feedback with n either less than or greater than 1, the system sustained a steady oscillation as shown in Figures 110 and 111.

It is interesting to note in connection with Figure 111 that, throughout the bulk of the thesis, the phase trajectories are all shown without isochrones (time ticks). Toward the end of the research, the idea of modulating the z axis of the oscilloscope with a series of timed negative spikes occurred. With the simple circuit Figure 112, the square-wave voltage is differentiated, producing regularly positive and negative spikes. A diode is used to eliminate all positive pulses,

and the negative spikes appearing on the z axis of the oscilloscope result in a dark space. Hence, although this simple but indeed useful idea was not used until this late time, the author hopes that future researchers may benefit from this isochrone generator. The isochrones on the oscillograms of Figures 113 and 114 are spaced 1 millisec apart.

Oscillograms of Figures 113 and 114 demonstrate again the phenomenon mentioned in connection with positive nonlinear rate feedback (Figures 102 and 103). In both of these oscillograms, the position feedback is linear plus cubic ($\alpha x + \beta x^3$). In both oscillograms (Figures 113 and 114) the system starts at a large value and damps to a limit cycle. But in both cases the momentum of the energy storage elements carries the system through, and a position of rest results. In Figure 114 the x^3 term was increased 2 percent. The arc of a circle on the left portion of both oscillograms should be disregarded since this line is the trajectory of the system before shorting the dc driving supply. An investigation proved that, for this phenomenon to occur, the system should have a saturating amplifier and have near-cubic rate feedback or linear-plus-cubic positive feedback. The author believes that this same phenomenon could exist with any type of nonlinear function which produced a stationary value. In the present case, the effects of the saturated amplifier and the nonlinear feedback function combine to form this interesting result.

Figure 110

Figure 111

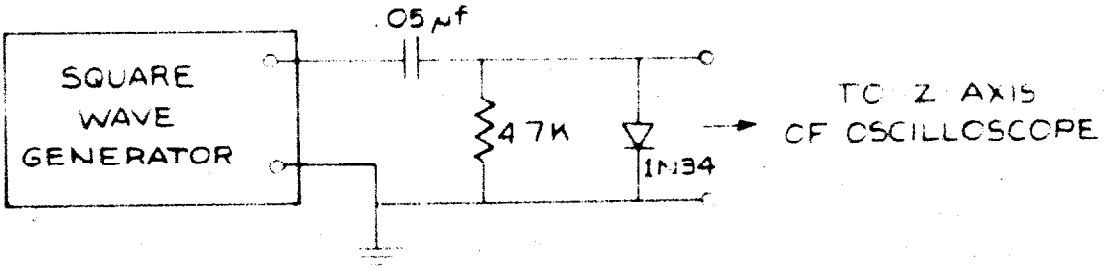

FIGURE 112 ISOCHRONE GENERATOR

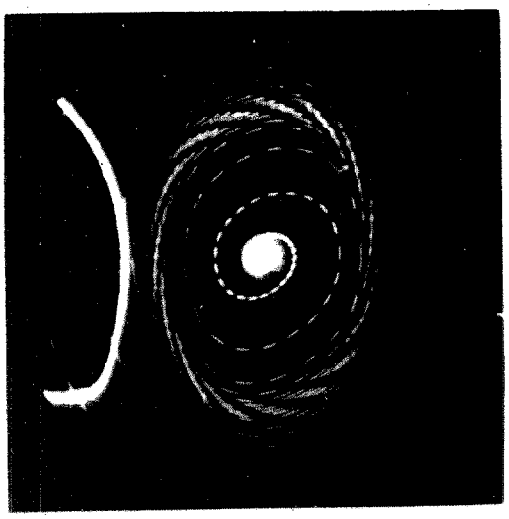

Figure 113

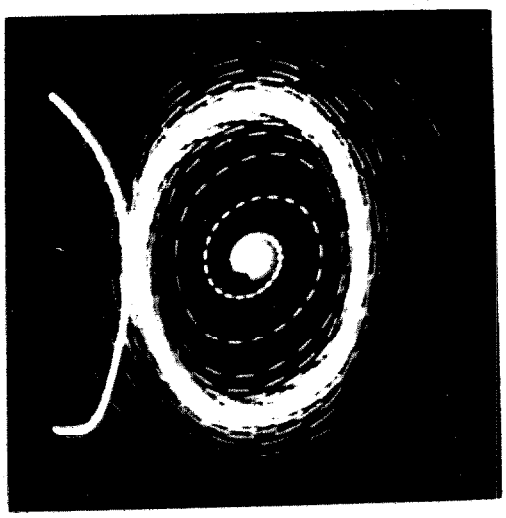

Figure 114

VIII. CONCLUSIONS

One can read about the phenomena resulting from the solution of nonlinear differential equations and can further build up a belief in these phenomena from topological or analytical results. But to observe these phenomena on an oscilloscope screen is conclusive proof of their existence. Even more fascinating is the use of the computer in the feedback path of servo systems. Here one obtains the feeling that he is doing something that hitherto was not possible. The author concludes that this feeling is somewhat justified, since the computer offers a most versatile and useful tool for the solution of these problems. True it is that the AFDEV described herein is less accurate (about 5 percent) than other forms of function generator. But because of its versatility in producing functions of a dependent variable, one must conclude that this function generator serves a real need in the field of analog computing.

With regard to the optimization of closed-loop systems by means of nonlinear functions, the author believes that the surface has just been scratched. A general statement as to the improvement of nonlinear systems or even certain classes of nonlinear problems is not yet possible. The author concludes, however, that with further work and with the aid of the function generator herein described, engineers will one day push back the shroud of ignorance which surrounds the subject of nonlinear mechanics and will begin to solve the mass of these unsolved problems.

References

1. N. Minorsky, Introduction to Non-linear Mechanics (1947), J. W. Edwards.

2. J. J. Stoker, Nonlinear Vibrations in Mechanical and Electrical Systems (1950), Interscience Publishers.

3. A. Andronow and S. Chaikin, Theory of Oscillations (1937), Moscow.

4. Arthur C. Hardy, "A Recording Photoelectric Color Analyzer," Jour. of Opt. Soc. of Amer. (Feb. 1929), Vol. 18, No. 2, pp. 96-117.

5. Stuart Ballantine, "Variable-mu Tetrodes in Logarithmic Recording," Electronics (Jan. 1931), Vol. II, pp. 472-473, 490.

6. Frederick V. Hunt, "A Vacuum-Tube Voltmeter with Logarithmic Response," Rev. Sci. Instruments (Dec. 1933), Vol. 4, pp. 672-675.

7. John P. Taylor, "A D.C. Amplifier for Logarithmic Recording," Electronics (Mar. 1937), Vol. 10, pp. 24-27, 35.

8. Ralph E. Meagher and Edward P. Bentley, "Vacuum Tube Circuit to Measure the Logarithm of a Direct Current," Rev. of Sci. Instrum. (Nov. 1939), Vol. 10, pp. 336-339.

9. I. A. Greenwood, J. V. Holdam, and D. MacRae, Electronic Instruments (1948), M.I.T. Rad. Lab Series, Vol. 21, p. 125.

10. H. B. Dwight, Tables of Integrals and Other Mathematical Data (1947), Macmillan Company.

11. R. C. Howard, "A Special-Purpose Electric Analog Computer and Its Application to the Solution of Certain Nonlinear Differential Equations" (1953), thesis, California Institute of Technology.

12. Shih-Ying Lee and J. F. Blackburn, "Axial Forces on Control-Valve Pistons," Meteor Guided Missile Project Report No. 65 (June, 1950), Dynamic Analysis and Control Laboratory, Massachusetts Institute of Technology (Unclassified).

APPENDIX A

DC Power Source

Early in the development stage of the linear-to-logarithm converter, it was realized that a well-regulated, reliable power supply with versatile output connections was a necessity. Since a variety of voltages, both positive and negative, would be necessary for experimental and computing work, it was decided that four identical power supplies should be built in such a manner that voltages from -600 to +600 would be available in 300-volt steps. The outputs of these supplies are brought out to a common distribution panel located in the center of the experimental test bench, which is discussed in Appendix B.

The power supplies used in this system are designed to deliver 300 volts at currents up to 300 ma. The drift at the output is less than 10 mv/hr, measured with a Brown potentiometer, and the internal impedance is held to the order of 10^{-2} ohm by the regulator. The principal time constant of the regulator results from the 2000- μf stabilizing capacitor and the plate load of the 12AX7 which, in magnitude, is approximately 1 millisec.

The design employs a unique balance of economy, reliability, and accuracy. Referring to Figure A-1 in which a complete schematic diagram of the power supply is displayed, one can see that use is made of two transformers and two rectifiers to supply one filter network and regulator. This arrangement permits the use of inexpensive lower-current

109

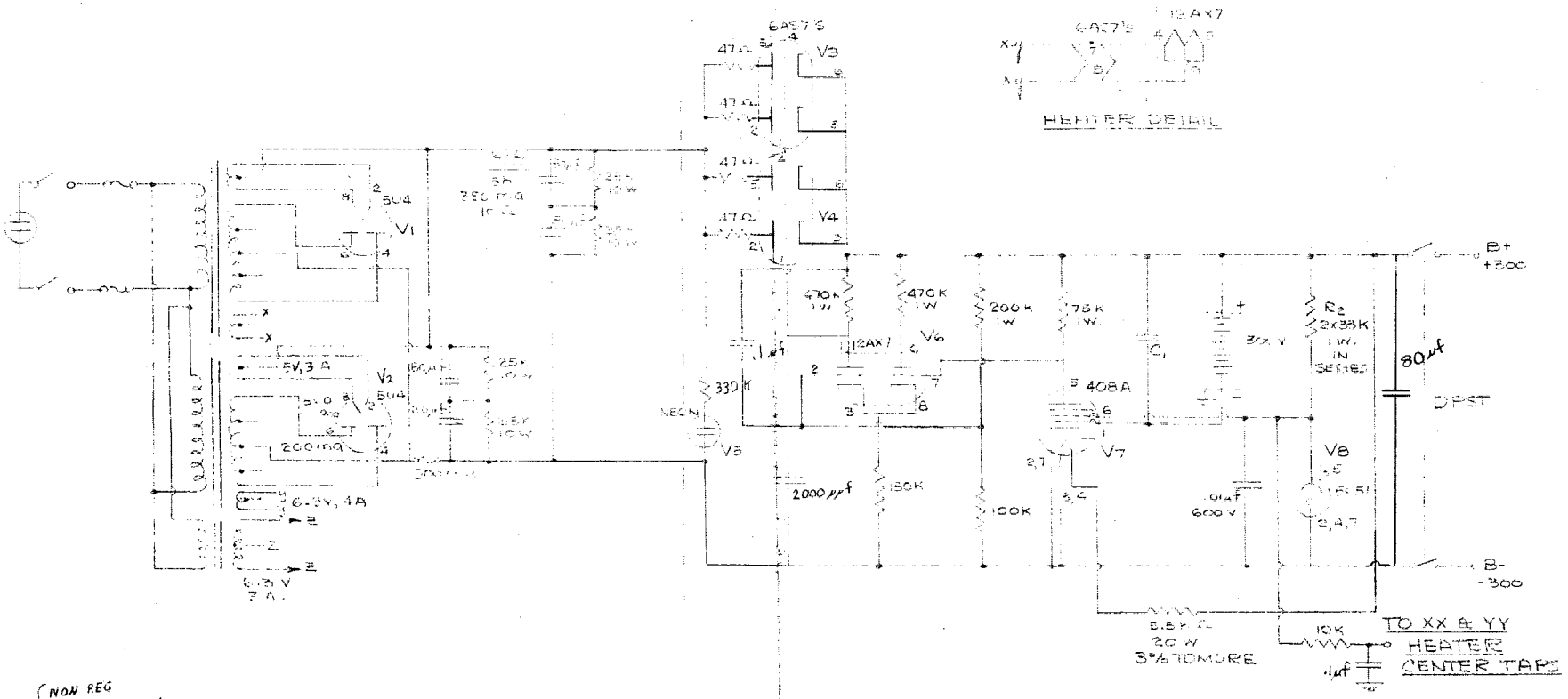

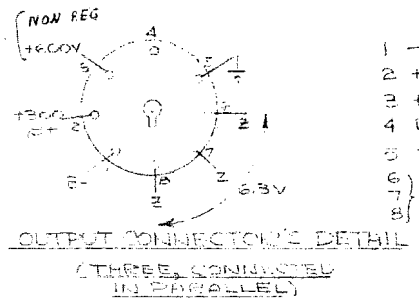

OUTPUT CONNECTION'S DETAIL
(THREE CONNECTED IN PARALLEL)

1 –
2 + 300
3 + 600
4 BLANK
5 ⏚ CHASSIS
6, 7, 8 6.3 V.

NOTES – POWER SUPPLIES NOS. 1-4 –
1- CHASSIS IS NOT CONNECTED TO B-, BUT IS BROUGHT OUT TO A TERMINAL.

NOTES – POWER SUPPLY NO. 5 –
1- COMMON TRANSFORMER
2- 6B66 TRIODE CONNECTED REGULATOR TUBES
3- GAIN E COMPARISON TUBE, AC HEATED
4- MAXIMUM CURRENT IS 175 MILLIAMPERES

300V., 300 MILLIAMPERE REGULATED POWER SUPPLY
FIGURE A-1

transformers and rectifier tubes and at the same time provides quite a sizable power by paralleling the transformers. Any undesirable circulating current, caused by slight transformer unbalance, is avoided because a separate rectifier is used for each transformer. Electrolytic capacitors are used in the filter network, again in the interests of economy.

The accuracy which is achieved with this design can easily be understood from a consideration of the details of the regulator circuit. This circuit has a gain of about 10,000 and uses a 300-volt battery for reference. The first stage employs a 408A* pentode which is electrically equivalent to the 6AK5 pentode except that the heater requires 20 volts at only 50 ma. Because of this low heater-current requirement, the filaments can be heated from the regulated output. This last feature would be impractical unless resistors with very nearly zero temperature coefficient were available. The tomore resistors which were used vary less than 1/2 percent over the entire range of temperature involved; after these special resistors have reached operating temperature, the variation in heater current is less than 1/10 percent. To improve the stability of the regulator further, the screen voltage on the first stage (408A pentode) is maintained constant with a 5651 voltage reference tube. The remainder of the regulator employs a 12AX7 twin triode, used as a differential amplifier, which drives two 6AS7 twin triodes, sections of which are connected in parallel to provide the necessary

---

*Supplied by Western Electric.

capacity for controlling the 300 ma. As can be seen from the photographs of Figure A-2, numerous binding posts, carrying the plus and minus terminals of the power supply, the chassis, and the 6.3-volt ac filament supply, are brought out to the front. All voltages are readily accessible for permanent connection with an octal socket from the rear.

After the power supplies had been in service for an adequate aging period (2 months), tests were performed to ascertain the accuracy of the supply. It was concluded from these tests that the drift (as previously stated) of 10 mv/hr was satisfactorily low. Although it was feared at first that the primary-secondary insulation of the transformers might not stand the added stress resulting from the series connection, no failures have occurred in the 10 months of operation.

APPENDIX B

Experimental Test Bench and Laboratory Facilities

This appendix describes (for the reference of any future researchers) the layout of the laboratory in which the computer was developed and ultimately used. Considerable time was spent in the layout and construction of a convenient work area, and since the equipment has been used for a period of a year, it is concluded that the time was well invested.

All necessary power is readily accessible and controllable by one master distribution box mounted in the center of the bench. All the power supplies are in shelves, with the Sola constant-voltage transformers and filament storage

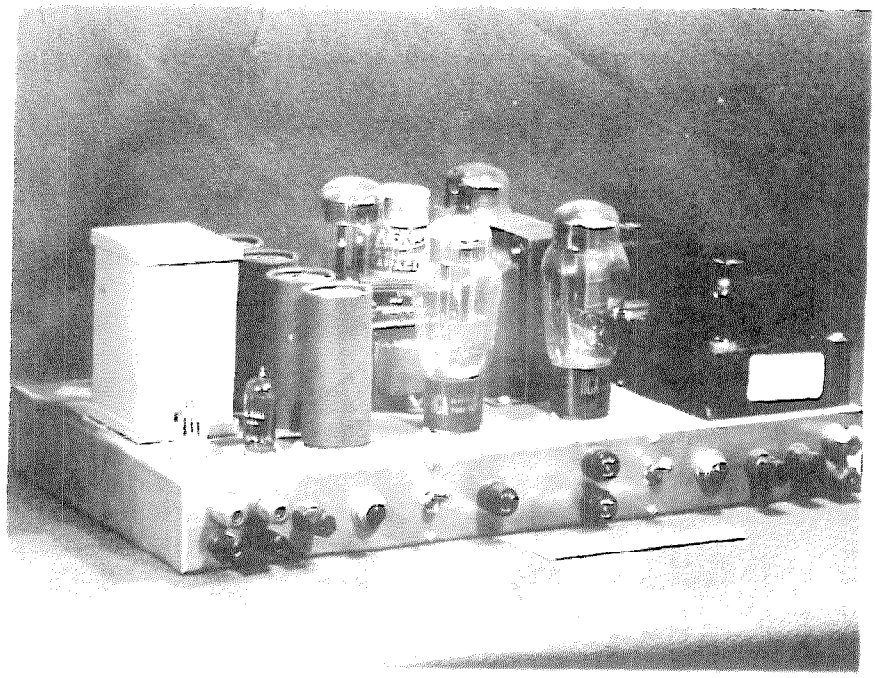

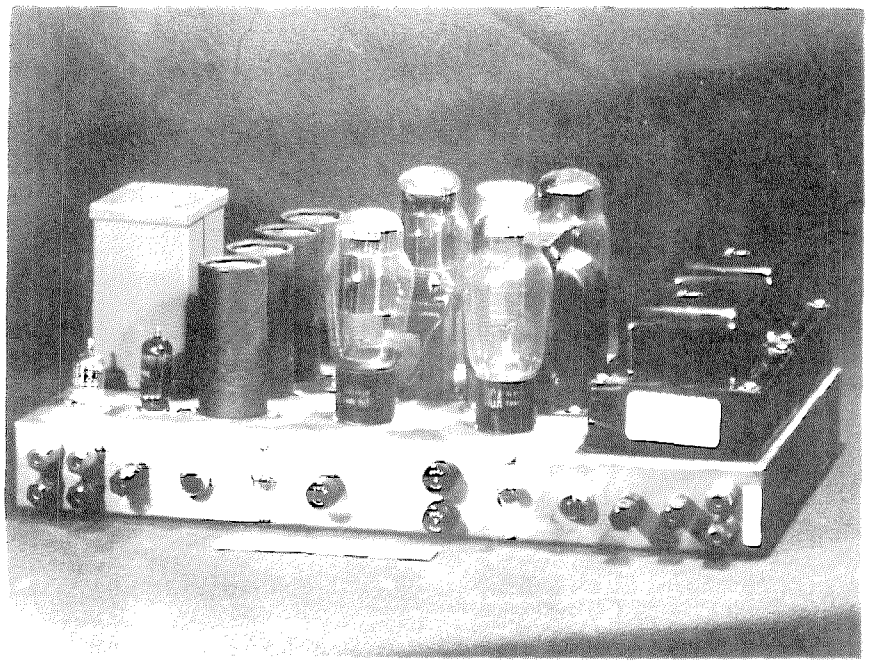

Figure A-2. Two Views of the Power Supply

battery mounted below. A master power switch, mounted on the wall, removes the power from all equipment except the tube ager and the battery charger, which is mounted to the right of the power supplies. The bench is equipped with a common ground that permits various types of terminals to be used conveniently with clip leads, banana plugs, or spade terminals. Figure B-1 shows two photographs of the laboratory facility. The central distribution board, shown in detail on Figure B-2, contains eleven-prong receptacles for the reception of standard power plugs wired to each permanent piece of equipment and numerous binding posts for use with experimental equipment. Both ac and dc 6.3-volt filament supplies also are available and are indicated as being available with appropriate pilot lights. Each high-voltage supply can be disconnected independently by four double-pole, double-throw switches mounted on the panel.

APPENDIX C

Linear Sweep Generator

During the initial stages of LTE testing and during the operation of the nonlinear computer an arbitrary function of an independent variable (AFINV), a linear sweep generator was employed to generate the function x. This generator (LSG) has a 300-volt peak sweep. The LSG was designed to deliver a saw-tooth voltage wave of constant repetition rate, variable amplitude, and low output impedance. A schematic diagram is included in Figure C-1, and Figure C-2 shows photographs of

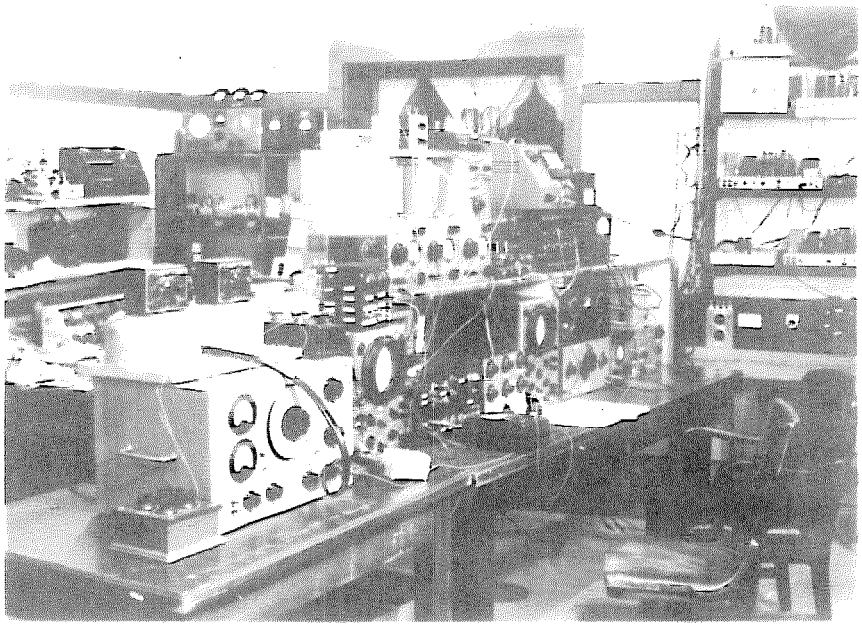

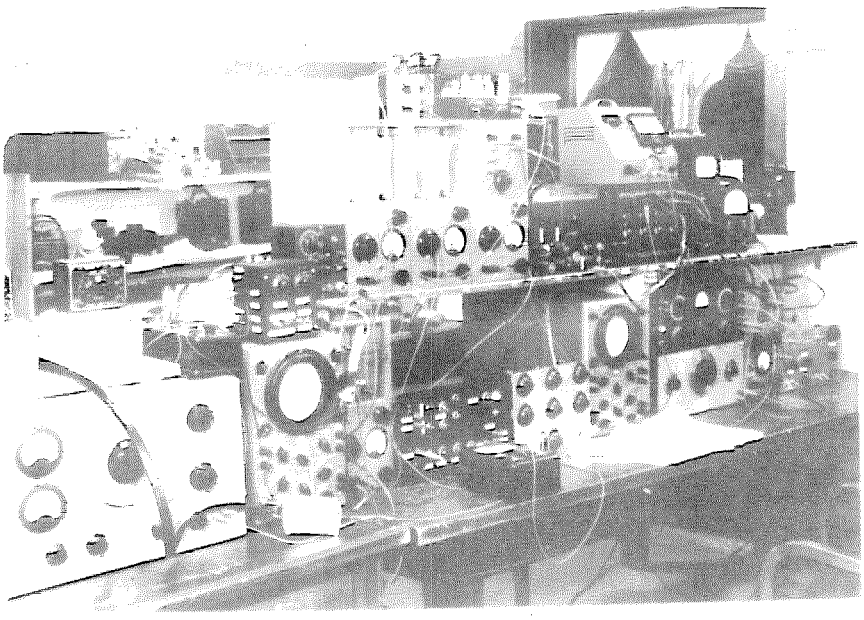

Figure B-1. Two Views of the Laboratory Facility

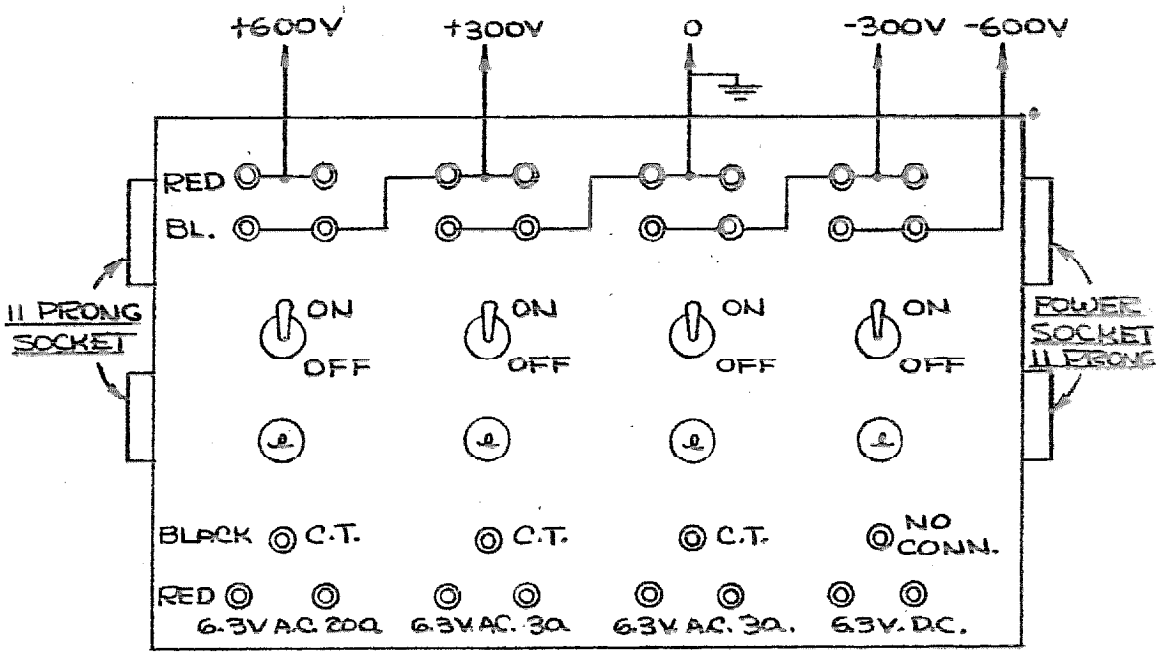

(BOTTOM POWER SUPPLIES ON SHELVES TOP)

NOTE:
SWITCHES CONTROL BOTH BINDING POSTS AND POWER SOCKETS

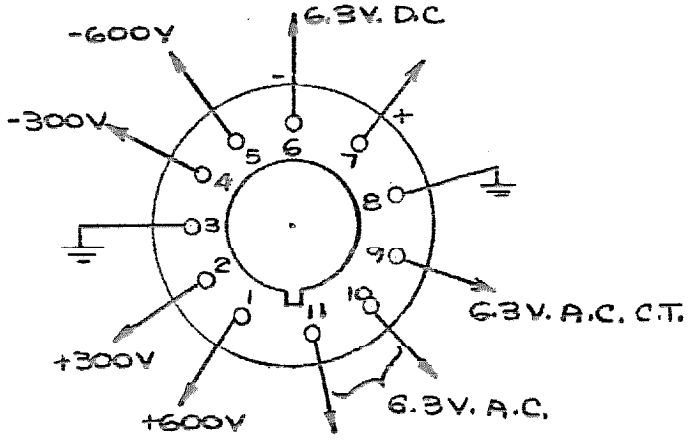

POWER PLUG
(FOR 11 PRONG SOCKET)

POWER PANELS
FIGURE B-2

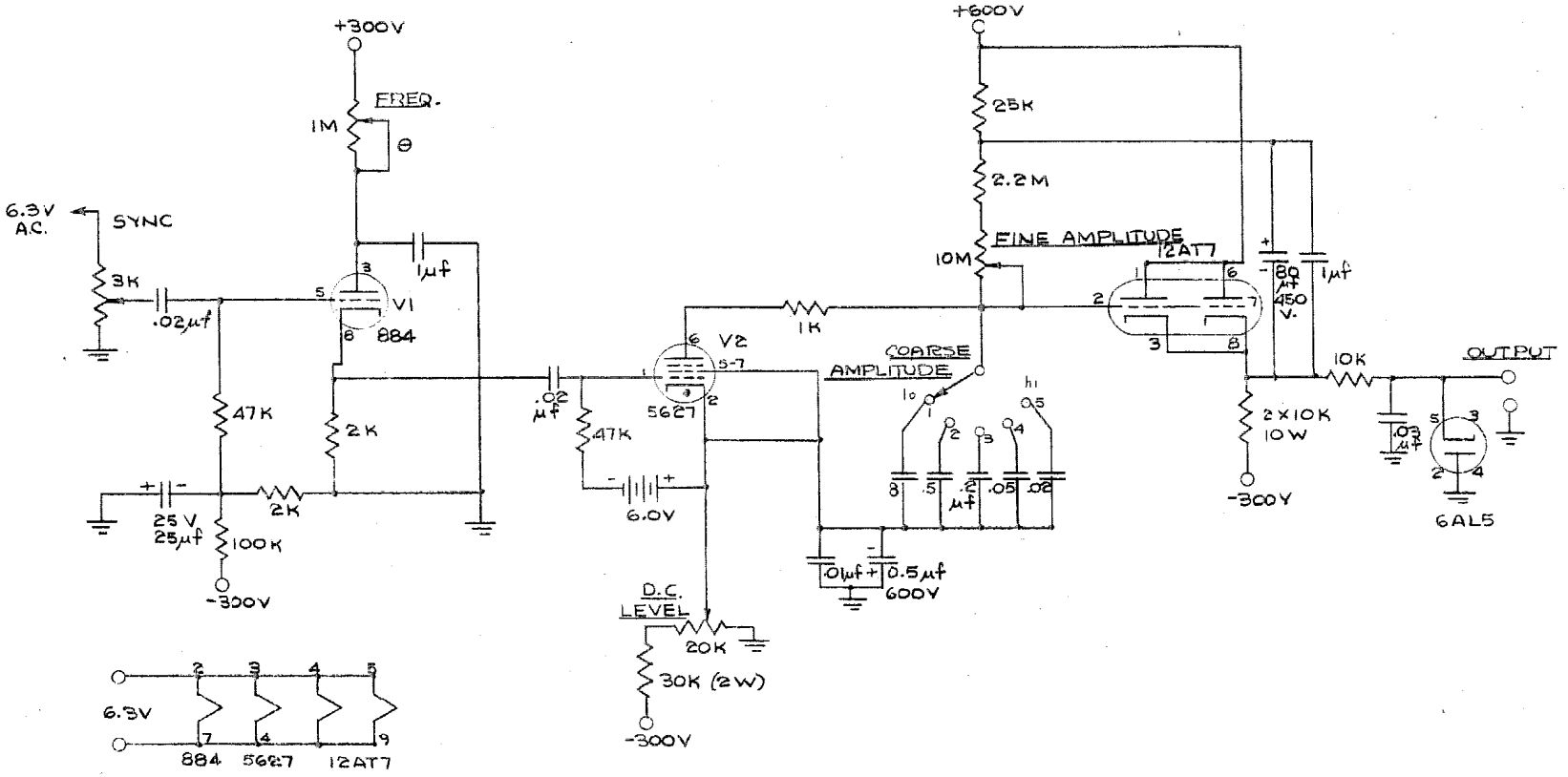

FIGURE C-1

LINEAR SWEEP GENERATOR

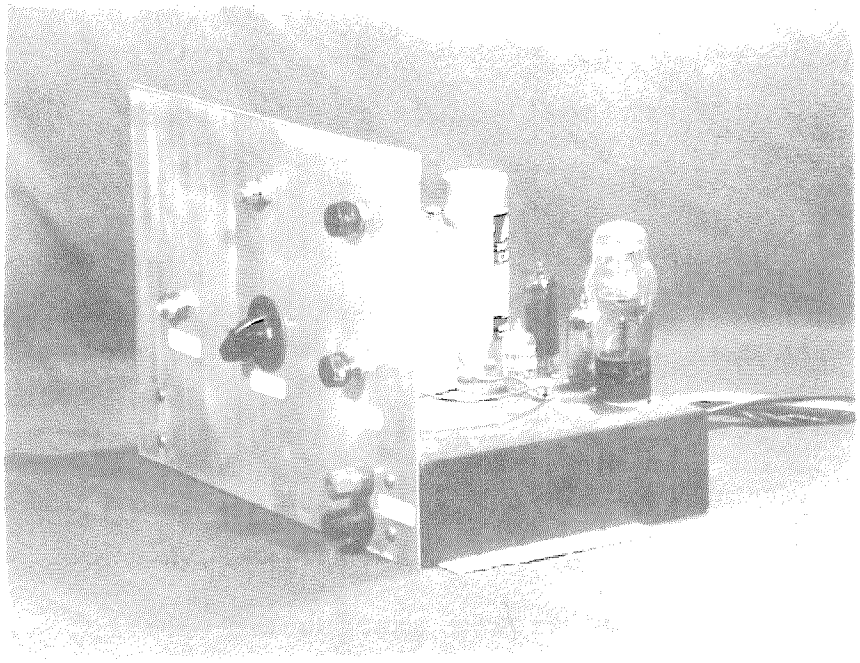

Figure C-2. Photograph of Linear Sweep Generator

the device.

In the use of the LSG, an 884 thyratron (V1) operates as a relaxation oscillator. The frequency is controlled by a 1-megohm, five-frequency-control potentiometer which alters the charging current of the 1-μf capacitor. A 60-cyc/sec, 6.3-volt signal is applied from the ac line to the grid of the 884 thyratron through the 3000-ohm synchronizing potentiometer. The frequency of oscillation is thus synchronized at the following submultiples of 60 cyc/sec: 10, 20, 30, or 60.

The output of this oscillator is taken from the cathode in the form of spikes which are applied to the grid of V2 (a 5627 thryatron). With the application of a spike, V2 conducts, and the sweep capacitor is quickly discharged. The capacitor begins charging toward +600 volts through the fine-amplitude resistor. The voltage across the capacitors is fed to the output through the cathode follower V3 (a 12AT7 parallel-connected).

Since a maximum amplitude of +300 volts, which is continuously adjustable down to 20 volts, is desired, the output voltage is fed back to the top of the charging capacitor. This scheme corresponds to constant current charging with a great improvement in linearity. The resulting curve was measured linear to within 1 percent.

The firing potential of the saw-tooth output voltage is controlled by the setting of the dc level control. The total drift results from the output tube V3, which operates

in an amplifier of gain less than unity. Since the amplifier has low gain, and since the LSG is supplied with regulated filament and dc requirements, the drift is less than 0.3 volt (0.1 percent of full-scale voltage). The output impedance of the LSG is approximately 200 ohms.

APPENDIX D

Additional Computer Components

This appendix describes five devices which are used in conjunction with the computer. A circuit diagram, together with an explanation of each device, is included for the benefit of future users of the equipment which has been discussed in this thesis.

1. Voltage control box.

In testing and using the computer, one often requires a calibrated voltage or accurate voltage divider. The voltage control box, which is shown in the schematic diagram of Figure D-1, satisfies this need. The unit, which is shown in the photograph of Figure D-2, consists of six Helipots. Terminals are brought out for convenient availability of each potentiometer, and appropriate fusing is provided.

2. Oscilloscope calibrator and function selector.

The need was felt for an oscilloscope calibrator such that peak magnitudes of the various oscillograms could be obtained. Built in one unit, which is shown in Figure D-3, are a voltage calibrator and a function selector. The latter device has as its input the important junctions in the analog

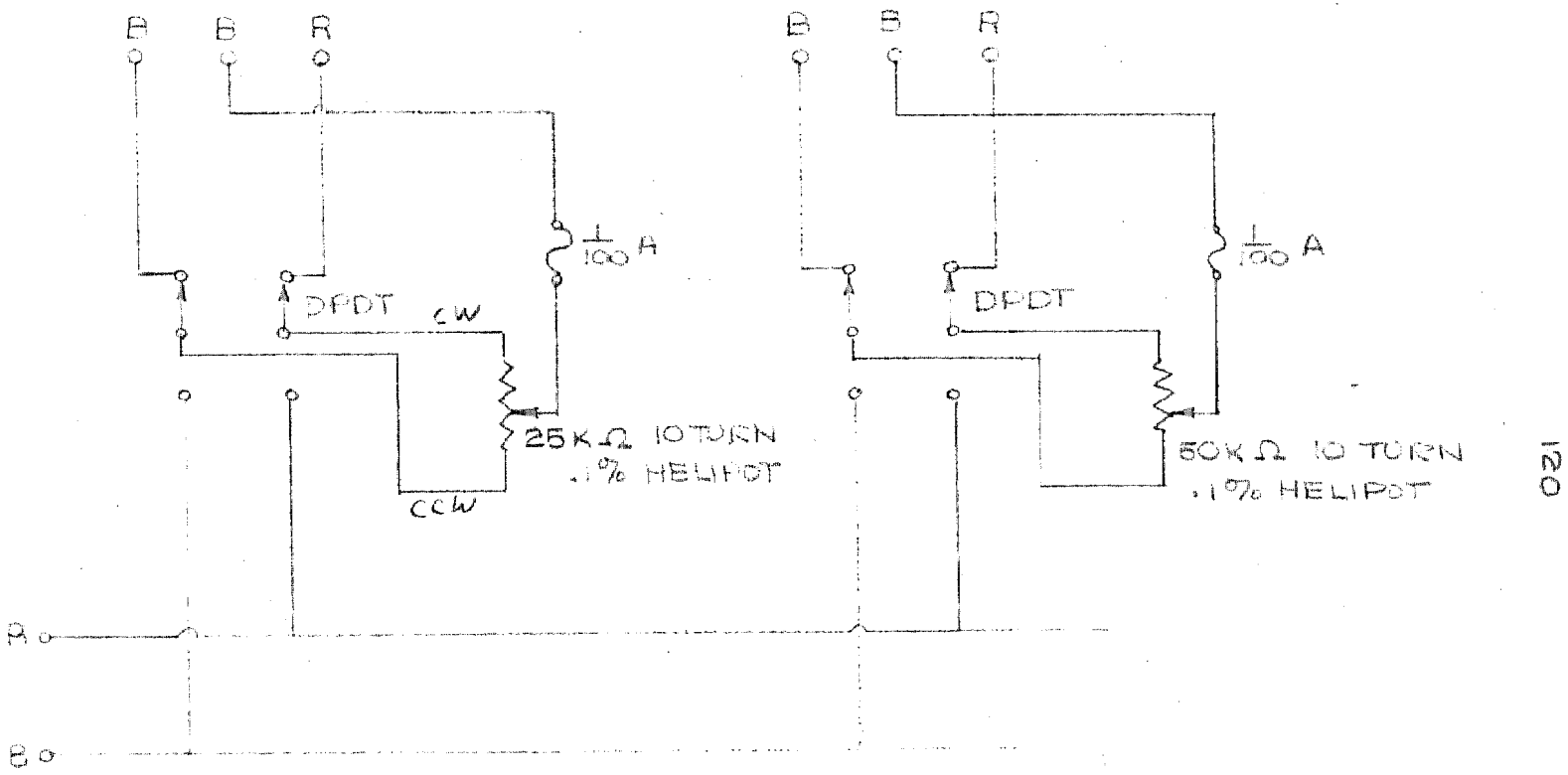

SWITCHES SHOWN WITH HANDLES IN "UP" POSITION
25 KΩ HELIPOTS IN BOTTOM ROW
THREE SETS AS SHOWN ABOVE

FIGURE D-1 VOLTAGE CONTROL BOX

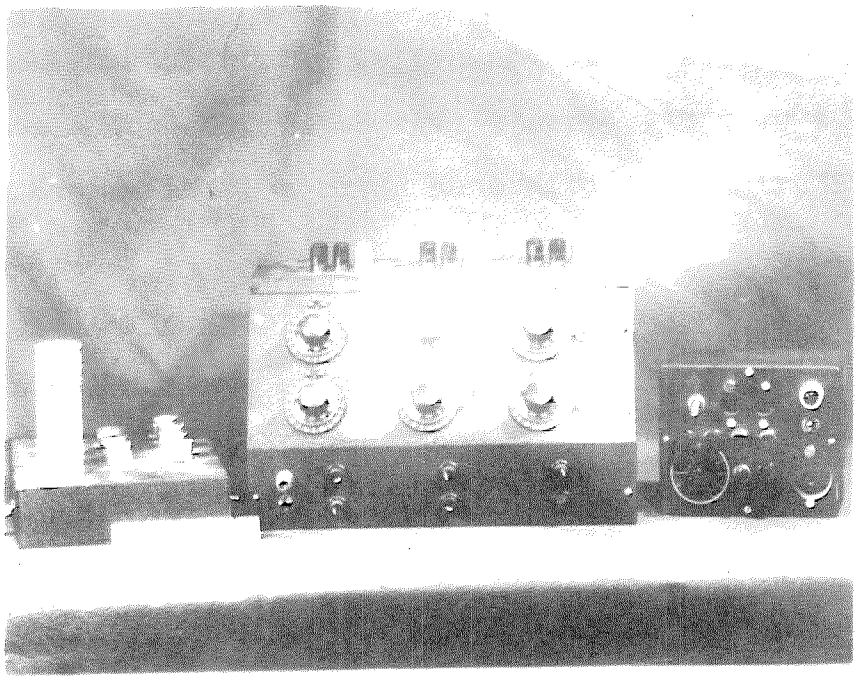

Figure D-2. Photograph of Voltage Control Box

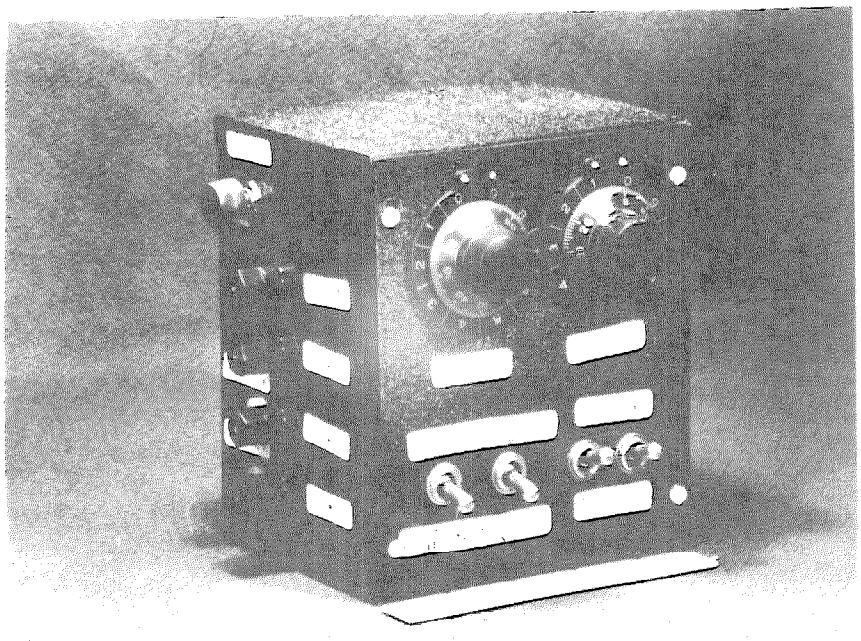

Figure D-3. Photograph of Oscilloscope Calibrator and Function Selector

solution. With appropriate switching one is able to obtain either a phase trajectory, an x vs t curve, an $\dot{x}$ vs t curve, or the nonlinear function being generated. The circuit diagram of this unit is given in Figure D-4.

3. The computer connector unit.

Into this unit are plugged the three LTE units for interconnection with the other computer elements. All necessary power for the LTE is brought into this chassis. As is shown on the schematic diagram of Figure D-5, the input and output Helipots, which adjust the base and exponent of each element, are also included on this unit. A center-tapped Helipot provides the necessary scale changing for the computer. All important leads are brought to the front through standard jacks. Figure D-6 shows a photograph of the unit.

4. The test voltage unit.

The test voltage unit shown photographed on Figure D-7 provides fixed voltages of 300, 180, 90, 30, 9, and 3. The output voltages of this unit are used to plot the static characteristics of the LTE. The circuit arrangement is shown on Figure D-8.

5. Stability voltmeter.

This unit provides a wide range of small voltages and an appropriate null meter. The unit was used first to measure the stability of power supplies and other equipment. Later, terminals 3 and 4 were used as a variable step-function generator. In the latter application the device provided easy change of exciting function for the phase trajectories of

of Sections V and VI of the text. The circuit diagram is included in Figure D-9.

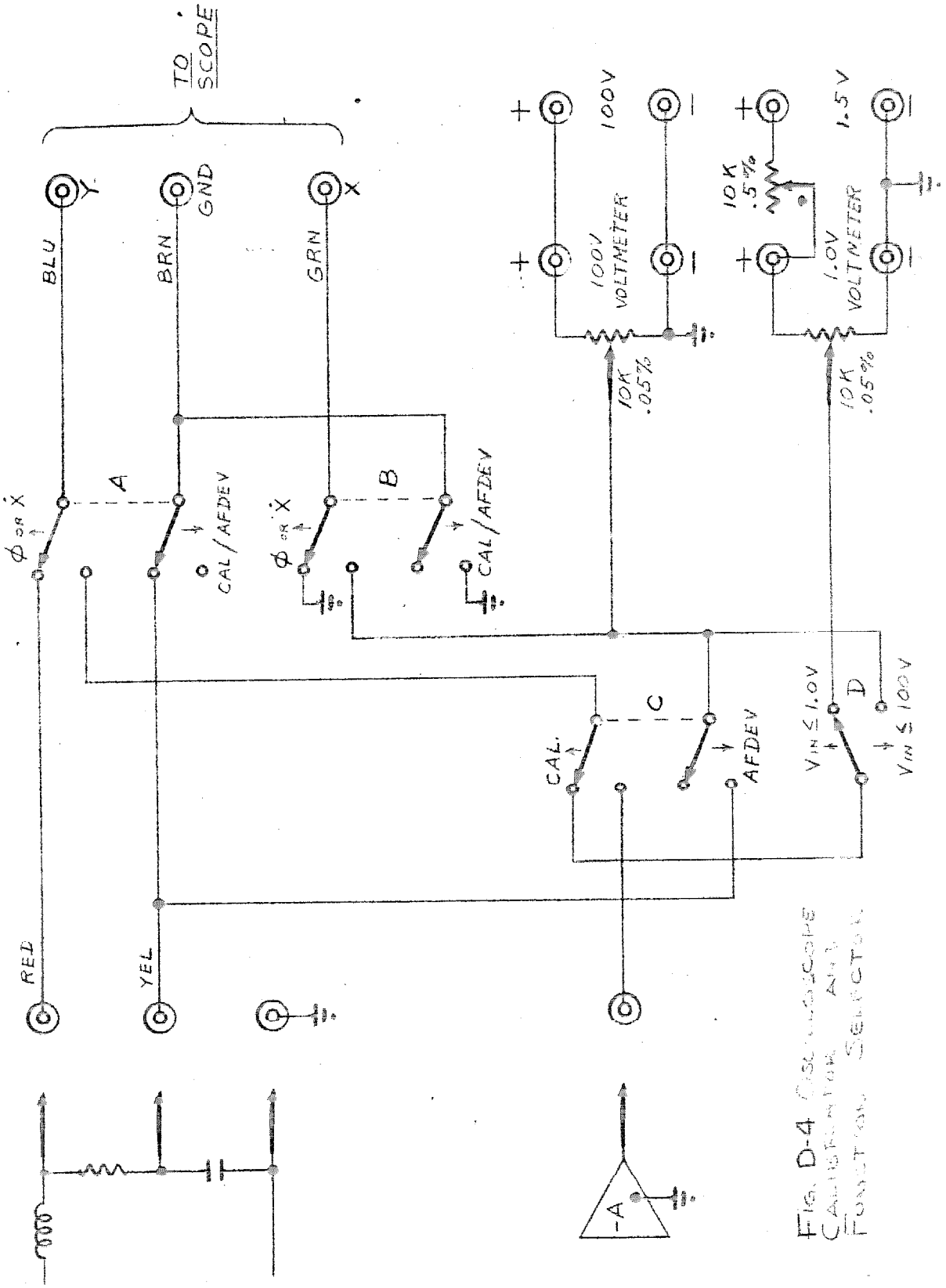

Fig. D-4 Oscilloscope Calibration and Function Selector

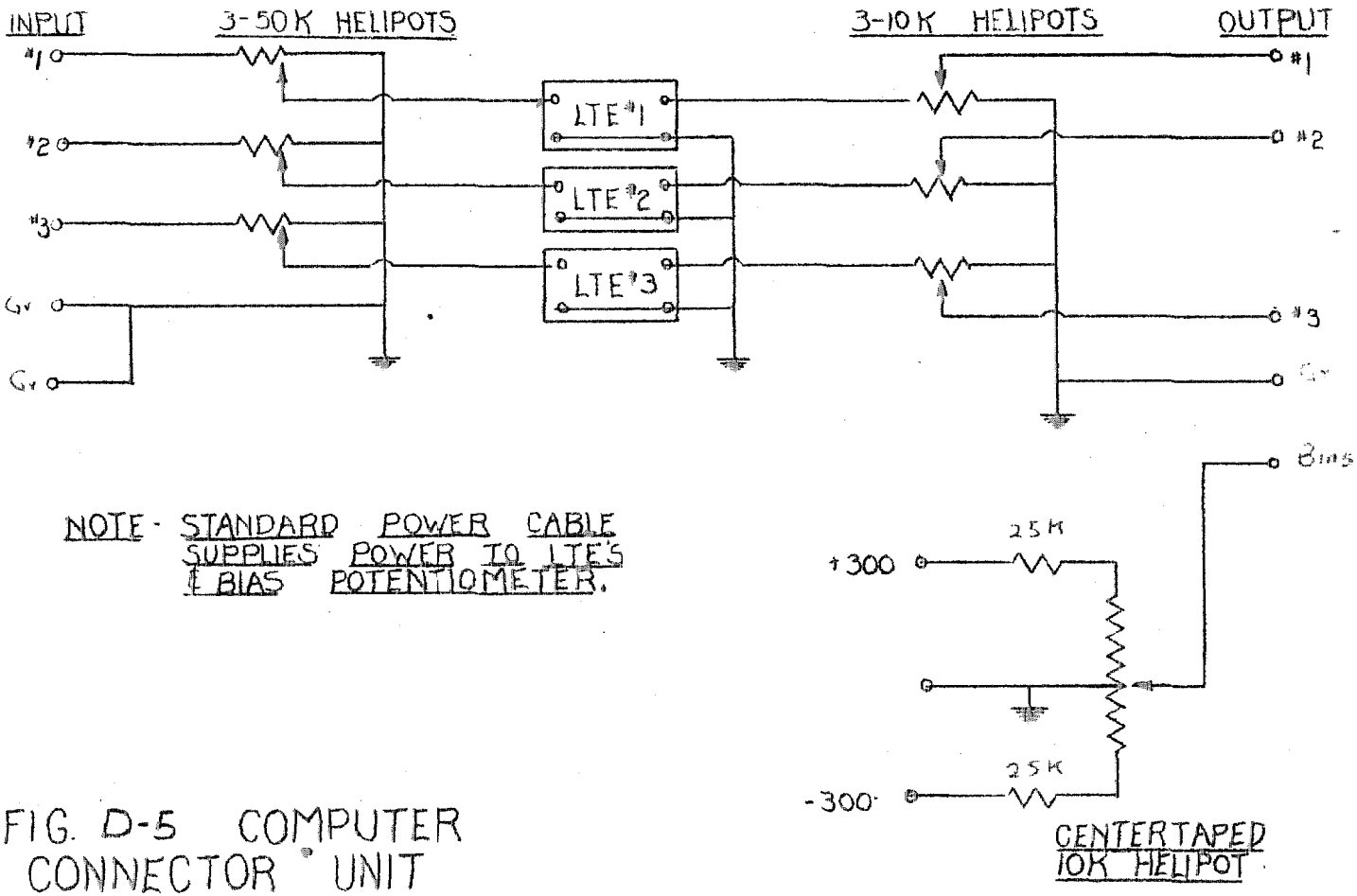

NOTE - STANDARD POWER CABLE SUPPLIES POWER TO LTE'S & BIAS POTENTIOMETER.

FIG. D-5 COMPUTER CONNECTOR UNIT

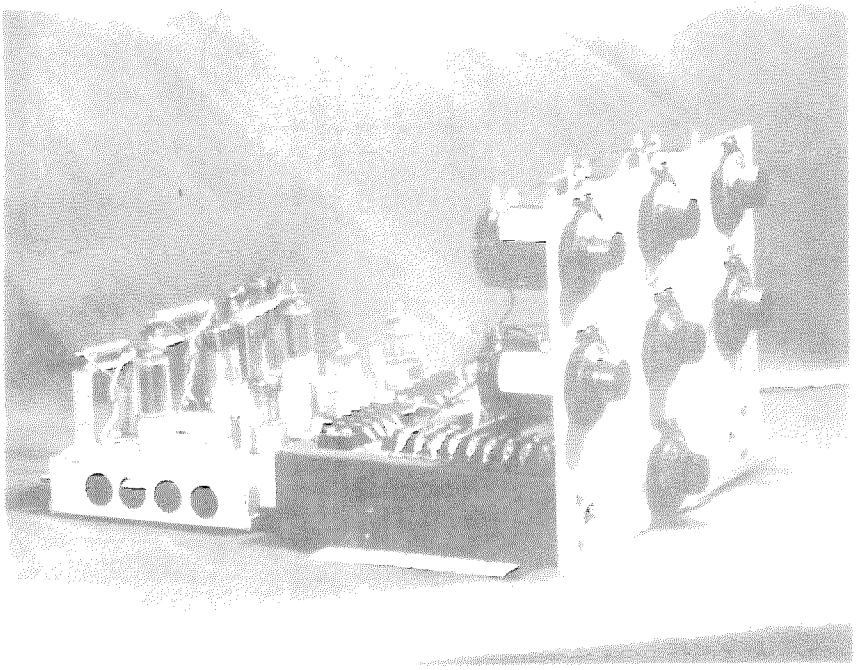

Figure D-6. Photograph of Computer Connector Unit

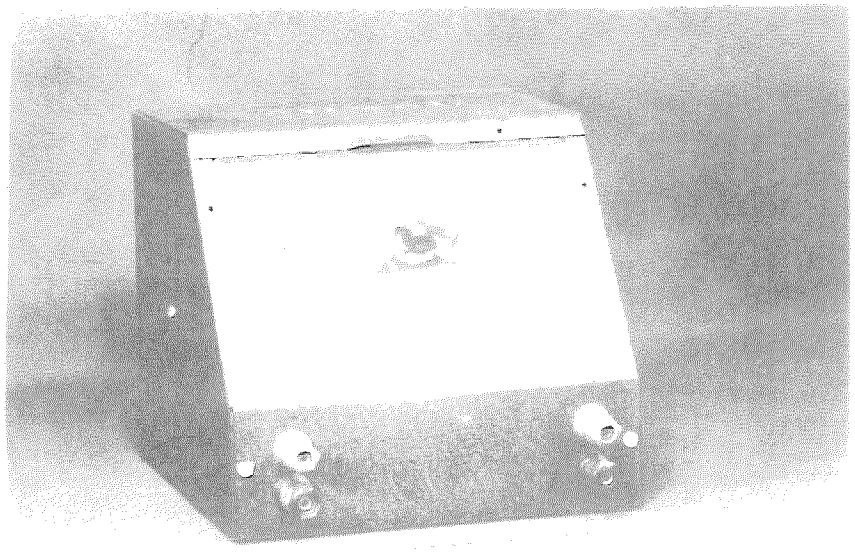

Figure D-7. Photograph of Test Voltage Unit

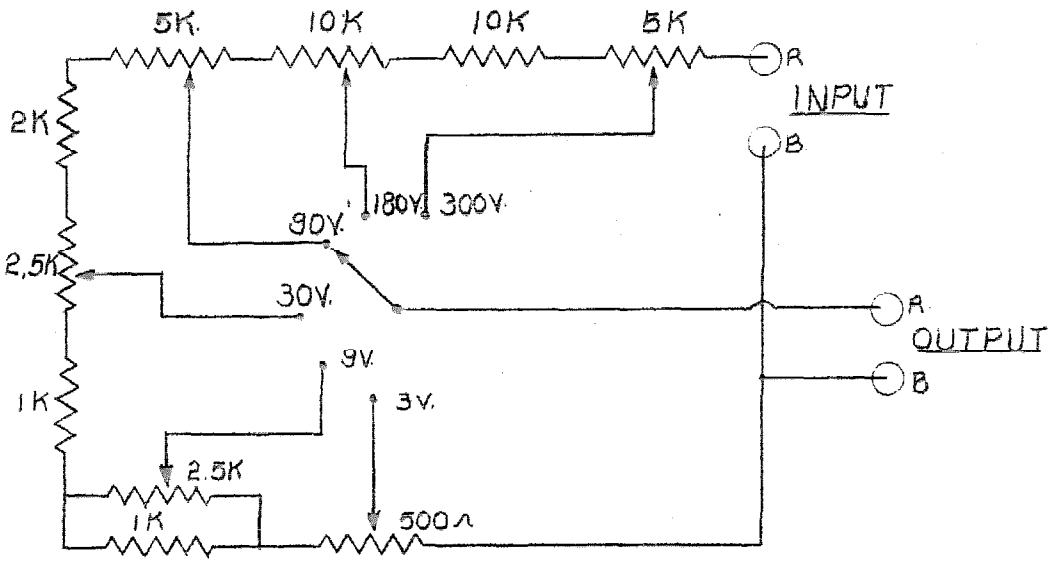

TEST VOLTAGE UNIT
FIG. D8

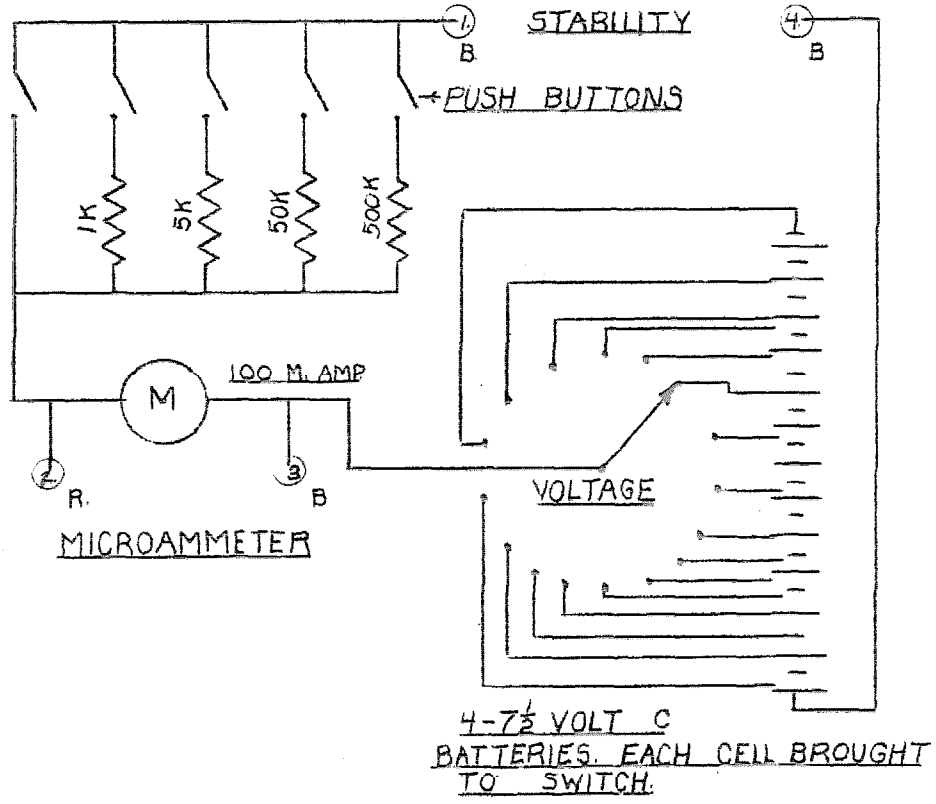

STABILITY VOLTMETER
FIG. D-9